

SAMMENDRAG

Konseptuell design er en unik mulighet til å ta del i designprosessen som en helhet, og skape konstruksjoner som både er meningsfulle for ingeniøren, arkitekten og de som skal få jobben gjort. Ikke minst er det en fordel fra et miljøperspektiv, og den som skulle betale for prosjektet. Fordelen med metoden kommer av de digitale parametriske verktøyene, som gir muligheten til en kontinuerlig oppdatering av formen på konstruksjonen. Dette gjør at den strukturelle effektiviteten kan vurderes underveis som formen trer frem. Denne optimaliseringsprosessen utfordrer tradisjonelle metoder, der endring i form fort skaper konflikter og resulter i høye kostnader. Med en kontinuerlig mulighet til å vurdere det konstruktive, får komplekse former muligheten til å tre frem. Dette gir konstruksjoner med spennende geometriske former. Skallkonstruksjoner er eksempler på dette. Effektive, stabile former med en spennende arkitektonisk fremtreden. Disse kompliserte formene kan være bærekraftige med sin høye materialeffektivitet. Det er likevel utfordringer i slike komplekse former. Komplekse former, følger også komplekse konstruksjons-elementer, knutepunkter og konstruksjon med. I dag har utviklingen på den parametriske arbeidsflyten kommet langt med tanke på å finne den globale effektive formen. Digitale verktøy blir i større grad integrert i større ingeniørfirmaer. Likevel er det mye igjen å forske på for å få slike konstruksjoner til å fungere. Mange ikke-standard konstruksjons elementer som skal settes sammen til komplekse konstruksjoner, kan føre til at de tradisjonelle metodene lønner seg både økonomisk og miljømessig. Krevende knutepunktshåndtering og avfall fra forskallinger kan gjøre konstruksjonen ulønnsomme. Ved å benytte nettopp disse parametriske verktøyene kan likevel designet bli lønnsomt. Ved bruk av industrielle roboter, kan krevende arbeid ved å montere konstruksjonen, bli mye lettere. Industrielle roboter kan montere kompliserte konstruksjoner hurtig med høy presisjon, også på steder som er ansett som farlige omgivelser. Dette setter likevel krav til knutepunktene mellom elementene. Knutepunktene må være mulige å produseres og monteres med robotene, uten at det går ut over knutepunktets evne til å overføre krefter. I denne masteroppgaven har jeg derfor fokusert på å finne en «form finding method», en algoritme som kan implementeres i den globale parametriske modellen og finne den optimale knutepunktsutformingen analogt med optimaliseringen av den globale formen. Det må også settes krav til at knutepunktet kan settes sammen av robotene med den gitte knutepunktsutformingen. I denne forskingen har jeg valgt å utforske trelementer som knyttes sammen i knutepunkter kun ved hjelp av sin egen geometri. Dette muliggjør robot montering, der kompliserte skrueforbindelser og andre eksterne festingsmetoder unngås. For å finne en felles måte å optimalisere konstruksjonselementenes utforming med hensyn til den globale formen, kreves det det en grundig undersøkelse av elementenes begrensninger, og kjennskap til materielt. I dette tilfellet har jeg vurdere kapasiteten til rene treknutepunkter. I undersøkelser (elementmetoden) av ulike treknutepunktsgeometrier, viste det seg at slike treknutepunkter er svært sårbare for høye spenningskonstruksjoner. Treverk er et anisotrop materiale, og har svake plan parallelt med fiberretningen. Skarpe kanter i knutepunkts geometri kan føre til høye spenningskonsentrasjoner som injiserer til splitting langs de svake planene. Også treknutepunkter i rent trykk er sårbare for slik «splitting». For å vurdere kapasitet til slike treknutepunkter, må de svake planene som gir brudd av knutepunktet må oppdages, og tas hensyn til i hver enkelt geometri. I denne forskningen ble det anisotrope material kriteriet «Tsai Wu» benyttet for å sjekke kapasiteten til treknutepunktene. Denne metoden må videre utvikles og testes empirisk for å kunne tas i bruk.

PREFACE

I wanted to write my master thesis within Conceptual Structural Design, because this department represents what I want to achieve and contribute with as a future structural engineer. I want to contribute in making as beautiful, meaningful, innovative and interesting architecture as possible.

The research group at NTNU “Conceptual structural Design” represents the platform between architecture and structural design. Believing that if architects and structural engineer work close together in finding the form, we can develop structures that unites the structural functionality and visual form into a meaningful and interesting whole. By working together, we can also find innovative shapes and create projects where architectural form and structural functionality are interlinked. In Conceptual Structural Design, the architect and engineer are both part of the designers finding the optimal form of the structure.

Through the year as NTNU student, I have learned theoretical structural approaches to evaluate structural components and find the most efficient shape. I am very grateful for have been given this opportunity to merge this knowledge with the philosophy of beautiful architecture.

I want to express my sincere gratitude to our advisors, Marcin Luczkowski and Professor Anders Rønquist. A special thanks to Marcin Luczkowski for helping me with digital models and my many questions at all hours, and Anders Rønquist for being an inspiring professor. I would also like to thank Katarzyna O. Luckowska, and Marie Louise Seeberg.

Hanne Seeberg

INTRODUCTION

Advances in computer technology have facilitated the design of structures of high complexity and extraordinary geometry. To realize these complex structures, the technology is implemented throughout the design process, from finding the shape of the structure to fabrication and final construction.

Elegant, thin-shell structures with irregular shapes are examples of structures with high complexity that create extraordinary geometry. In previous work by the research group “Conceptual Structural Design Group (CSDG)” at NTNU, the design process of advanced shell structures has been investigated. This has contributed to the work of developing digital workflows of parametric structural design.

Complex shapes with irregular geometry require nonstandard structural elements assembled in joint configurations of unit complexity. Hence, complex shapes require sophisticated joint design. This design connections needs to consider both structural load-bearing efficiency and the logic of assembling the structural elements into one, sophisticated structure. As the joint configuration and its internal loads are derived from the global shape, the joint design should be implemented in the *Digital Workflow of Parametric Structural Design*. As the shape itself is continuously modified, so should the joints be.

With complex shapes revolving in sophisticated joints, complex construction and fabrication follow. Fabrication and assembly of nonstandard structural elements into sophisticated configurations using traditional methods can be time consuming and expensive. With digital production and assembly such as 3D printing techniques and industrial robots, technology can handle complexity particularly well, and extraordinary architectural design can be carried out. Use of these digital methods requires an “assembly logical” design. This means that the construction must be considered in the design of the shape and its elements. The construction becomes an integral part of the design process as it is integrated in the Digital Workflow of Parametric Structural Design.

Considering the construction of these complex structures in the design of the joints, the investigation of pure geometrical interlocking between joint members is done. Today’s tradition of timber joints by metal fastening does not facilitate robot assembly. Metal fastening methods increase the time of assembly and make the construction more complicated and more instable during construction. In contrast, integral attachment timber joints with their pure geometrical interlocking design facilitate robot assembly and the construction of complex shapes.

Thereby, in this master thesis I will investigate the structural behavior of integral attachment timber joints and collect information to find a potential form finding method for timber joints. The aim is to implement timber joint design in a digital workflow of parametric structural design, that enables robot manufacturing and assembly.

Content

Abstract.....	Feil! Bokmerke er ikke definert.
Sammendrag	1
Preface.....	1
Introduction.....	2
1 Background.....	7
1.1 Architects, engineers and construction	7
2 Japanese joinery.....	9
2.1 Conceptual structural design.....	Feil! Bokmerke er ikke definert.
2.2 Shell structures - complex structures	10
3 Structural joints.....	11
3.1 Definitions.....	11
3.2 Joints – classification	12
3.3 Mechanical joints	13
4 Implementation of joint design in the digital workflow of parametric structural design	15
General Workflow	81
4.1 Design and production tools	15
4.1.1 3.1.1 Software	15
4.1.2 Industrial robots	17
4.2 Advances in Architectural Geometry (AAG) 2018	19
4.3 Advantages of integral attachment joints.....	20
4.4 Requirements and constraints	21
4.5 Interlocking strategy	22
5 Wood	25
5.1 Wood connection design.....	25
5.2 Characteristics of wood.....	27
5.3 Eurocode	30
6 Structural analysis of mechanical wood joints	31
6.1 Joint - tension.....	32
6.1.1 The basic analysis	36
7 Case study: apply in General workflow	81

8	Conclusion marks	90
9	References	91
10	Appendix.....	92

1 BACKGROUND

1.1 ARCHITECTS, ENGINEERS AND CONSTRUCTION

Historical structures

Structures have always been vital for humans and their societies. Shelters and dwellings, religious meeting points, vehicles and monuments are all central to human lives. Astonishing structures have been erected and are impressive accomplishments from both an aesthetic, structural and a constructive point of view. One may wonder how people managed, more than 5000 years ago[19], to build the monumental Stonehenge, with its nine meters high and 20 tons heavy stones. Examples on historical structures requiring labor intense and complex work is many, Egyptian pyramids, Greek temples and the Great Wall of China are some to be mentioned. Mainly facilitated by cheap labor, and in many cases on the expense of construction workers lives.



FIGURE 1) STONGEHENGE [19]



FIGURE 2) PANTHEON IN ROME [20]

Throughout history, the shape and complexity of structures have evolved, and increasable architecture created, still appreciated today. An example of this is one of the most famous historical buildings, the Pantheon in Rome, a concrete dome spanning 44 meters. The building was constructed between year 110 and 130 AD, during a time before the existence of any digital structural analysis tools as we know them today. Notably, this was also before the current separation between the architect and the civil engineer was created. The architects, or constructors, were artists or mathematicians, finding the shape through their knowledge of physics and geometry. The architects behind great historical buildings had a scientific approach to physical and mathematical problems applicable to civil engineering.

Method of design

In the 18th century, through polytechnic schools, specialisation in technical fields was established and civil engineering became a separate discipline. Since then, specialized knowledge about structural design has accumulated on each side of the disciplinary boundary between architecture and civil engineering, and caused separate understandings of the nature of good design.

Hence, in traditional methods of design, the engineer rarely takes part in the conceptual phase. The engineer optimises and evaluates the structural behavior of a finalised concept, created by the architects. As changes must be done to secure structural stability, the result can end far from the vision.

Modern technology challenges the traditional method of design, and has enabled geometric computation providing a variety of tools for efficient design, analysis, and manufacturing of complex shapes[10]. *Parametric design* uses variables and algorithms to allow the designer to investigate the shape by adjusting parameters. This gives the opportunity to examine the effect of changes in shapes, both regards to structural behavior and architectural points of view. It opens up a new horizon for architecture, where irregular and freeform shapes can rapidly be investigated. As shapes are explored, structural efficiency can be evaluated by implementing *form finding methods* in the parametric model. A form-finding method means “Finding an optimal shape of a [form-active structure] that is in (or approximates) a state of static equilibrium[21].

This has enhanced the synergy between architects and engineers. Working together, they can find innovative shapes and create projects where architectural form and structural functionality are inseparable. *The workflow of parametric design* gives the opportunity to explore the area between architecture and structural design. Along with the cooperation between engineers and architects, the construction phase can be implemented in the design. This can secure that the structure, both architectonically beautiful and structurally efficient, can be produced.

However, the method requires interest from all parts, learning required computer skills and taking part in a research area that rapidly evolves. In addition, the method gives no guarantee for a common understanding of optimal design, only the possibility of exploring it together.

1.2 INSPIRING JOINERY - JAPANESE WOODWORK

Japanese traditional architecture and construction are well known for their complex wood joinery performed with highly skilled handicraft, passed down through generations of Japanese woodworkers[22]. The work is seen as an artistic craft, requiring high precision, knowledge and experience with wood.

Japanese woodwork may have originated a long time before nails, screws or other any metal fasteners were invented. The tradition of using pure wood-wood connections with complex interlocking geometries have been learned through generations, and long been kept “secret” among Japanese woodworkers and carpenters.

The secret behind the strength and durability of these joints is not only to be found in their sophisticated geometry, but high precision creating tight interlockings. The joint designs are done without any structural calculations, but with considerable knowledge of wood characteristics and experience with interlockings. The flexibility of wood as a workable material combined with respect for the handicraft has resulted in many years of exploring geometrical shapes of wooden joints.

As well as providing strength to the overall structure, the joints are considered art simply based on its own geometry. An example of this type of sophisticated Japanese joint is the Kawai Tsugi. The joint can be assembled in three different ways, creating three different configurations- two at right angles and one a straight line. The wooden joint has pure geometrical interlocking, see Figure 3.

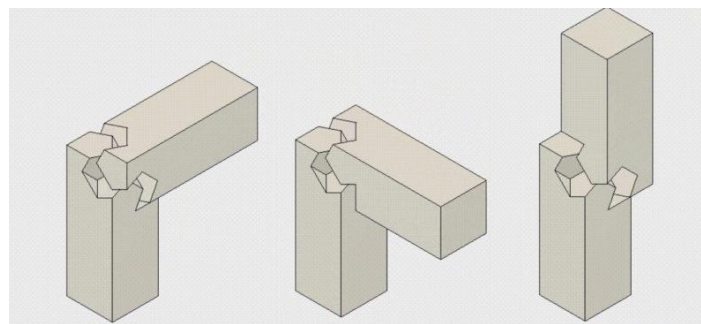


FIGURE 3) THE KAWAI TSUGI. [23]

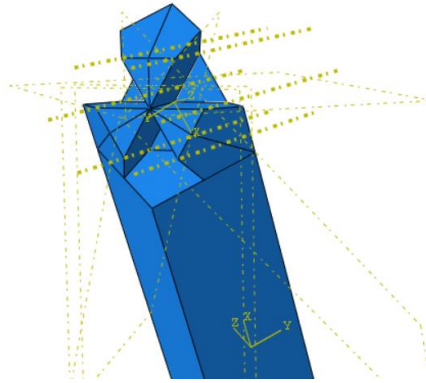


FIGURE 4) A MODEL CREATED OF THE KAWAI TSUGI IN ABAQUS/CAE, TO UNDERSTAND IT COMPLEXITY.

1.3 COMPLEX STRUCTURES – SHELL STRUCTURES

The Landesgartenschau Exhibition Hall is an example of a structure where sophisticated joinery can facilitate extraordinary shapes. The Landesgartenschau Exhibition Hall was conceived at the University of Stuttgart as part of the “Robotics in Timber Construction”. One of the most important challenges and innovations is the robotic fabrication of the 7600 individual finger joints, which, through their interlocking connection, are the main reason for the building’s structural stability. [17]



Shell structures with complex shapes can be considered as architecturally interesting and structurally efficient structures. A shell is a three-dimensional curved surface, where one dimension is smaller compared to the other two[1]. The structures reflect conceptual design as the structural efficiency and architectonic shapes are due to its geometry. Thus, the parametric design process, with its synergy of engineering and architecture, is highly relevant. By finding an ideal shape, shell structures can achieve efficient load bearing capacities with low material spending and expenditure. Together with an optimized joint, extraordinary shapes can be created.

There are different types of shell structures, constructed by a continuous surface or a by a grid of elements following the curvature of the surface, so-called grid shells.

2 STRUCTURAL JOINTS

This chapter will look into the characteristics of structural joints and discover how they achieve their structural interlocking behavior.

2.1 DEFINITIONS

Joint and connections

The definition of a joint may vary with the context. A wide definition is *an assembly of two or more objects*. In this thesis, the joint is defined by its structural purpose: A joint is a zone where two or more members are interconnected. For design purposes, it is the assembly of all the basic components required to represent the behavior during the transfer of the relevant internal forces and moments between the connected members.[24]

In situations where this structural feature is discussed, a *connection* is a common term used when referring to the joint.

A connection is the location at which two or more elements meet. For design purposes, it is the assembly of the basic components required to represent the behavior during the transfer of the relevant internal forces and moments at the connection.[25]

Based on these definitions, the difference between a *joint* and a *connection* is interpreted as the level of detail. A joint is defined as the assembly point between two structural members, whereas the connection is the detailing of the joint. In a joint, there can be several connections. For instance, in a column-beam joint, the flange of the beam can have one type of connection to a column, whereas the web can have another type of connection to the same column. [25]

Joining, assemblies and interlocking

Joining is the act or process of putting or bringing things together to make them continuous or to form a unit. As two parts are joined, they achieve a function that the simple components cannot do themselves. In civil engineering, the process is essential as structural elements of material components are joined together into structures. [3, pp.4] Using this definition, the term *assemble* in this thesis will refer to the process of joining.

As structural components are brought together by joining, an *assembly* is created. An assembly is further defined as a collection of manufactured parts with an aim of performing one or more functions. Based on its intended function, the assembly can be categorized as electrical, mechanical or structural. The primary function of a structural assembly is to carry either static or dynamic loads. In a structural assembly, the joint has a crucial role: to transfer forces between the structural elements in the assembly.

In this thesis, the term *interlock* is often used when the functionality of the joint is discussed. Interlock or *interlocking* refers to the ability of restricting a motion and to interfere with the structural components in the assembly. Interlocking can restrict one or up to six degrees of freedom[18].

2.2 JOINTS – CLASSIFICATION

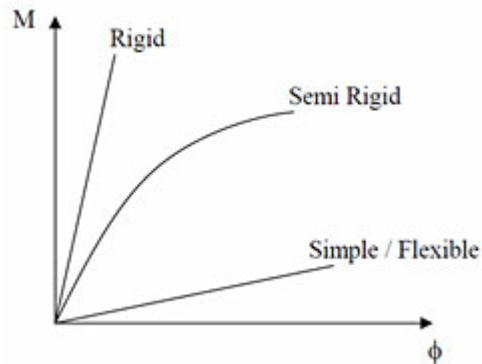
Rigid, semi-rigid and simple

All real structures are entities in three-dimensional space. In three-dimensional space, there are six directions of possible motion, referred to as degrees of freedom. Three of these are transversal movements along three orthogonal axes. The remaining three degrees of freedom are rotations around the three orthotropic directions.

The behavior of a joint has a significant effect on the structural performance of an assembly. By joining structural elements, unwanted motion and disassembly are prevented. The functionality of the joint decides how many degrees of freedom to restrict. To prevent disassembly, possible relative transversal movement between joint members must be restricted.

Based on the functionality of the joint, the permitted relative rotation between joining members classifies the joint. The ratio between the imposed bending moment and the resulting curvature of the joining members is defined as the moment stiffness. By its moment stiffness, the joint is classified as rigid, semi-rigid or simple. A rigid joint does not allow any relative rotation, and the joint is considered a continuous component. In contrast, a simple (pinned) joint has no rigidity against relative rotation and cannot transfer a moment. It works like a hinge. In real life, a joint is rarely completely rigid or simple. Most joints are semi-rigid. A semi-rigid joint allows certain

degree of rotation as well as provide some rigidity. Figure 1, shows the moment-curvature relation of a rigid, semi-rigid and simple joint.



FIGUR 1) MOMENT(M)-CURVATURE(Φ) RELATION.

2.3 MECHANICAL JOINTS

Mechanical joining

The function of mechanical joints is to transfer load from one structural component to another strictly through the development of purely mechanical forces arising from the interlocking and resulting interference of two or more components. The imposed loading of the interlocking members can be pure compression, tension, shear, bending, torsion or a complex combination of these loads. The mechanical joints are discontinuities, without any molecular or atomic binding, where all transfer of imposed load must be through normal contact pressure or friction. Contact pressure and friction between interlocking features are key aspects of mechanical joining.

Microscopic features naturally occur in the phenomenon of friction, through surface roughness, which is always yet to varying degrees present in material surfaces. Friction gives rise to transfer of shear stresses between bodies in contact. The frictional forces are proportional to the normal contact pressure. Normal contact pressure is transmitted normal stresses as the two surfaces are in contact.

The joint interlocks through geometric shapes that, in combination, interfere. These geometrical features are either external fasteners or integral attachments. Based on this observation, mechanical joining is divided into two subgroups: mechanical fastening and integral mechanical attachment. Mechanical fastening makes use of external devices such as screws, bolts, nails or pins. With integral mechanical attachments, the interlocking features are a part of the structural component's geometry.

Integral attachment joints

Compared to mechanical fasteners, integral attachment joints imply simpler motion for their insertion and engagement. Assembling mechanical fastening joints in complex structures requires intensive and skilled labor. This is less the case when it comes to integral mechanical attachment joints, which can easily be done by automatization. By this characteristic, integral attachment joints will be the type of joints further discussed in this thesis.

Integral attachment joints are connected through geometrical features, defined as integral attachment features. These are divided into “rigid attachment features”, “elastic attachment features” and “plastic attachment features” [4, pp.127]. A joint with elastic attachment features intentionally allows elastic deflection in desired direction(s). The plastic attachment features interlocks through plastic defamation and requires a ductile material. In contrast, a rigid attachment feature is expected to transfer load well within the elastic limit (yielding point of the material).

With rigid attachment features, two complementary joint members are engaged with simple motion in the same direction. The joint members interlock when engaged and carry load in desired directions, but different from the direction engaged. If the elastic limit of the material is exceeded, it will lead to failure of the joint (in plastic or brittle manner). The failure is often a result of crack propagation leading to a fracture mechanism of the interlocking feature (see chapter 5). [12]

Timber is a typical material for rigid interlocking integral attachment joints, which will be the key aspect for further investigation.

Structural design of integral attachment joints

Because of loading, structural elements are subjected to internal stress. The internal stress in the material, its stress state, decides the structural performance. Integral attachment joints are considered to be discontinuities and involve changes in cross-section areas and geometries. This leads to the accumulation of stress in so-called stress concentrations. In stress concentrations, stress levels are higher than in the rest of the material. For this reason, integral attachment joints are regarded as a critical part of the structure.

This illustrates the importance of careful integral attachment joint design. In the design process, the magnitude and complexity of forces that the joint should carry and transfer must be identified, along with the calculation of the resulting internal stress in the joint features.

3 IMPLEMENTATION OF JOINT DESIGN IN THE DIGITAL WORKFLOW OF PARAMETRIC STRUCTURAL DESIGN

In complex structures, joints are often relatively small but very important structural details in a greater structural assembly. The functionality of a structural joint is to interlock the structural elements into a configuration that serves the desired structural performance. Type of structure, materials, the imposed load, manufacturing tools and construction method are essential information that must be considered in the structural design of the joint. Hence, if the designing of the joints is implemented as part of the process of designing the global shape, and optimized accordingly, the joint can enable complex shapes instead of being a prescribed limitation.

Important features regarding the implementation of structural joint design in a digital workflow of parametric structural design will further be discussed in this chapter.

3.1 DESIGN AND PRODUCTION TOOLS

3.1.1 SOFTWARE

In this thesis, the following software will be implemented for geometric design of structural joints in addition to performance of structural analysis (FEA), optimization and investigation of potential form-finding methods. The selection of digital tools is based on software available to students at NTNU.

Rhinoceros 5.0

Rhinoceros (Rhino) is a CAD (computer-aided design) software which allows 3D modeling. The digital tool is created by Robert McNeel & Associates, who released Rhinoceros 5.0 in 2017. The three-dimensional geometry enables curves and freeform surfaces (arbitrary form not derived from any geometrical object) in computer graphics, which enables complex geometry modeling. Rhino provides a visual studio for geometries created in plug-in tools like Grasshopper. [26]

Grasshopper

The graphical algorithm editor Grasshopper (GH) was also developed by Robert McNeel & Associates[7]The software is a visual and intuitive method of scripting. As a plug-in tool, the geometry created in GH can be defined only by GH itself and visualised in Rhino or fetched

from Rhino and further parametrically controlled in GH. By being integrated in a parametric environment, the visual programming language enables parametric modeling. The graphical scripting in Grasshopper is done through embedded functional blocks, so-called “components”, which provide a diversity of actions. The components can receive inputs from other components by connecting them with visual “wires”. As previously mentioned, inputs can also be imported from geometries in Rhino. Grasshopper allows costume-made components, by allowing the designer to use programming languages like C# to create components performing desired actions.

To create a parametric geometry, GH offers adjustable “sliders”. A slider can be connected to one or more components. These components’ impact on the geometry can be parametrically changed by adjusting the connected slider. As the geometry adapts to the new configurations controlled by the slider, the graphical changes are visually simulated in the Rhino view port.

C Sharp

C Sharp (C#), is an object-oriented programming language developed by Microsoft, introduced in 2000. The language is based on the older programming languages C++ and Java [3]As an object-orientated language, C# combines data structures with C#-functions to create re-useable objects. The Grasshopper C#-component is an empty C#-script template. With the component, the designer can import data structures from GH, write a script with C# functions, and introduce the re-created objects as outputs. [3]

Abaqus/CAE

Abaqus/CAE (Complete Abaqus Environment) is a software tool that offers Finite Element Method (FEM) - analysis (FEA) of mechanical components and assemblies. It enables finite element modeling with further automatized numerical analysis (FEA) and visual post-processing of the FEA-results. The digital tool allows design with several types of finite elements such as solid-, shell-, beam- and truss finite elements. The geometry of the structural components analysed can be created in Abaqus/CAE or imported from a file. The Abaqus/CAE FEA results are visualized in its own viewport, which enables intuitive investigation and post-processing. With Microsoft Office Excel as a plug-in tool, data from analysis in Abaqus/CAE can be obtained and further processed. The procedure, from modeling to post-processing, in Abaqus/CAE is elaborated in chapter 5 [27]

Finite Element Method divides a system with complex behavior into several subsystems where the behavior is “known”. After assembling the system and applying boundary conditions, the result is a system of linear algebraic equations[2]. The division into subsystems is done through assigning the structural component a mesh of components, so-called finite elements. Choice of finite element type affects the structural behavior of the component. This will further be elaborated in chapter 5.2. In order to achieve a “known behavior” of the system, a mathematical model (finite element model) representing the component physical problem must be developed.

The structural behavior of the component is further described through a finite element analysis, which solves the linear algebraic equation represented by the finite element model.

The combination of Rhinoceros and Grasshopper offers a parametric model toolkit to create three-dimensional complex designs. To achieve a flexible digital workflow of parametric structural design, it requires the implementation of engineering software tools into the corporate toolkit. However, the plug-in tool performing structural analysis in the Rhino and GH environment, Karamba 3D (FEM-software), does not offer solid finite elements. In the work of this master thesis, it is assumed that solid elements are required to simulate the structural behavior of the joint components.

Thus, in this master thesis Abaqus/CAE will be used to perform structural analysis. Hence, the investigation of changes in the structural behavior of a joints as the interlocking geometry is parametrically changed, is limited by a simple selection of joint geometries. The joint geometries are parametrically modelled in GH and exported from Rhino to Abaqus/CAE as a SAT-file. A SAT-file can contain a three-dimensional model of pure geometrical information. This process requires a new creation of a finite element models (in Abaqus/CAE) for each parametric adjustment.

3.1.2 INDUSTRIAL ROBOTS

In this thesis, industrial robots are considered implemented in the digital workflow of parametric structural design, contributing with robot assembly and manufacturing of the assembly elements. These technologies make it possible to build structures in inaccessible or dangerous surroundings, as well as to build special architectural buildings with irregular shapes and complex constructions. [5]

3D printing

3D printing is the common term for creating three-dimensional objects by material manipulation under computer control. The process is done by adding material through joining or solidifying. In case of both rapid prototyping and additive manufacturing, 3D printing is an efficient technique of fabrication. Using 3D printing, objects of complex shapes and geometries can easily be produced from digital 3D model data. Use of 3D printing can easily be implemented in the digital workflow of parametric structural design. Industrial robots as fabricating systems can be used in the process of 3D printing.[5]

Industrial Robots

A robot is a machine capable of automatically carrying out a complex series of actions [28]

Industrial robot is a common term for all robot systems used for manufacturing. Robotic systems are automatically controlled, programmable and capable of movements on three or more axes.

Typical tasks performed by industrial robots, useful in construction, are welding, painting, pick and place, material handling, cutting and assembly. Simple, repetitive tasks as well as sophisticated manufacturing can be done with high endurance, speed and accuracy in challenging surroundings. Further advantages are a low noise level, flexible application and reduced production damage.[29]

The most common feature of industrial robots in construction is robotic arms. A robotic arm is a jointed mechanical arm, which is programmable with similar functions to a human arm. The mechanical arm with its joints allows linear translation displacement and rotational motion, controlled by computational programming. A device called end effector is attached to the end of the robot arm. The device interacts with the surroundings by holding and manipulating the tool performing the fabrication process. By special devices attached to the end effector, the geometry each structural element can be created. In robot assembly, the robot physically places the structural elements together in the correct configuration, through a prescribed assembly path.

A wide range of models provides industrial robots with different reach distance, payload capacity and number of axes of travel. The choice of robot model defines the machine constraints, hence the possibilities during fabrication of the structure.

Parametric robot control

The performance of industrial robots can be programmed and simulated in the digital parametric environment of the three-dimensional model that is to be manufactured. This is done through a digital plug-in tool, created by the robot producers.

This can be explained with KUKA PRC plug-in implemented in Grasshopper, representing KUKA-robots (KUKA is a company of robot supplement)[29]. With KUKA PRC in Grasshopper, a KUKA-robot is directly integrated in the parametric environment of Rhino and GH. The industrial robot performance can be controlled by function-blocks (like other GH components) or by custom scripted algorithms (like C# components).

As an important feature of the parametric robot control, the performance can be visually simulated inside the parametric model. With feedback from this visualization, the designer can quickly move between design and fabrication. The simulation of the robot performance gives the possibility to check for collisions, unreachable points or other fabrication mistakes, and further solve these problems by interacting with the parametric model. Fabrication becomes part of the design process. Together with other plug-in tools in the same parametric environment, the robotic performance code can be optimized. These software tools will not be elaborated in this thesis, but more information can be found in KUKA home page[29]

3.2 ADVANCES IN ARCHITECTURAL GEOMETRY (AAG) 2018

Advances in Architectural Geometry (AAG) is a biennial event started in 2008. In September 2018, it was held at Chalmers University of Technology in Gothenburg. AAG is a conference and workshop event, where new geometrical developments in architecture are presented in theoretical sessions and in practical workshops. The biennial includes architects, engineers, computer scientists, mathematicians, software and algorithms designers and contractors. AAG aims at “connecting researchers from architectural and engineering practices, academia and industry”[11], to develop the possibilities of architectural geometry by modern technology.

Geometry lies at the core of the architectural design process. It is omnipresent, from the initial form-finding stages, to novel manufacturing techniques, to the construction, and to post occupancy monitoring. But the role of geometry in architecture and engineering is also continuously evolving. Geometry increasingly plays a role in modelling environments and processing sensing information. Modern geometric computing provides a variety of tools for the efficient design, analysis, and manufacturing of complex shapes. Besides descriptive geometry controlling form, algorithmic processes play a crucial role in integrating disciplinary input. On the one hand this opens new horizons for architecture. On the other hand, the architectural context also poses new problems to geometry. Around these problems the research area of architectural geometry has emerged. It is located at the common border of architecture with applied geometry, computational design, mathematics, and manufacturing. [10]

Advances in Architectural Geometry deals with the core of conceptual design, which is the geometry. In conceptual design, everything in the design process, from structural performance to architectural shape, is considered in the geometry of the structure.

As part of researching for this master thesis, I attended the workshop *interlocking-based Robotic Fabrication of Segmented Shells: Formwork-free and mortar-free assembly* at the AAG event 2018. The workshop investigated the importance of geometrical shape, not just on a global scale, but in the joinery details of a structure. The AAG workshop investigation is based on complex continuous shell structures in compression only, divided into segmental blocks or plates.

The workshop demonstrates the advantages of interlocking strategy using robot assembly and computational design on shell elements. This involves working with parametric algorithms in Grasshopper, and robot fabrication experience with an industrial 6-axis robotic arm. The workshop includes fabricating prototypes of self-designed interlocking shell elements, using 3D printing technique, in an iterative manner... Workshop participants will develop their own digital robotic simulation code which will be tested physically on KUKA Agilus mobile robot. [11]

Briefly summarized, the workshop involved: form-finding of a shell structure, designing its interlocking segments, robot fabrication of these elements and final robotic assembly. The structural validation of the segmented shell was done through scaled down models of 3D printed prototypes further tested physically.

3.3 ADVANTAGES OF INTEGRAL ATTACHMENT JOINTS

The AAG workshop attended (see chap) introduced the implementation of designing the joints into a digital workflow of parametric structural design. This design approach challenges today's separation between design, element fabrication and final construction. The incorporation is enabled by the method of integral attachment joining.

Parametric modeling - Geometrical relations

With an integral attachment joint, the integral interlocking feature uniquely enables a geometrical relation between the joint and the shape of the structure. This geometrical relation can be defined through parametric modeling. In a parametric model, when a geometric change is done to a component by adjusting a parameter, the rest of the connected geometry will adapt to the new configuration. Using this method, the joint can be optimized to satisfy the desired global shape.

The incorporation facilitates complex shapes with structural efficiency. It also results in complex nonstandard elements with sophisticated interlockings, which may pose challenges to more traditional methods of manufacturing and construction. However, with integral attachment joints such challenges can be met by the use of industrial robots.

Fabrication and construction

Nonstandard integral attachment joint members can rapidly be produced and assembled by industrial robots, as its geometry and location (in assembly) is embedded in the global shape.

With the joinery concept of integral attachment joint design, the construction phase can be simplified by being formwork free. The instability during construction of an incomplete shell requires the utilisation of formwork which is labor intensive in construction, takes time and effort to be designed, and produces a large amount of waste material. Applying the design of the integral attachment feature, a stability without formwork can be achieved.

In addition to the possibility of a formwork free construction, the interlocking geometry concept enables metal fastener and adhesive free joinery. Joining methods using fasteners and adhesives increase the time of assembly and makes the construction more complicated. The joinery details of external fasteners do not have the same direct coherence with the geometry of the global

shape. In contrast, with pure geometrical interlocking elements the fabrication and global construction “information” lies within the shape of the global structure, without any extra need of detailing. This enables the use of industrial robots, which can gather fabrication data directly from the global model.

When external fasteners are used, the structural members are often made of standard elements, which can be a fabrication advantage. However, the global shape is limited by standard elements, and its structural performance highly affected by the joinery details. We want to be able to achieve the desired global shape without limitations beyond its own shape. In addition, using external fasteners or adhesives would require supplemental production of the external fastening elements. In case of complex shapes, the fasteners might require tailor-made design and production.

Architectural advantages

From an architectural point of view, in addition to enable complex shapes on a global level, the integral attachment joint itself can be considered aesthetically advantageous. A connection without any external fastener gives a smooth transition between structural elements, hence a clean look without any involvement of undesired materials due to structural performance.

3.4 REQUIREMENTS AND CONSTRAINTS

The integral attachment joint needs to fulfill several requirements to be incorporated in the digital workflow of parametric structural design. The design of the members needs to be interlocking with interfering members, possible to produce with robotic fabrication tools and it must allow robotic assembly. These requirements need to be considered and incorporated in the joint design.

Assembly logic

In use of robot assembly, certain challenges and limitations to the design of the integral attachment joint need to be considered. The geometry must allow the joint member to follow an “assembly path” and be placed in the correct configuration without being prevented by its own or other members geometry. It introduces a dilemma between the ability to interlock (prevent disassembling) and allow engagement. This challenge is only present with integral attachment joining. In contrast, interlocking by external fasteners, adhesives or chemical bonding can be applied after the interfering members are placed together in the correct configuration. However, by ensuring an assembly logic into the design of the interlocking geometry robot, assembly will be possible. This illustrates the importance of assembly simulations before real construction to be incorporated in the parametric model

Production constraints

Robotic manufacturing of the joint geometry also includes challenges and limitations, despite the many advantages. With an industrial robot, the manufacturing tools attached to the end effector decided the production constraints of the geometric design. An example of this is a hot wire cutter used at the AAG workshop. The tool was used to cut through Styrofoam as the wire is heated up. A wire can only cut ruled surfaces. A ruled surface can be described as the set of points swept by a moving straight line (the wire). [15]A cone is an example of a ruled surface, as it is formed by keeping one point of a line fixed whilst moving another point along a circle see Figure 5

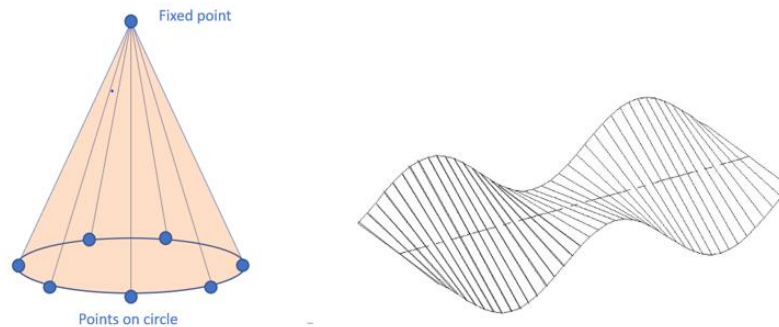


FIGURE 5 LEFT, A CONE REPRESENTING A RULED SURFACE. RIGHT, A RULED SURFACE OF AN ABSTRACT GEOMETRY [10]

Unit complexity

A complex assembly of nonstandard elements results in a unique interlocking design of each single structural member. It requires an automated process where an interlocking geometry design adapts to every joint configuration in the structural assembly while still maintaining its characteristics. The ability to interlock, robot assemble and be produced must be considered in the process of nonstandard adjustment of the interlocking geometry.

To fulfill the requirements discussed in this subchapter an interlocking strategy, as a set of principles (constraints), must be included in the design of the joints.

3.5 INTERLOCKING STRATEGY

To ensure interlocking, automatized production and robot assembly of nonstandard elements, a design method to fulfil these requirements in the interlocking geometry design must be developed. This will be further explained by the method of joint design performed at the Advances in Architectural Geometry (AAG) workshop, see Figure 6

At the AAG workshop (see chapter 3.2) an “interlocking strategy” was developed. This interlocking strategy is performed on a standard interlocking component, referred to as a base element. Together, these base elements interlock into a “base assembly”, an interlocking pattern of several base elements. The assembly can consist of one or several types of base elements.

The base element was designed in Grasshopper. By the technique of morphing, the base element is be transposed into the nonstandard elements which constitute the shape of the shell. The definition of morphing is *to gradually change, or change someone or something from one thing to another*[30]. With the “box morphed”-component in Grasshopper (see 3.1), a reference geometry is transposed into a target geometry in accordance with a prescribed relation between the two geometries.

The interlocking strategy performed on the base elements involves a set of geometric principles and constrains which ensure that the ability to interlock, assemble and be produced is provided. In addition, the interlocking strategy ensures that these characteristics are maintained in the transition to nonstandard element

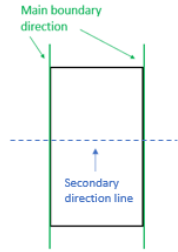
An interlocking strategy must be customized according to the functionality of the global assembly and the available robotic tools. The principles of the interlocking strategy developed at the AAG workshop will further be elaborated. The requirements at the AAG workshop was to design interlocking segments of a shell structure only working in compression, with a hot wire cutter as the manufacturing tool and a formwork and adhesive free robot assembly. The robot was a KUKA Agilus mobile robot, which is an industrial 6-axis robotic arm [29].

Within these constraints the interlocking segments designed at the AAG workshop must transfer compression force. Without adhesives or formwork, the interlocking geometry also needs to restrict relative shear movements between segments during construction. In addition, the available production tool requires a ruled interlocking surface design (see chapter 3.4). The digital workflow of parametric joint design, involving an interlocking strategy we developed as workshop contestants, is described in ten steps, see Figure 6



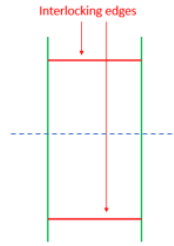
1. Base element

As base element, a rectangular 2D element was created.



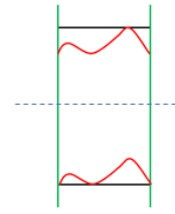
2. Main direction

The element was given “main boundary direction lines”, and a “secondary direction line”. To make sure that the nonstandard (morphed) elements are not hindered from its assembly path, the interlocking pattern cannot cross the main boundary lines.



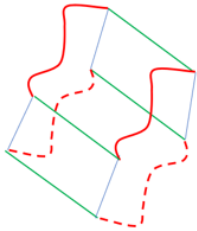
3. Interlocking edges

The elements interlocking edges, are between the main boundary lines. One on the top and one on the bottom, separated by the secondary line. Each line represent a interactive interlocking area with adjacent elements.



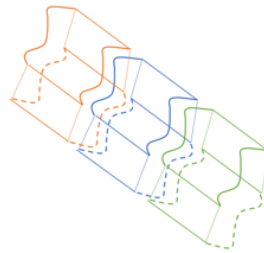
4. Interlocking geometry

The interlocking geometry is created, inside the base element geometry and between the main boundary direction lines. The bottom and top geometry are identical. Create a curvature which will restrict shear movement between adjacent elements.



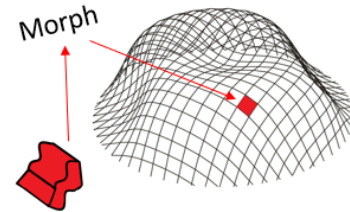
5. Base interlocking segment

The plane geometry in step four is offset in perpendicular direction to the rectangular plane, and rotated in-plane 180 degrees. Then the solid segment is created by lofting between the two surfaces. Lofting makes it possible to cut with a hotwire cutter. Rotation creates geometrical interlocking components that restrict shear movement between segments.



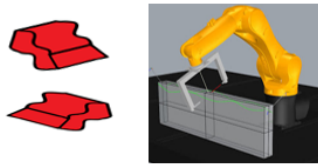
6. Interlocking base pattern

Identical segments of the same base geometry created in step five will fit together in an interlocking pattern. With rectangles and only one type of base elements the segment will only interlock in one direction. More sophisticated interlocking can be achieved with a hexagonal base elements of two types.



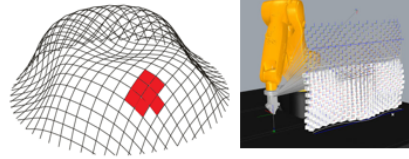
7. Box Morph

The “Box Morph” component in Grasshopper will “Morph an object into a twisted box”. With the base geometry (base interlocking segment, step 5), reference box (base rectangular geometry, step 1) and target box (deformed rectangle element in 3D shell grid) as inputs. The output is the translated geometry (nonstandard element).



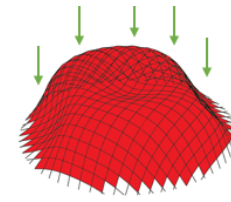
8. Fabrication simulation

With KUKA PRC, provides simulation of cutting each nonstandard segment with a hotwire cutter. With this visualization, the morphed nonstandard elements production can be validated. If not, retrieve to step four.



9. Assembly simulation

With KUKA PRC the assembly is simulated, and investigated. If not possible, retrieve to step four.



10. Structural validation

Structural validation through testing 3D printed prototype (small scale). Not verified, return to step four.

FIGURE 6) THE DIGITAL WORKFLOW OF PARAMETRIC JOINT DESIGN DEVELOPED AT THE AAG WORKSHOP 2018.

4 WOOD

Any components to be joined consist of a material. Some joined products are natural elements that fit together, but in most cases, joining involves components, hence material manipulation. In order for joint and joining to be possible and successful, investigation and knowledge of the material involved and of its properties are crucial. [14]

In the investigation of integral attachment joints, solid timber is considered as the appropriate material. As discussed in chapter 3, rigid interlocks (integral attachment joints) were considered a suitable integral attachment type for robot assembly. Solid timber will be used as the structural material further investigated.

4.1 TIMBER CONNECTION DESIGN

There are three primary types of traditional joinery in timber structures. These joinery methods are glued connections, mechanical fasteners (see chap. 3), and integral attachments joinery (see chap. 3). Glued connection uses an adhesive supplemental material to create fastening between joining members. These are typically structural finger joints or glued in steel ring connections [31] see Figure 7

In civil engineering, standards are frequently used in design to ensure structural stability. In Norway, Eurocode is commonly adopted in structural design both regarding materials and loads.

Eurocode 5 covers design of timber structures, including connections design with metal fasteners. As a result, metal fasteners is a common method of joinery in timber structures. Metal fasteners in timber connection design as elaborated in Eurocode 5 are nails, staples, punch metal plates, screws, dowels, bolts as well as shear plates and split rings. [31]

Structural design of glued connections and integral attachment joints are not included in the Eurocode. Guidelines for structural design of these joint methods are usually given by the manufacturing companies, producing the joint members.

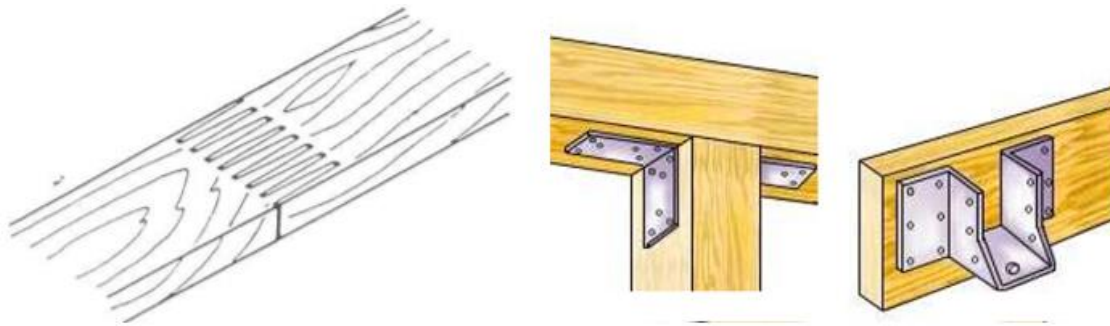


FIGURE 7 LEFT, FINGER JOINTS. RIGHT, METAL FASTENERS. (KILDE)

Wood is a suitable material for integral mechanical joints, as the desired geometry is easy and cheap to cut from the material. However, calculation of the load-carrying capability of fasteners is far more manageable than wood-to-wood joints. Extensive analysis and comprehensive tables of load-bearing capacity have been compiled by manufactures of metal fasteners and are invaluable resources to engineers, architects, and planners. Comparable tables, not to mention comparable analyses, for wood-to-wood joinery methods simply do not exist and would be prohibitively time-consuming and expensive to generate today. In the past, such wood-to-wood joints developed with experience and success, and any design and analysis were largely, if not exclusively, empirical in nature. [14]

By creating a form-finding method for integral attachment joints, the joinery method can be frequently used in common civil engineering design. However, it requires a careful understanding of the material characteristics.

4.2 CHARACTERISTICS OF WOOD

Wood is a unique material, the most sustainable resource in the construction industry. The reason for its sustainability is its renewable nature and the natural process of manufacturing from growing trees. Wood has a relatively low density compared to its strength, which makes it a preferable structural material in many projects. From an aesthetic point of view, the material is often favourably considered, given its natural colours, variation and texture.

Solid- and Engineering timber

The structural material comes from the trunk of a tree, of various species. Different species have different structural and aesthetic properties. In the industry of structural timber, there are solid timber and engineering wood products. Solid timber is lumber cut directly from the length of the tree, with its knots and imperfections, while engineering timber products are processed. Processing is done to overcome shortcomings inherent in the natural imperfections, size and strength of solid timber. Laminated timber and structural composite lumber are examples of engineering products. [9]

Anisotropic material

As a natural polymeric composite, wood is a complex anisotropic material. The anisotropy means that the material property varies according to the directions in the material, which has great impact on the structural behavior. The anisotropy of solid timber can be simplified and idealized as orthotropy. An orthotropic material has material properties in three orthogonal directions, as described by a three-dimensional coordinate system.[9]

Structure

In the cross section of a tree trunk (Figure xxx), the structure and its features illustrate the complexity and the reason behind its structural behavior. These features are, as seen from the surface of the trunk towards its center: outer bark, inner bark, cambium, sapwood, heartwood and pith.

Outer bark is dead tissue which protects the tree from unwanted bacteria, fungus and insects. In contrast, the inner bark is a living tissue, which contributes to the transportation of water and nutrition in the tree. The cambium is a thin layer of cells that forms new bark and new wood cells. These cells are created in growth periods. During a single growth period, a *growth ring* is created. This makes up the “ring” structure observed in the cross section. Wood cells from the cambium give rise to the light-colored layer of sapwood. Sapwood consists of active living cells, which contribute to the transportation of water and nutrition from the roots to the crown of the tree. The darker layer closer to the core is heartwood, which consists of dead, compressed wood cells from earlier sapwood. The heartwood provides structural strength to the trunk of the tree, as

well as storage of energy reserve. The pith is the core of the tree trunk, which also participates in the transport and storage of nutrition.

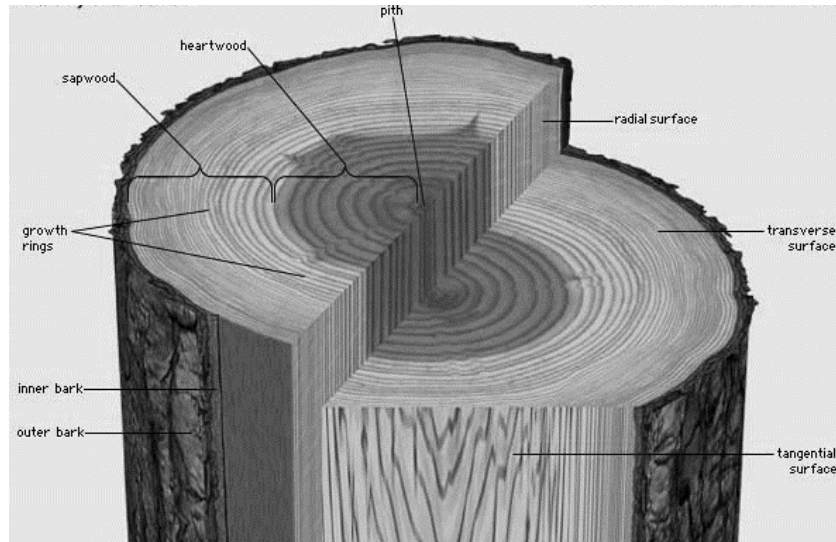


FIGURE 8) GENERAL CROSS SECTION OF A TREE THRUNK, WITH STRCUTRAL FEATURES MARKED ACCORDAGLY. [32]

Softwood and hardwood

But there is more than this to the complexity of wood as a material. On a microscopic level, the configuration and fibrous structure of wood cells are the main reason for the direction dependent behavior of wood. There are different cell types depending on the species, and on their location and function in the structure. Tree species are classified as either softwood or hardwood. Softwood are cone bearing trees from naked seeds. Typically pine and spruce. They often have a quick growth rate, and relatively low density and strength. Hardwood trees generally have broad leaves, which they shed at the end of each growth season. They grow more slowly than softwood and have higher density and strength. Thus, hardwood is generally more expensive than softwood.[9]

Wood cells

The material is a natural polymer, made of cells like other plants. The cells consist of three substances: cellulose, lignin and hemicellulose. Cellulose is a polysaccharide, which is the important structural component of the cell walls. Wood, in general, consists of parallel strands of cellulose fiberfibers held together by the adhesive substance lignin.[9]

Softwood and heartwood contain slightly different cells. Further investigation in this master thesis is based on Norwegian spruce, which is classified as a softwood. As a softwood, Norwegian spruce contains tracheid and parenchyma cells. About 90 % of the wood volume consists of vertical tracheid cells [28]. These cells are typically 100 times longer than they are

wide, with their longitudinal axis parallel with the longitudinal direction of the tree trunk. In the radial direction of the growth rings, you find horizontal shorter tracheid cells, called ray cells. Both cell types provide transport and structural support in their longitudinal direction. Parenchyma cells are another, less common, cell present in softwood, both in radial and axial directions. The main function of these relatively small prismatic shaped cells is storage. The vertical tracheid cell will from now on be referred to as fiber.

Orthotropic mechanical properties

The fibers define the orientation of the orthotropic directions in the wooden member. They are lined up as thousands of straws packed and glued together by the adhesive substance lignin, orientated in parallel with the length of the tree. Each straw is weak but glued together the material becomes much stronger.

When tensile stress perpendicular to the fiber reaches the strength limit, lignin bonds will break. This causes splitting in parallel with the fibers. Relatively weak lignin bonds explain a low strength against tensile stress perpendicular to the fibers. This also results in low strength against shear stresses on a plane parallel with the fibers. Breaking across the fibers requires snapping of cellulose fibers. This can be triggered by tensile stress in the direction parallel with the fibers, which requires a much higher level of stress.

Subjected to high enough compressive stress parallel with the fibers, the fibers will buckle. The packed and glued fibers causes relatively high strength against buckling. The shear strength stresses perpendicular to the fibers is determined by tearing of the cellulose fibers. When the thin-walled wood cells are subjected to compressive stress perpendicular to the fibers, the cell-wall easily collapse. From this, the material axial strength perpendicular to the fibers in a wooden member is of an appreciably lower level than the strength parallel with the fibers. [9]

Until now, only two of the three orthogonal directions have been discussed (perpendicular and parallel to the fibers). The perpendicular direction of the fibers in a wood member represents a plane of two orthotropic directions: tangential and radial to the growth rings. Accordingly, the orthogonal directions in a wooden member is described by a longitudinal (parallel with the fibers), radial (perpendicular with the fibers) and tangential (perpendicular with the fibers) direction, see Figure 9. The difference in tangential and radial mechanical properties is not considered in further investigations of this thesis. The “perpendicular properties” will represent both directions.

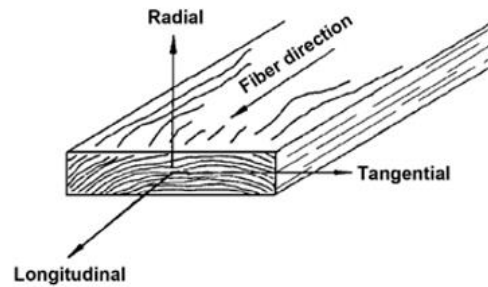


FIGURE 9) ORTHOTROPIC DIRECTION OF TIMBER. LONGITUDINAL, RADIAL AND TANGENTIAL DIRECTION [32]

Discontinuities and natural variation

As it is a natural material, there is little production control of a solid timber component. A solid timber component contains knots, imperfections and other discontinuities, which all affect its structural behavior. Moisture content, temperatures and environmental effects are also highly relevant to its performance. However, the variation in structural behavior due to the complex interplay of these factors are a research area in itself. Thus, the timber material further investigated in this thesis is assumed to be without any special defects, with a temperature of 20 degrees Celsius and 65 % relative humidity[9].

4.3 EUROCODE

In subchapter 4.1, Eurocode 5 was introduced as the frequently-used Standard for design of timber structures. The design of timber joints further investigated in this thesis will not be based on joint methods described by the Eurocode.

However, the type of structural analysis is done in accordance with recommendations in the Standard. Hence, because of the brittle nature of timber under tension-induced stress configurations, a plastic analysis should not be used, and EC5 requires that the forces in the elements of structure to be determined by a linear static analysis [33]

In addition, the properties of the material analyzed, represented by mean characteristic values, are found in Eurocode 5. See Table 1) Characteristic strength properties of solid timber, softwood class C24 [34] (chapter 5)

5 STRUCTURAL ANALYSIS OF MECHANICAL TIMBER JOINTS

In this chapter an investigation of integral mechanical attachment timber joints, discussed in Chapter 3, will be performed using Abaqus/CAE (chapter 3.1). The investigation requires the analysis of their structural behavior, to create a potential form-finding method adapted to this type of mechanical joint. The aim is to observe important features of the integral attachment timber joints and to understand their structural limitations. To detect the structural behavior of integral attachment timber joints, the investigations are based on simple joint configurations subjected to simple load conditions.

Further, in Chapter 5 two joint configurations are investigated, one subjected to pure tension force and another subjected to pure compression force. The interlocking geometry of the joints are designed parametrical. This is done to observe changes in their structural performance due to changes in their interlocking geometry.

The integral attachment timber joint investigated in this chapter is not chosen based on structural efficiency. Intuitively, the designs might seem unreasonable. Structural shortcomings are considered important information to develop a potential form-finding method. Final capacity calculation for these exact joints will not be considered necessary.

C24 – Softwood – Norwegian spruce

The material used in further investigation is solid timber of Norwegian spruce softwood strength class C24[30]. The characteristic strength properties from the choice of material are of great importance in the investigation and are provided in Table 1) Characteristic strength properties of solid timber, softwood class C24 [34]

TABLE 1) CHARACTERISTIC STRENGTH PROPERTIES OF SOLID TIMBER, SOFTWOOD CLASS C24 [34]

Characteristic strength properties	Value [MPa]
$f_{t, 0, k}$ = Tension strength parallel to the grains	14
$f_{t, 90, k}$ = Tension strength perpendicular to the grains	0.4
$f_{v, k}$ = Shear strength	4
$f_{c, 0, k}$ = Compression strength perpendicular to the grains	21
$f_{c, 90, k}$ =Compression strength perpendicular to the grains	2,5

5.1 JOINT - TENSION

The first integral mechanical attachment timber joint investigated is a configuration of two adjacent interlocking joint members subjected to pure tensile force. A simple three-dimensional solid model of the joint geometry is created in Grasshopper, with a parametric interlocking geometry controlled by sliders (chapter 3.1). Rhino is used as a visual environment for the Grasshopper model (Figure 10) Left in the picture the three-dimensional solid model visualized in Rhino is illustrated both from a front- and perspective view. To the right an overview of the GH-components creating the model is shown.

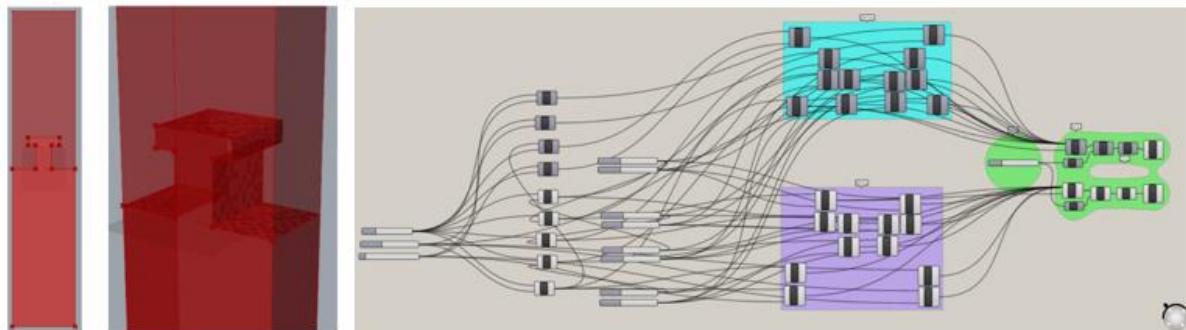
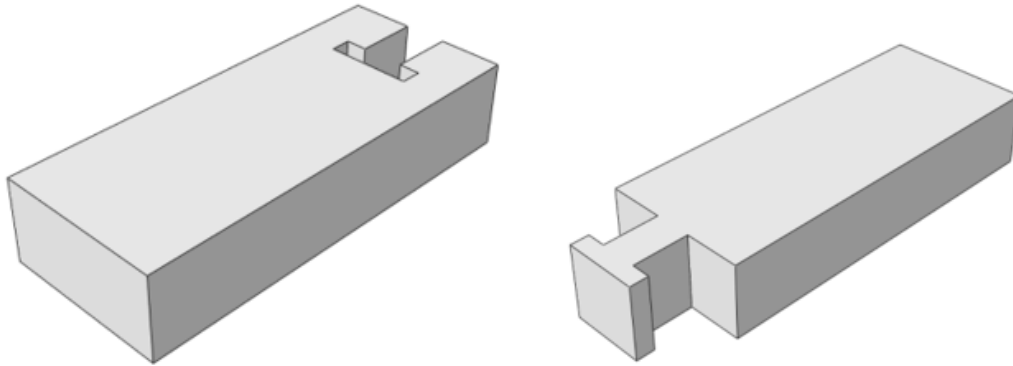


FIGURE 10) LEFT IN THE PICTURE THE THREE-DIMENSIONAL SOLID MODEL VISUALIZED IN RHINO IS ILLUSTRATED BOTH FROM A FRONT- AND PERSPECTIVE VIEW. TO THE RIGHT AN OVERVIEW OF THE GH-COMPONENTS CREATING THE MODEL IS SHOWN.

Tenon and Mortise

Figure 11 shows the joint design concept which will be investigated in this subchapter. The joint design is based on the traditional *mortise and tenon-joint*. [16] This traditional joint consists of two joint members, a mortise and a tenon. The tenon is a timber joint member with a protruding integral interlocking geometry that fits into the interlocking geometry of a mortise. The specific design of the tenon and mortise is made as simple as possible to evaluate the structural behavior as a result of parametrical changes of the interlocking geometry.



**FIGURE 11) TENON AND MORTISE DESIGN FOR INVESTIGATION OF INTEGRAL ATTACHMENT TIMBER JOINTS
SUBJECTED TO TENSION**

Parameters considered

The integral attachment feature of the tenon is illustrated in Figure 11. The interlocking surface interfering with the mortise is defined by three parameters: height (h), width (w) and length (l). In further parametric investigation, these parameters are changed separately, giving 18 different geometries, see Table 2) In the tables above, 18 geometries which will be investigated, are displayed with their interlocking width-, length- and height variables. The rest of the variables defining the geometry of the joint are fixed. The dimensions of the joint members' cross-section are a height of 100 millimeters (mm) and width of 200 millimeters (mm).

The reason for choosing these parameters as parametric variables is because they define the geometry of the integral attachment feature of the tenon and mortise. Integral attachment features are the components which ensure the interlocking functionality of the joint. In addition, the parameters are easy to model parametrically. Thus, a simple investigation of the structural behavior due to geometrical changes of the interlocking geometry can be done.

TABLE 2) IN THE TABLES ABOVE, 18 GEOMETRIES WHICH WILL BE INVESTIGATED, ARE DISPLAYED WITH THEIR INTERLOCKING WIDTH-, LENGTH- AND HEIGHT VARIABLES

Changes of width:

Geometry	Width (mm)	Length (mm)	Height (mm)
1	10	25	75
2	15	25	75
3	20	25	75
4	25	25	75
5	30	25	75
6	35	25	75

Change of length

Geometry	Length (mm)	Height (mm)	Width (mm)
7	10	75	25
8	15	75	25
9	20	75	25
10	25	75	25
11	30	75	25
12	35	75	25

Change of height

Geometry	Height (mm)	Length (mm)	Width (mm)
13	50	25	25
14	75	25	25
15	100	25	25
16	125	25	25
17	140	25	25
18	160	25	25

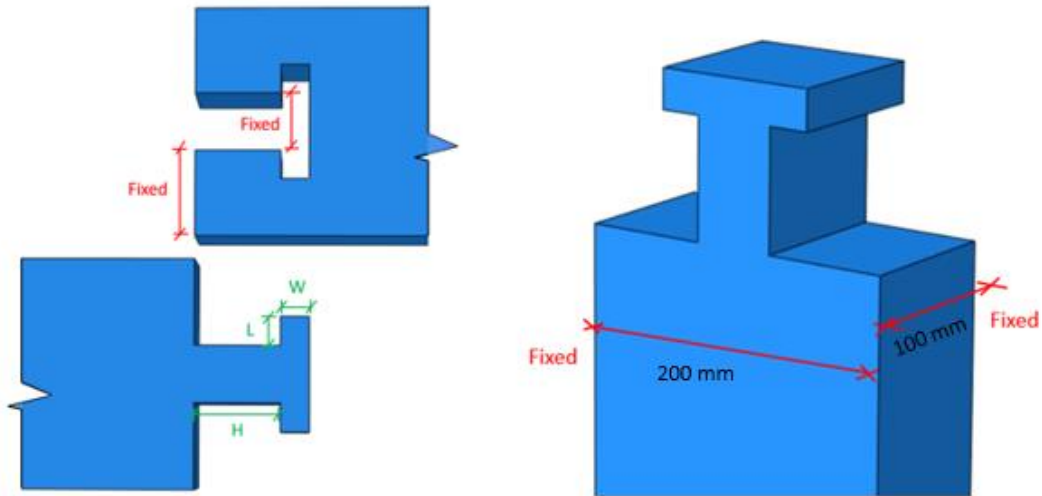


FIGURE 12) TO THE LEFT IN THE FIGURE, THE PARAMETERS CONTROLLING THE INTERLOCKING GEOMETRY OF THE TENON IS ILLUSTRATED IN GREEN CAPITAL LETTERS (H, L, W).

Nomenclature

The report, investigation and discussion of the mortise and tension joint in chapter 5.1 will refer to the nomenclature in Figure 13) Nomenclature used in chapter 2. As the mortise geometry is the inverted geometry of the tenon, further descriptions will be based on the tenon member.

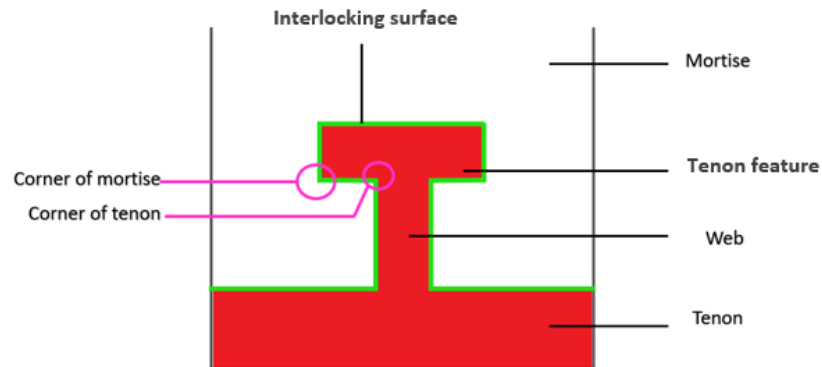


FIGURE 13) NOMENCLATURE USED IN CHAPTER 2

Active area

In considerations of the joint, the most important thing is to observe and understand the way of transferring force from one member to another. Before any structural analysis is performed, the phenomena are intuitively considered. As a result, the tension force is assumed to be transferred via the connection area called “active area” through contact pressure, illustrated in Figure 14

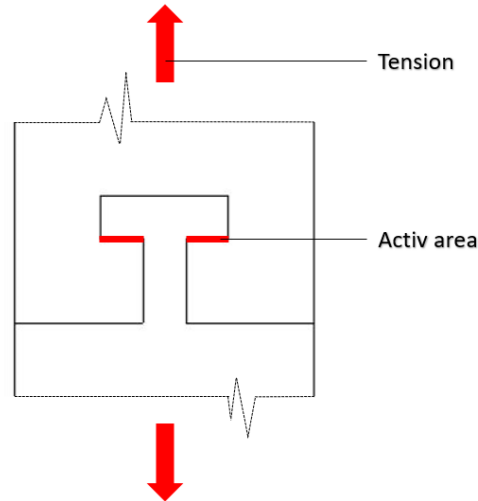


FIGURE 14) THE “ACTIVE AREA” DISTRIBUTING THE STRESS BETWEEN THE MORTISE AND THE TENDON IS THE RED AREA SHOWN IN

5.1.1 THE BASIC ANALYSIS

Before the parametric part of the analysis, a basic analysis is carried out on a basic interlocking geometry of the tenon and mortise. The basic interlocking geometry is defined by the parameters of length(l): 25 mm, height(h): 75 mm and width(w): 25 mm. Through that analysis, information on pre- and post-processing for further parametric study is obtained and discussed.

Abaqus analysis

The solid joint model created in Grasshopper is *baked* into Rhino (See webpage of Rhinoceros[35]). This enables the geometry to be exported as SAT file (file which holds 3D geometries) to Abaqus/CAE. Hence, the imported solid geometry in Abaqus/CAE is a pure geometrical model.

In Abaqus/CAE, the imported geometry is made into a finite element model (FEM). The joint geometry members are imported as two independent geometries. This is done to create independent instances of each joint member, with defined interaction properties between the members in the joint assembly

ADDIN ZOTERO_ITEM CSL_CITATION {"citationID":"x8G4bQvK","properties":{"formattedCitation":"[4]","plainCitation":"[4]","noteIndex":0},"citationItems":[{"id":130,"uris":["http://zotero.org/users/local/gQ6k7A9l/items/AI6HEKDS"],"uri":["http://zotero.org/users/local/gQ6k7A9l/items/AI6HEKDS"],"itemData":{"id":130,"type":"article-journal","title":"Mechanical properties of clear wood from Norway spruce","page":"140","source":"Zotero","language":"en","author":[{"family":"Dahl","given":"Kr

istian Berbom"]} } } }], "schema": "https://github.com/citation-style-language/schema/raw/master/csl-citation.json" } [4](Annex A). Further, a static linear elastic finite element analysis is performed to evaluate the structural performance of the joint.

To create a finite element model in Abaqus/CAE that will simulate the actual physical behavior of the joint, input data describing the geometry, material properties, loads, and boundary need to be defined.

5.1.1.1 PRE-PROCESSING – FINITE ELEMENT MODEL

The pre-processing stage of the basic analysis, where the finite element model is created, is described in given in Appendix A.

Finite element model considerations

The choice of finite element model and analysis in Abaqus/CAE have great impact on the simulated results. These results are used to describe the structural behavior of the joint. Thus, the choice of modeling must be considered carefully. Before any results are obtained and used in the investigation of the structural behavior, the finite element model (see Appendix) is considered.

Thus, following features are discussed:

- Material model
- Section properties
- Mesh and elements
- Analysis type
- Interaction properties
- Load simulation
- Output request

- **Material model**

To perform a finite element analysis, a material model describing the object's behavior is crucial. As the analysis performed is elastic analysis, the material of the structural joint needs to be described by elastic material properties. In Abaqus/CAE a linear elastic material model can be isotropic, orthotropic or fully anisotropic depending on the material to be analysed.

In chapter 4, the anisotropic nature of wood is described. Thus, the structural performance of the tenon and mortise is determined by the anisotropic behavior of solid timber. Figure 15 illustrate the orientation of the wood fibers in the tenon. The orthotropic simplification is describing the

timber member by a longitudinal, radial and tangential direction. The definitions of these directions, with corresponding identification in Abaqus/CAE, are displayed in table 3.

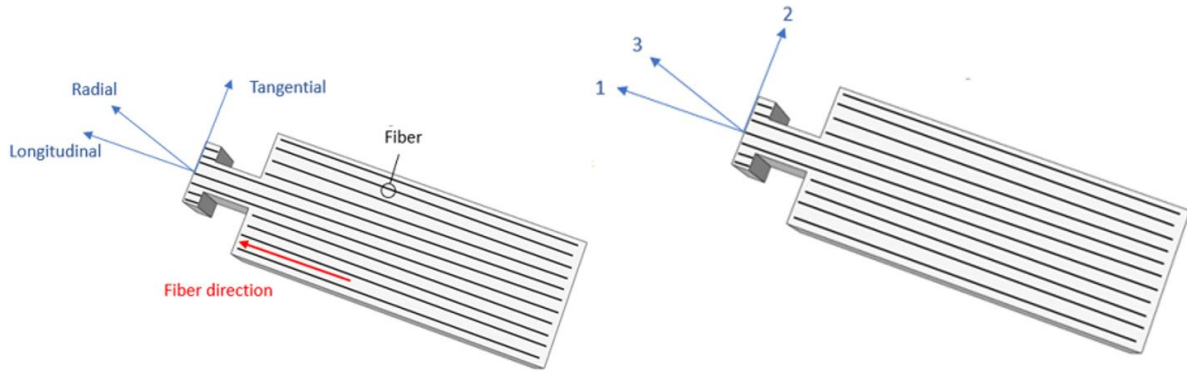


FIGURE 15) (TO THE LEFT, THE TENON IS ILLUSTRATED WITH ITS FIBERS AND ORTHOTROPIC DIRECTION CONFIGURATION. TO THE RIGHT, CORRESPONDING IDENTIFICATION IN ABAQUS/CAE IS DISPLAYED

TABLE 3) DEFINITION OF ORTHOTROPIC DIRECTING-MODELING IN ABAQUS/CAE

Axis in Abaqus/CAE	Explanation
1	Longitudinal direction of the member, parallel with wood fibers
2	Transverse direction of member, perpendicular to wood fibers and tangential to growth rings
3	Radial direction of member, perpendicular to fibers and radial to growth rings

- **Engineering constants – Norwegian spruce**

To simulate the orthotropic behavior, the geometries need to be assigned the material properties representing each direction. This is done through defining nine independent *engineering constants* when the material description is created in Abaqus/CAE. The engineering constants

are physically measured characterizations of the elastic behavior obtained by empirical studies of the given material.[4]

These nine material properties are three elastic modulus (E), three shear modulus (G) and three Poisson's ratios (ν). Further definitions of these material constant can be found in [27]The engineering constants of Norwegian spruce used in this Abaqus/CAE analysis is presented in Table 4, with corresponding definition and labeling of the material properties.

TABLE 4) ENGINEERING CONSTANT OF NORWEGIAN SPRUCE WITH ASSIGNED DIRECTION AND DEFINITION IN ABAQUS/CAE[4]

Engineering constants	Explanation	Norwegian spruce
E1	Modulus of elasticity in direction 1.	10991
E2	Modulus of elasticity in direction 2.	716
E3	Modulus of elasticity in direction 3.	435
G12	Shear modulus, shear stress acting in direction 1 on a plane with normal in direction 2.	0.42
G13	Shear modulus, shear stress acting in 1 direction on a plane with normal in direction 3.	0.48
G23	Shear modulus (Rolling shear modulus), shear stress acting in 2 direction on a plane with normal in direction 3.	0.5
Nu12	Poisson's ratio, when acting axial stress in direction 1 giving lateral deformation in direction 2.	682
Nu13	Poisson's ratio, when acting axial stress in direction 1 giving lateral deformation in direction 3.	693
Nu23	Poisson's ratio, when acting axial stress in direction 2 giving lateral deformation in direction 3.	49

- **Solid homogeneous section**

When the joint members are defined as a *solid, homogeneous* sections in Abaqus/CAE, the geometries are assigned the solid state of matter[36]. As for the description of homogeneity, the section is set to be composed with the same material regardless of location along its body [37].There is no such thing as a completely homogeneous solid section in reality, but this is an adequate simplification for analysis in Abaqus/CAE.

- **Mesh and choice of elements**

The meshing of the basic geometry finite element model (Appendix A) is performed by structured meshing technique, which generates structured meshing using simple predefined mesh geometry. Abaqus/CAE transforms a mesh of a regular shaped region onto a chosen region on the geometry of the component which is analysed. In this case a three-dimensional mesh with hexagonal finite elements is applied onto the tenon and mortise.

Global and local seed size

The size of the hexagonal finite elements is of great importance. As the finite elements are smaller, the analysis becomes more accurate. A denser mesh means more degrees of freedom[2] (see chapter 3.2) hence increased computational cost. The size of the elements in Abaqus/CAE are given by globally or locally seed size. [36]Global seed size[36] defines the approximate element size for all edges of the analysed component. If one wishes the mesh to be denser at specific locations, a local seed size with desired value can be applied to the edges surrounding this location. [2]

Typically, the local seed size is applied where the results are of more interest (on the component analysed). In the analysis of the basic geometry this location is not known at this stage, thus all the components in the assembly are applied with a global seed sized mesh of 5 mm.

Element type - C3D8R

By default, Abaqus/CAE uses a mesh of C3D8R- finite element in the basic analysis. A C3D8R- finite element is an eight-node solid hexahedral linear finite element with reduced integration[2]. The integration point is located in the geometric center of the finite element, Figure 16. It is important to be aware of the behavior and shortcomings when using the C3D8R. If the shortcomings are taken into account, good quality results with high accuracy can be achieved.

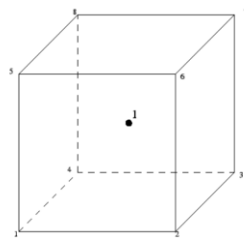


FIGURE 16) C3D8R- FINITE ELEMENT

To capture accurate stress and strain values close to the boundary of a structural component with C3D8R- finite element, it is important to use small finite elements, as the most accurate values are at the integration point inside the finite element. As the size of the finite element decreases, the accurate integration point comes closer to the boundary.

With only one integration point, the reduced integration saves computer costs. The disadvantage of reduced integration is that it can result in hour-glassing(deformation error)[36]. By default,

Abaqus/CAE takes care of this problem by *hour-glass control*. However, even though hour-glass control is used, the finite elements should be used with a reasonably fine mesh.

A mesh with hexahedral elements is more sensitive to distortion compared with a mesh of tetrahedral solid elements. Geometrical distortion of the finite elements reduces the accuracy of the results. If the result of interest is located where the mesh is distorted, reduced accuracy needs to be considered. In areas where finite elements are distorted, the mesh can be improved by partitioning the geometry into appropriate cells or reduce the local finite element size. The simple geometry of the tenon and mortise does not give significant finite element distortion.

Another character of the C3D8R-finite element is that the finite element tends not to be stiff enough in bending[2]. As the joint is subjected to pure tension, this limitation is not considered to be of great importance.

- **Analysis**

The numerical analysis done by Abaqus is defined in the analysis step. The problem is defined as static and linear elastic in Abaqus/CAE, and with the embedded default setting, it is assumed to be appropriate in this investigation.

- **Contact area**

As discussed in previous chapter, the main purpose of the joint is to transfer the flow of forces from one member to another distributing the stress to rest of the structure and into the ground. Thus, the contact area, active area and choice of modeling has great impact on the behavior of the joint.

Master and slave surface

When two surfaces are interacting between disconnected objects, the character of each surface needs to be defined. In Abaqus/CAE, a master- slave approach assigns each surface in contact a “role”. One surface is assigned a master-role and the other a slave-role. In interaction, the master-surface can only penetrate the slave-surface, and not opposite[36]. Abaqus/CAE requires the user to decide which surface is to be master and which is the slave. The role decision is based on difference in material, size, stiffness and mesh density between the objects in contact. Thus, in this investigation of the mortise and tenon interaction this is not considered to affect the result.

Interaction properties

The interaction properties of the surfaces on the tenon and mortise in contact are modelled as frictionless tangential behavior, and “hard” contact pressure as normal behavior[36]. With frictionless tangential behavior, there will be no transport of shear stresses between the interacting surfaces. They are free to slide relative to each other. Hard contact pressures imply that tensile stresses cannot be transferred between the contact surfaces. In addition, the

penetration between master and slave surfaces is minimized. [36] This means that if the surfaces are in contact, any contact pressure can be transmitted. As the pressure is reduced to zero, the surfaces will separate.

The finite element models created in this master thesis is assumed not to simulate the real interaction between the joint members. However, it is assumed to be a simplification accurate enough for the purpose of this investigations. In future design of integral attachment timber joints, a sophisticated contact behavior model should be developed.

- **Load simulation**

To simulate the tenon and mortise joint configuration subjected to pure tension, the applied load is modelled as negative pressure on the boundary surfaces. The magnitude of the load in the basic analysis is 0.5 megapascal (MPa).

- **Output request: Stress tensor components**

Before the finite element analysis is performed by Abaqus/CAE, the FEA-results of interest are specified through *output request*. In the investigation of the joint the result of interest from the Abaqus/CAE analysis are the stress tensor components of a solid finite element (variables S11, S22, S33, S12, S13, S23). The stress tensor components are the nodal stresses calculated by the finite element method (automatic numerical analysis of the FEM-model in Abaqus/CAE), represent the internal stresses in the structural object analysed. The components refer to the orthogonal directions assigned the component analysed (in Abaqus/CAE, see Appendix A), and are defined in Table 1 and illustrated in Figure 17

The stress tensor components are automatically calculated from the integration point of the finite elements. In the Abaqus/CAE computation process the calculations done at the integration points are extrapolated [2] to the nodes. Each node receives extrapolated values from all contributing finite elements. The nodes receiving values from several finite elements are averaged. Contour plots of these stress tensor components are visualized in Abaqus/Viewer [36]

TABLE 5) TENSOR STRESS COMPONENTS RESULTS.

Tensor stress component	Definition (by choice of modeling)
S11 +	Nodal stress tensor components, positive value, tensile stress in direction 1.
S11-	Nodal stress tensor components, negative value, compression stress in direction 1.
S22+	Nodal stress tensor components, positive value, tension stress in direction 2.
S22-	Nodal stress tensor components, positive value, compression stress in direction 2.
S33+	Nodal stress tensor components, positive value, tension stress in direction 3.
S33-	Nodal stress tensor components, positive value, compression stress in direction 3.
S12	Nodal stress tensor components, shear stress acting in direction 1 on a plane with normal in direction 2.
S13	Nodal stress tensor components, shear stress acting in 1 direction on a plane with normal in direction 3.
S23	Nodal stress tensor components, shear stress acting in 2 direction on a plane with normal in direction 3.

“+” indicates tension stress and “-” indicates compression stress

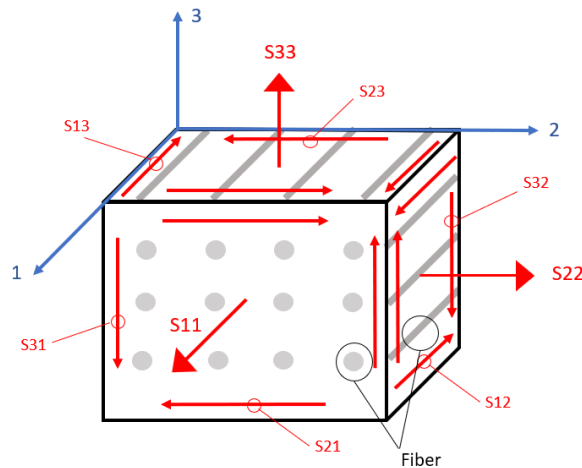


FIGURE 17) THE ORIENTATION OF THE STRESS TENSOR COMPONENTS IS VISUALIZED ON AN INFINITESIMALLY SMALL ELEMENT ACCORDING TO THE ORIENTATION OF THE FIBERS (IN GREY).

5.1.1.2 FINITE ELEMENT METHOD ANALYSIS

The finite element method model created is further submitted for automatically finite element analysis in Abaqus/CAE.

5.1.1.3 POST-PROCESSING

From pre-processing, we are examining the stress tensor components (S11, S22, S33, S12, S13, S23) obtained from the Finite Element Method in Abaqus/CAE.

Stress tensor components – utilization

To evaluate the structural behavior of the joint, the most critical stress tensor component is detected. The most critical stress tensor component is defined as the most utilized stress component, obtained by calculating the stress tensor components utilization ratio, equation 1 (p. 43). The utilization ratio is obtained by dividing the *highest* value of a stress tensor component (FEM-results in Abaqus/CAE) by the corresponding strength value, Table 6. In this investigation the characteristic values are assumed to be sufficient.

TABLE 6) TENSOR STRESS COMPONENTS RESULTS WITH CORRESPONDING STRENGTH.

Characteristic strength properties	Value [MPa]	Corresponding stress tensor component
$f_{t,0,k}$ = Tension strength parallel to the grains	14	S11+
$f_{t,90,k}$ = Tension strength perpendicular to the grains	0,4	S22+, S33+
$f_{v,k}$ = Shear strength	4	S12, S13, S23
$f_{c,0,k}$ = Compression strength perpendicular to the grains	21	S11-
$f_{c,90,k}$ = Compression strength perpendicular to the grains	2,5	S22-, S33-

$$1. \text{ Utilization ratio} = \frac{S22+}{f_{t,0,k,90}}$$

$f_{t,0,k,90}$ = Characteristic tensile strength perpendicular fibers

S22+= tensile stress tensor components (perpendicular to fibers)

The utilization ratios calculated of each stress tensor component is given in Figure 18) Utilization ratio of stress tensor components. The S22 tensile stress component has a remarkably higher utilization ratio than the rest of the stress tensor components. This is expected as the tensile stress strength perpendicular to the fibers in wood is low.

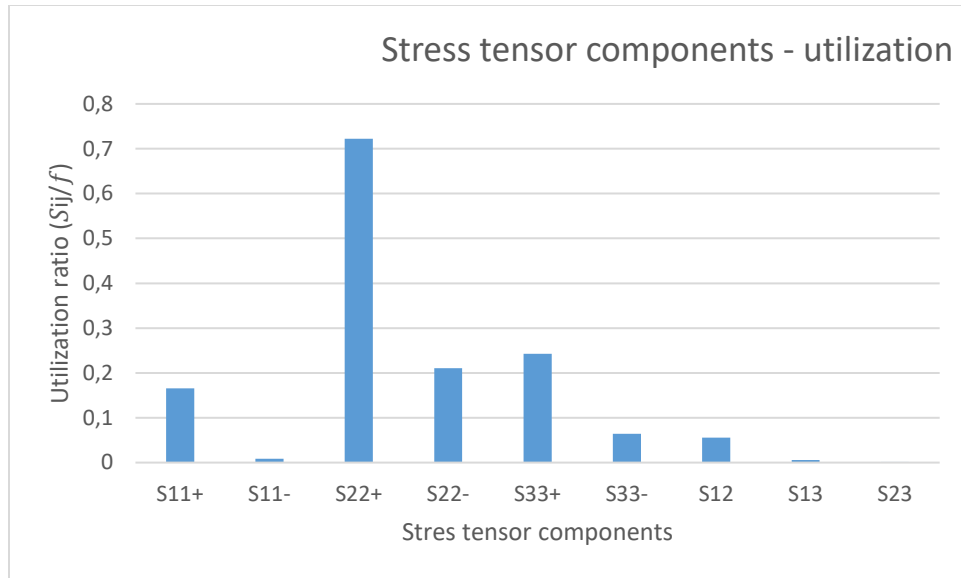


FIGURE 18) UTILIZATION RATIO OF STRESS TENSOR COMPONENTS

Localization – stress concentration

By observations of the S22 stress tensor component contour plot in Abaqus/Viewer, the highest level of S22 tensile stress are concentrated in the corners of the tenon and mortise (Figure 19) The S22 stress contour plot from Abaqus.. Further, the node with *the highest* S22 tensile stress is in the corner of the tenon feature. The high accumulation of stress this small area, indicates stress concentration. The phenomenon comes about typically due to sudden changes of geometry like cracks, sharp corners, holes, and decreasing cross-section areas.

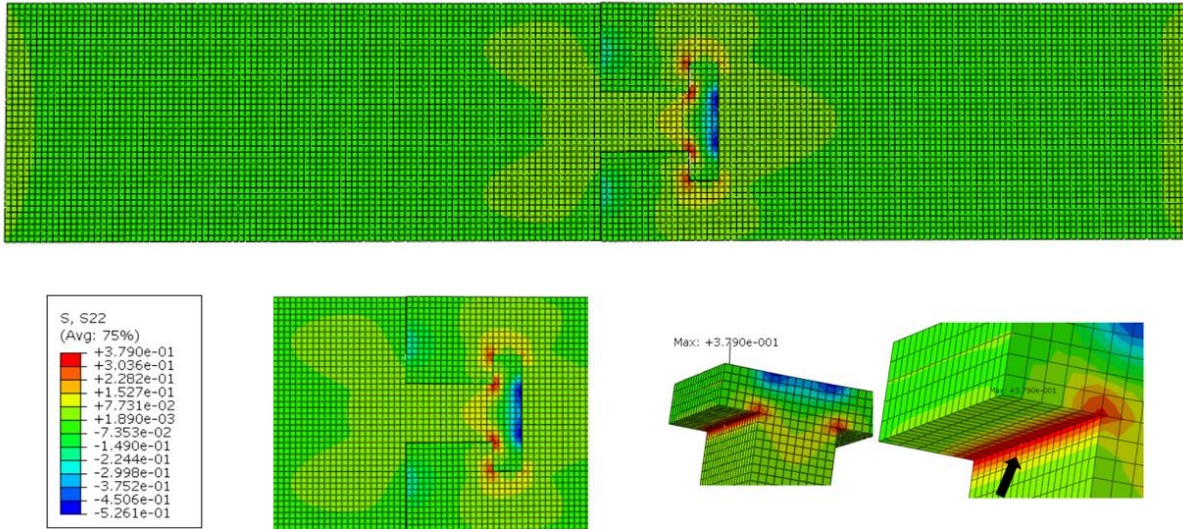


FIGURE 19) THE S22 STRESS CONTOUR PLOT FROM ABAQUS.

5.1.1.4 CONVERGENCE STUDY

A convergence test is conducted to evaluate the finite element model. This is done by refining the mesh until the FEM-results converge, with required accuracy.

Redefined mesh

Before the convergence test is performed, the mesh is modified to avoid unnecessary use of computer time. With a very dense mesh, the analysis is too heavy for the available computer resources. After locating *the most critical stress* (highest S22 tensile stress), a refined mesh is created (by local seed size) in this area only. The rest of the tenon and mortise FEM-model is applied with a more course mesh, see Figure 20

The FEM-results and computer time used on the model with the modified mesh is compared with the model (same model, but with original mesh from Appendix), see in table 7. The computer time is reduced with approx. 93,47 % while the result differs with approx. 5 %. The modified mesh is further used in the basic analysis.

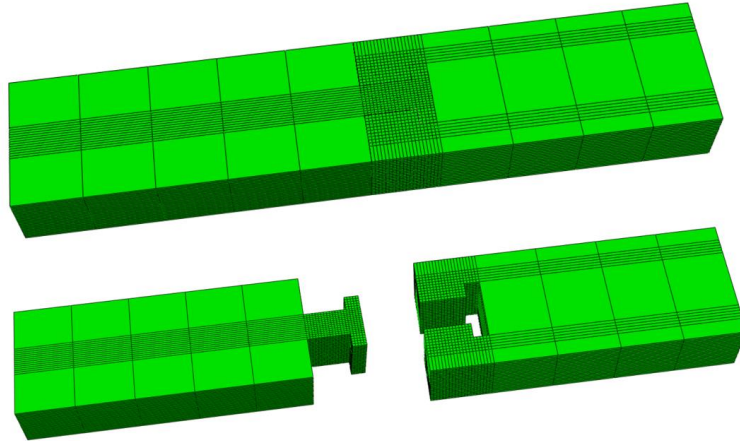


FIGURE 20) MODIFIED MESH

TABLE 7) COMPARED RESULTS WITH A MODIFIED MESH

	Homogeneous mesh, global seed size 5 mm:	Global seed size 100 mm, local seed size 5 mm:
S22:	0,3790 MPa	0,3933 MPa
Computer time:	46 minutes	3 minutes

Convergence test

The convergence test is conducted by comparing the FEM-results (highest S22 tensile stress component) from each mesh refinement, Figure 21. The convergence curve is shown in Figure 22

Modified mesh h	Local seed size finite element (mm)	Number of finite elements on tenon feature
Mesh 1	20	5
Mesh 2	15	98
Mesh 3	8	468
Mesh 4	5	2000
Mesh 5	3	8712
Mesh 6	2	33150

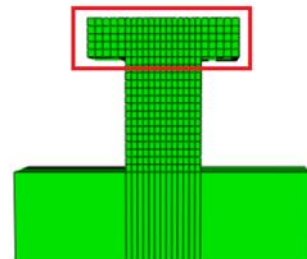


FIGURE 21) FROM LEFT, CONVERGENCE DATA (LOCAL SEED SIZE IS IN MILLIMETERS). TO THE RIGHT, AREA OF COUNTED FINITE ELEMENTS.

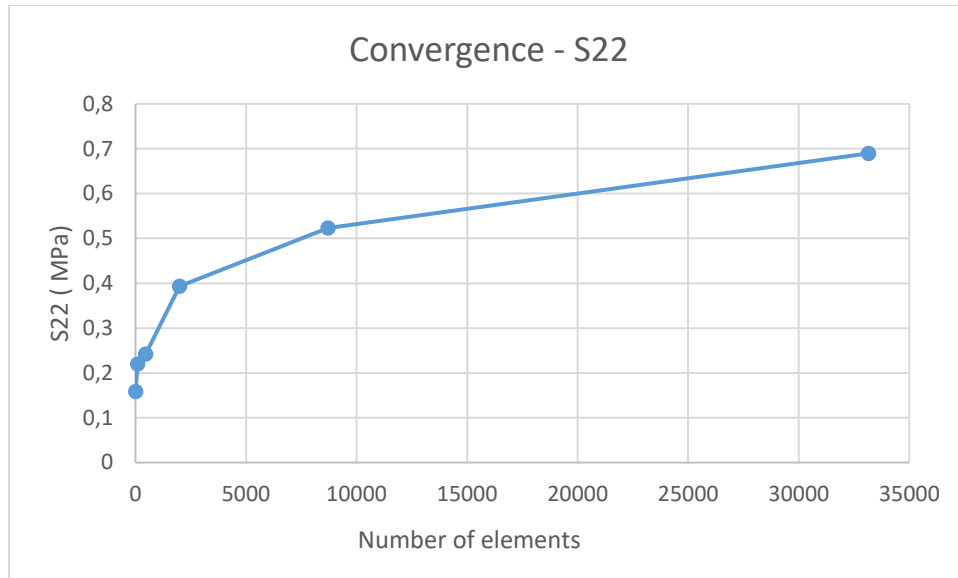


FIGURE 22) CONVERGENCE CURVE

As seen with the naked eye, the curve appears to converge. However, if the S22 tensile stress component obtained from a mesh of 2 mm finite elements and a mesh of 3 mm finite elements are compared (error to previous run), the results differ with 31.8 %, from equation 2.

$$mesh(h) = mesh \text{ refinement } h$$

$$mesh(h + 1) = mesh \text{ refinement } h + 1$$

$$2. \quad e(\%) = \text{percentage error to previous run} = \frac{S22_{mesh(h)} - S22_{mesh(h+1)}}{S22_{mesh(h+1)}}$$

Singularity

Finite Element Method involving a mesh with 2 mm finite elements is expected to reach a higher accuracy of convergence. Observing the S22 contour plots, the stress concentration of S22 stress (highest tensile S22) in the corner of the tenon tends to accumulate as the mesh is refined, see Figure 23. This observation indicates an important error in the finite analyses model. As a result of the convergence test and this observation, the high level of S22 stress in the corner of the tenon is assumed to be a singularity.

Where the geometry of the finite element model involves a sharp corner, the radius is assumed to be zero, which is not physically meaningful. In this case, the stresses are theoretically infinite.

This phenomenon is referred to as singularity. If a stress concentration is not a singularity, the stress will converge towards a finite value, as the mesh is sufficiently refined.[2]

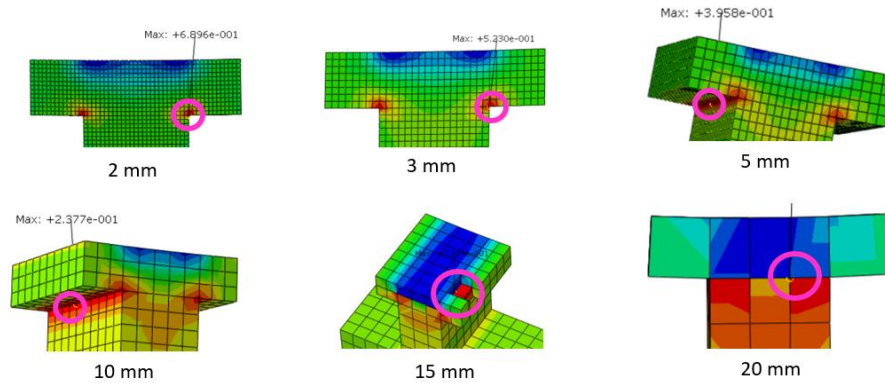


FIGURE 23) LOCATION OF THE CRITICAL S22 STRESS WITH REFINED MESH FROM 20 MM TO 2 MM.

Retrieve - Changing element type

To investigate if the high level of S22 stress in the corner of the tenon is a singularity, the convergence test is performed with more accurate finite elements, see table 8.

TABLE 8) FINITE SOLID ELEMENTS

Solid finite element	
C3D8	Full integration linear solid element
C3D20R	Reduced integration quadratic solid element
C3D20	Full integration quadratic solid element

Full integration) gives more integration points in each finite element, and therefore more accurate results. However, the computer cost increases. With full integration, the finite element C3D8 contains 8 integration points. By using quadratic solid finite element, the nodes are increased to 20 nodes per finite element. The stress tensor components are, as previously mentioned, nodal results. As the number of nodes per finite element are increased, the number of integration points increases, and even more so as the finite element is fully integrated. This change in nodes and integration points can be compared to a refined mesh. As the finite element is changed to the quadratic C3D20 finite element, the concentration of nodes and integration points, is locally increased in the same way as a finer mesh. This is illustrated in figure 24.

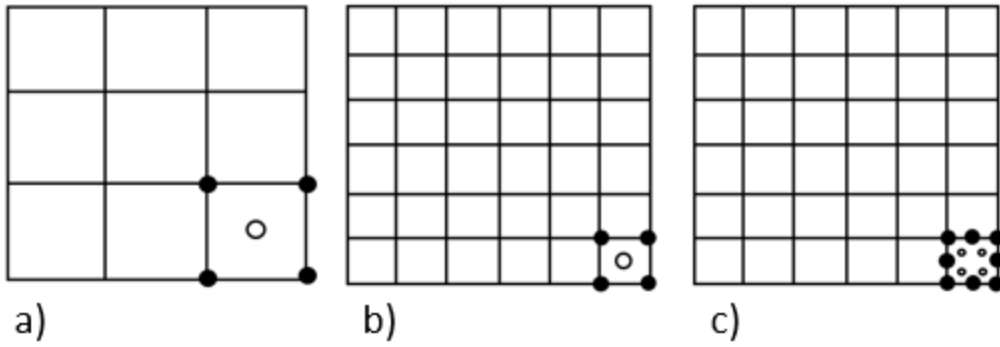


FIGURE 24) A) AND B) ILLUSTRATES THE SAME FINITE ELEMENT, BUT B) IS A REFINED MESH OF A). B) AND C) ILLUSTRATES THE SAME MESH DENSITY, BUT C) HAS FINITE ELEMENTS WITH MORE NODES.

The conducted convergence curves with the finite elements from table 8 are visualized in figure 25. The convergence test with quadratic finite elements was not performed with finite elements of 2 mm, because the computer costs were too high for the available resources. The critical stress (S22 in the corner of the tenon) tends to change significantly with continued mesh refinement. On the basis of these observations, it is assumed that we are dealing with a singular point.

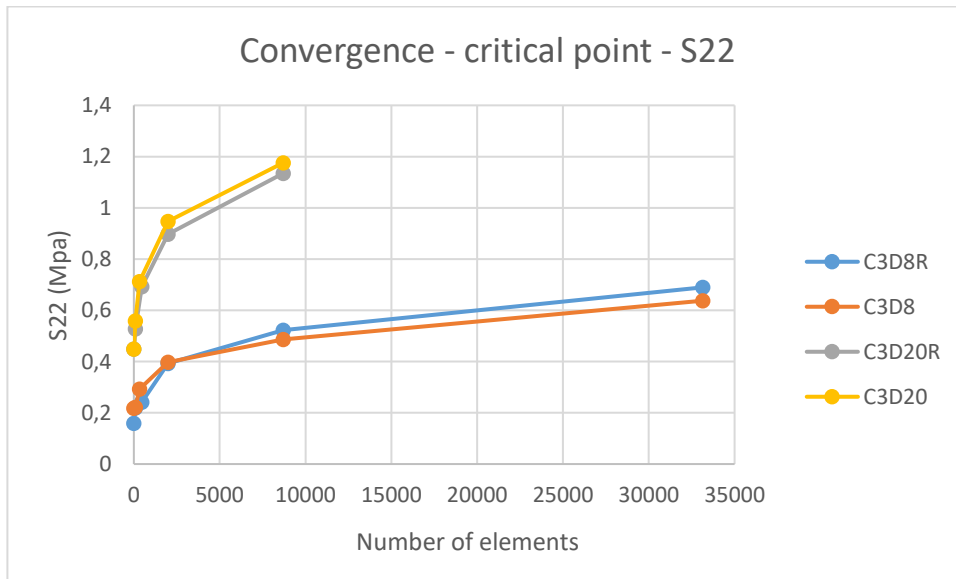


FIGURE 25) CONVERGENCE TEST WITH C3D8R, C3D8, C3D20R, C3D20

Discussion

A singularity can often be neglected where the result of interest is assumed to be at a distance from the singular point. In this analysis, the singular point is located at the integral attachment feature. A stress concentration of great importance to the structural performance of the joint is expected in this location.

There are different methods of dealing with stress singularity in sharp corners[34]. In this thesis, a simplified method by intuitive assumptions will be done. Based on the results from the FEM-model outside the singular area, the stresses in the corner of the tenon will be approximated.

As a result of the investigation described in chapter 5.1, important observations and reflections about the structural behavior of integral attachment timber joints will contribute to further investigations of their structural possibilities and limitations.

Critical section – failure of joint

To create a potential form-finding method for integral attachment timber joints, their structural limitations needs to be evaluated. In this chapter the most utilized stress tensor component (the tensile stress component S_{22}) and its location in the mortise and tenon joint was obtained. However, if the stress level in a point of the material reaches its strength limit, it does not necessarily entail failure of the joint. In addition, as shown in this chapter, the phenomena of singularity must be considered in further investigation.

The interlocking feature ensures the interlocking functionality of the joint. If these features are not fully utilized, the interlocking function of the joint is maintained. Still, a locally high level of S_{22} stress can initiate a failure mechanism of the interlocking feature. As the material fails locally, a crack can propagate under certain conditions.

Based on fracture mechanics, the failure of a solid is assumed to be a result of crack propagations in the material, leaving a crack surface. [8] The crack propagation requires modes of loading. The theory of fracture mechanics describes three pure modes of loading and the associated crack propagation Mode 1 is a result of pure tension load perpendicular to the cracking surface. The failure appears as the crack surfaces move directly apart. Mode 2 and 3, are due to shearing of the crack surfaces. In mode 2, the crack surfaces slide across one another in the direction perpendicular to the leading edge of the crack. In Mode 3, the crack surfaces are “teared” apart, as they move parallel to the leading edge of the crack.

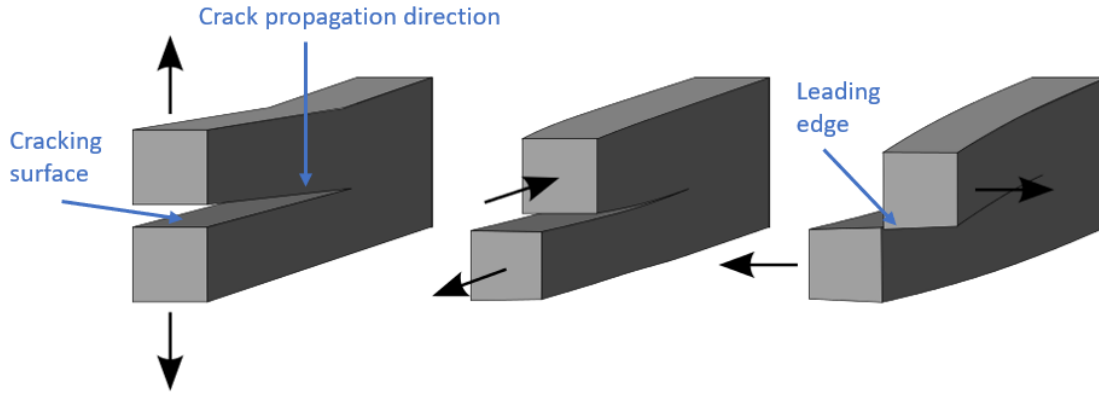


FIGURE 26) CRACK PROPAGATION MODE 1, MODE 2, MODE 3

In the investigation of timber components, failure due to crack propagations depends on the orthotropic behavior of the material. Studies of resistance against crack propagation in solid timber shows that crack propagation, under required loading conditions, along the fibers is most likely to occur. [8] This leaves two “weak-planes” in the tenon and mortise joint, see figure 27. From the finite element model of the basic geometry in Abaqus/CAE and the corresponding stress tensor components notation given in table 5, the load “acting” on the weak planes is represented by the stress tensor components S_{22} , S_{12} , S_{33} and S_{13} , see figure 28.

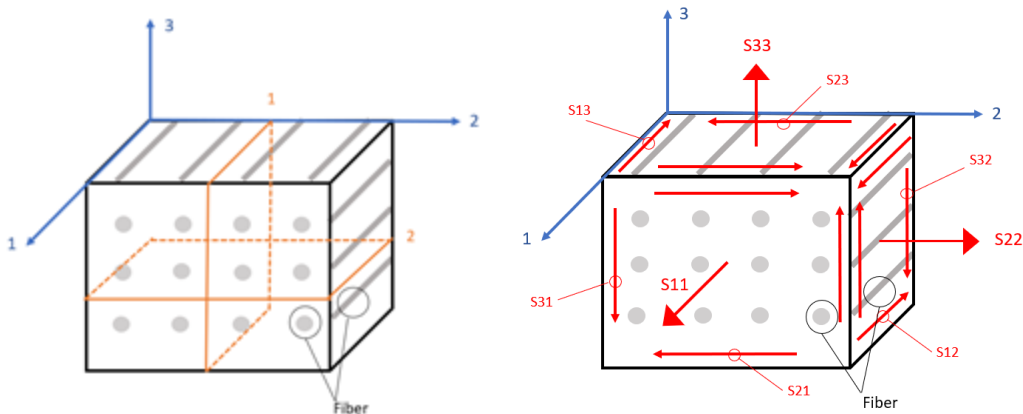


FIGURE 27) CRITICAL PLANE 1 AND 2 IN THE ANALYSED TIMBER JOINT.

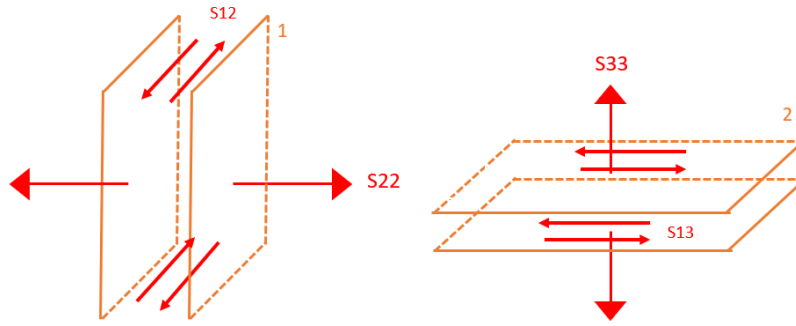


FIGURE 28) WEAK-PLANES WITH ASSOCIATED STRESS TENSOR COMPONENT.

Considering the geometry of the interlocking feature, fractures mechanics in timber and the stress tensor components results (from FEM in Abaqus/CAE) of the mortise and tenon joint, crack propagation along weak-plane 1 is assumed dimensioning for the capacity of the joint. The location of this weak-plane on the mortise and tenon joint is illustrated in figure 29 and will further be referred to as *the critical section*. The contour plots of the associated stress tensor components, S22 and S12, are displayed below (see figure 30).

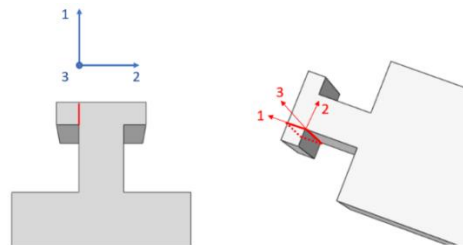


FIGURE 29) THE CRITICAL SECTION OF THE TENON AND MORTISE JOINT

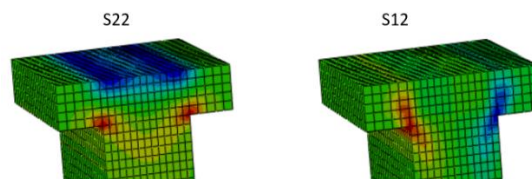


FIGURE 30) CONTOUR PLOT OF S22 (LEFT) AND S12 (RIGHT). RED COLOR IS HIGH TENSION STRESS, AND BLUE IS HIGH LEVEL COMPRESSION STRESS, GREEN IS CLOSE LOW STRESS LEVEL

Tsai Wu criterion

The consideration of failure due to crack propagation along the critical section, introduces both S22 tensile stress and S12 shear stress as parameter determining the capacity of the joint. Hence, the combination of stress components must be considered in the calculation of the joint capacity.

To predict the conditions under which solid anisotropic materials will fail, the Tsai Wu criterion is further suggested as a material failure criterion. The Tsai Wu criterion takes all strength parameters of solid timber into consideration. [38]

The criterion can be described by the equation 3, where f_i and f_{ij} are the tensor strength parameters, and σ_i and σ_j are the tensor stress components. The Tsai Wu tensor stress variables with corresponding tensor stress component results in Abaqus/CAE is displayed in table 9. [38]

$$3. f_i \sigma_i + f_{ij} \sigma_i \sigma_j = 1$$
$$i, j = 1, 2, 3, 4, 5, 6$$

TABLE 9) TSAI WU VARIABLES WITH CORRESPONDING TENSOR STRESS COMPONENT RESULTS IN ABAQUS/CAE

Tsai Wu stress components:	Corresponding tensor stress components in Abaqus/CAE:
σ_1	S11
σ_2	S22
σ_3	S33
σ_4	S23
σ_5	S13
σ_6	S12

In a coordinate system representing the stress state in an anisotropic material, the Tsai Wu failure criterion defines a “boundary curve”, see figure 31. If a point representing the stress state in the material is inside the boundary curve, the material will not fail. Opposite to this, if the point is outside the Tsai Wu boundary curve, the capacity of the material is exceeded. [38]

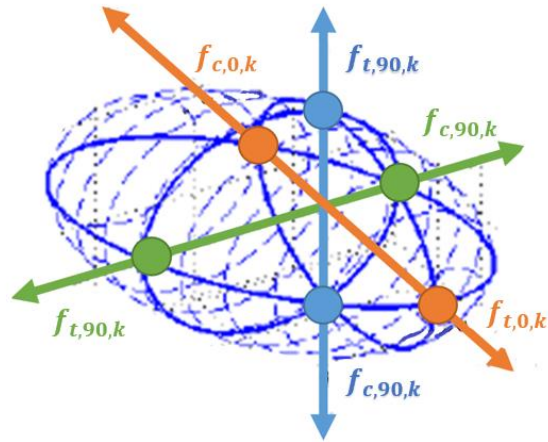


FIGURE 31) A ELLIPTIC THREE-DIMENSIONAL TSAI WU BOUNDARY SURFACES IN A COORDINATE SYSTEM SPANNED BY THE PRINCIPAL DIRECTION OF THE TIMBER, WITH THE STRENGTH PARAMETER LOCATED WHERE THE BOUNDARY CURVE INTERSECTS THE AXES.

In investigation of the critical section and its capacity, we are considering a plane stress situation of an orthotropic material. The tensor strength parameters f_4 , f_5 and f_6 are equal to zero for orthotropic materials. Thus, with a plane stress situation of an orthotropic material the Tsai Wu equation is simplified, see equation 4. The tensor strength parameters f_2 , f_{22} and f_{66} are defined below.

$$4. \quad f_2 \sigma_2 + f_{22} \sigma_2^2 + f_{66} \sigma_6^2 = 1$$

$$f_2 = \frac{1}{f_{t,90,k}} - \frac{1}{f_{c,90,k}}$$

$$f_{22} = \frac{1}{f_{t,90,k} * f_{c,90,k}}$$

$$f_{66} = \frac{1}{f_{v,k}^2}$$

Further, with the characteristic strength parameters of C24 solid timber inserted in equation 4, the Tsai Wu criterion curve is constructed in an axis-system spanned by tensor stress components S22 and S12 (see figure 32.)

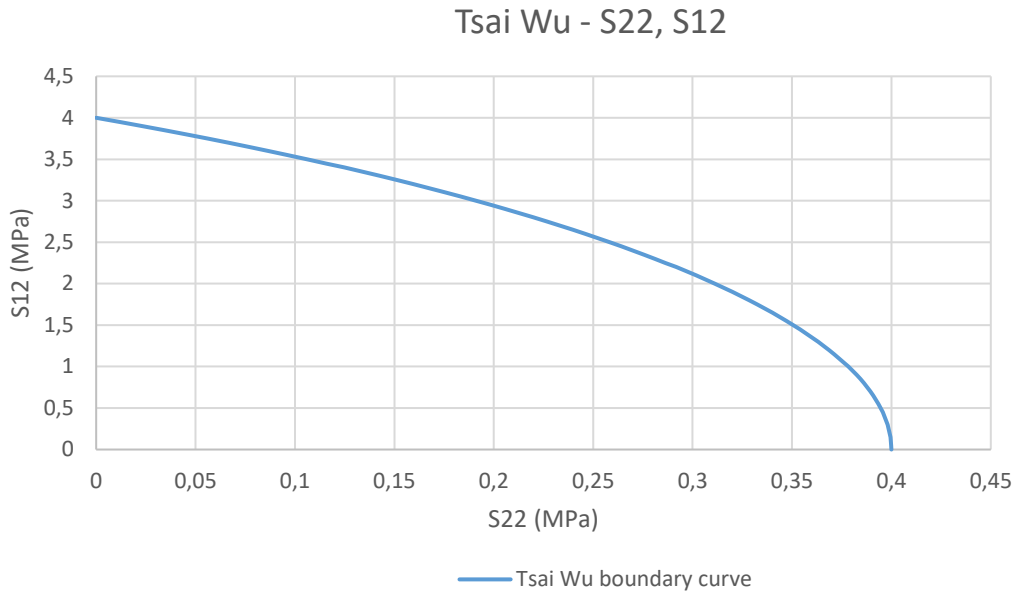


FIGURE 32) TSAI WU BOUNDARY CURVE OF C24 SOLID TIMBER

Critical section – path

Further, the S_{22} and S_{12} stresses that are “acting” on the critical section are obtained from FEM-basic geometry model in Abaqus/CAE. This is done by a linear path created from selected nodes on the surfaces of the tenon, see figure 33.

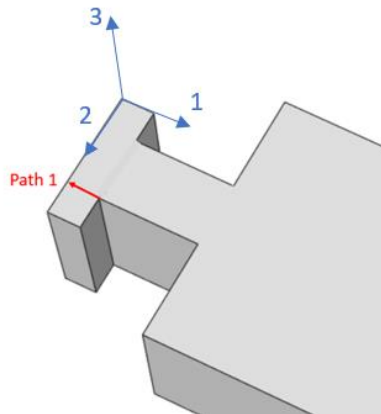


FIGURE 33) PATH 1 CREATED ON THE FINITE ELEMENT MODEL OF THE TENON IN ABAQUS/CAE

Based on the result of the FEM-model created in this chapter, the stress results are obtained from the nodes along the paths. Observation of the contour plot of the critical section indicates that both S_{22} and S_{12} stress tensor components are uniform in 3-direction. Thus, as a simplification the stresses along path 1 are assumed to represent the stresses along the critical section.

Stress along path - S_{22}

The S22 stress tensor component along the path are illustrated in figure 34. The singular point in the corner of the tenon, detected in previous investigation is in this path (position Length 0 mm). Thus, a convergence test of the path is conducted. This is done by comparing the S22 stress tensor component results along the path as the mesh is refined. As expected, the stress closest to the corner of the tenon (length 0 mm and length 25 mm) shows sign of singularity. However, the stress curves tend to converge at the middle of the path as the mesh is refined.

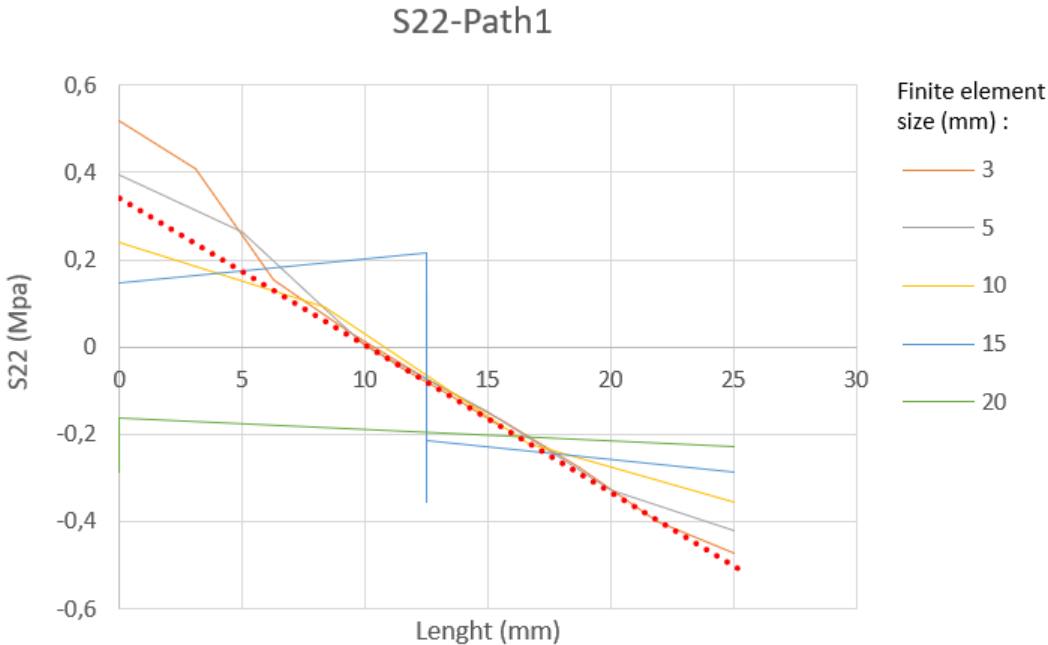


FIGURE 34) S22 STRESS ALONG PATH 1. THE STRESSES ALONG THE PATH REPRESENTED IN DIFFERENT COLOURED CURVES AS THE MESH IS REFINED, AND THE ASSOCIATED FINITE ELEMENT SIZE IS GIVEN TO THE RIGHT. THE HORIZONTAL AXIS GIVES THE LOCATION ALONG THE PATH. THE LINEAR REGRESSION IS THE RED DOTTED LINE.

Thereby, a linear regression made by the nodal S22 tensor stresses from 10 mm to 15 mm of the path is created. The linear regression is based on the mesh with 3 mm sized finite elements.

Looking back at in this chapter the *active area* is assumed to transferring the load between the joint members. Thus, the tenon feature is further assumed to be subjected to bending, se figure 35. By comparing this theoretical bending stress in figure 35 with the linear regression of S22 stress along the path in figure 34, the stress obtained from the FEM-model made in Abaqus/CAE is considered an appropriate estimation of the actual stress.

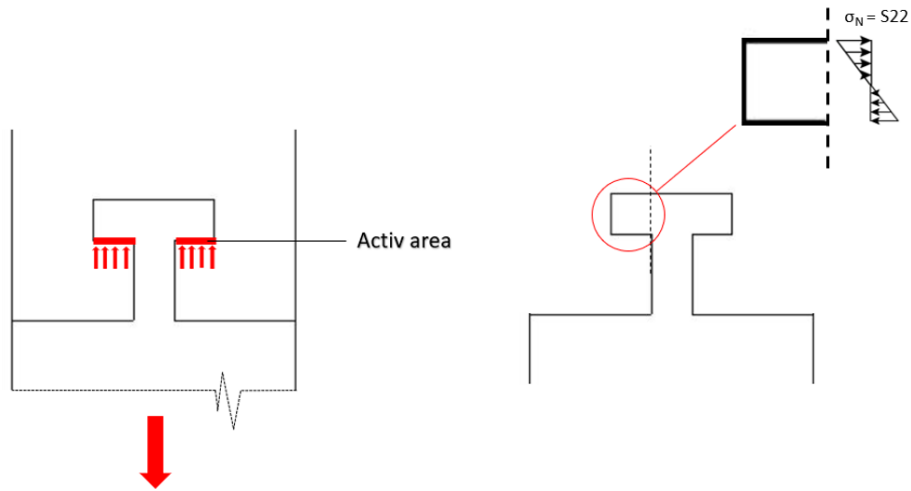


FIGURE 35) THE TRANSFER OF TENSION LOAD BETWEEN JOINT MEMBERS THROUGH CONTACT PRESSURE. RIGHT: STRESS DISTRIBUTION ON THE CRITICAL SECTION AS A RESULT OF BENDING

Stress along path - S12

The S12 stress along the path is obtained by the method explained above, see figure 36. The linear regression in figure 36 is based on the mesh with 3 mm sized elements from the same area of the path as the linear regression of S22 stress

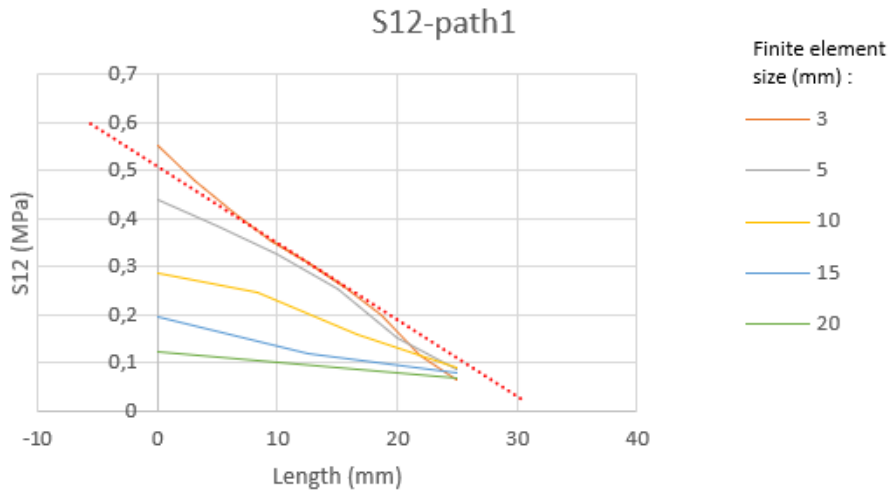


FIGURE 36) S22 STRESS ALONG PATH 1. THE RED DOTTED LINES IS THE LINEAR REGRESSION

The stresses (S22 and S12) along the path with a mesh of 15 mm and 20 mm sized finite elements show values far from the results of the finer meshes. With 15 mm finite elements, there are only two finite elements along the path, and with 20 mm finite elements there is only one finite

element along the path. Thus, it is assumed that the results obtained with these meshes do not represent the actual stress along the critical section. However, a mesh with 5 mm finite elements is assumed to be sufficient and will be used in further calculations.

Enable crack propagation

Before the combination of S22 and S12 stress along the path is checked with the Tsai Wu failure criterion, another observation is made. The S22 stress in figure 34 shows negative values along path. By the Abaqus/CAE sign convention, the S22 stress changes from tension to compression at 10 mm (following the arrow direction in figure 33). From the theory of fracture mechanics, it requires *tensile* S22 to enable crack propagation. In the same area as S22 is compressive stress, the S12 stress is decreasing. Therefore, only the first 10 mm of the path is assumed to be the part of the path exposed to failure by crack propagation, see figure 37.

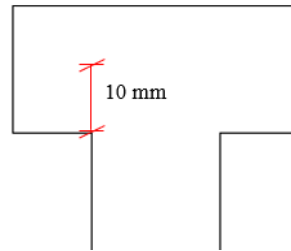


FIGURE 37) THE PART OF THE CRITICAL SECTION WHICH WILL MOST LIKELY FAIL BY CRACK PROPAGATION

Tsai Wu

The nodal tensor stress components (S22 and S12) from the mesh with 5 mm finite elements of the first 10 mm of the critical section are checked with the Tsai Wu criterion, see figure 38.

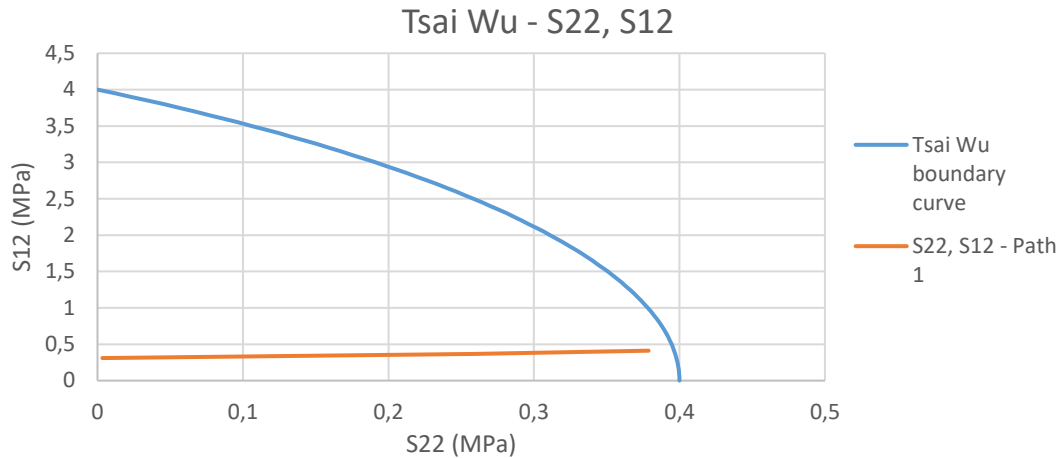


FIGURE 38) TSAI WU, S22 AND S12

The combination of S22 and S12 stress acting on the critical plane is “inside” the Tsai Wu boundary curve. Hence, the imposed load (tension force) causing the stress state will not lead to failure of the joint. Another observation from figure 38, is that the S22 stress tends to be dimensioning. The capacity of the joint can be found by increasing the imposed load until the stress state exceeds the Tsai Wu boundary curve. The purpose of this investigation was to find an approach that can determine the capacity of the joint. Thus, further calculation of the capacity of the basic geometry will not be performed.

In this thesis, this method of finding the capacity of an integral attachment timber joint will be referred to as “the Tsai Wu approach”.

5.1.2 PARAMETRIC STUDY

A parametrical study of the mortise and tenon joint is further performed to investigate how a potential form-finding method can evaluate the shape of an integral attachment timber joint.

This is done by performing the same structural investigation as done in chapter 5.1.1, on every geometry in table 2, chapter 5.1. This method implies finding the most utilized stress tensor components in the joint, detect where it is located and perform the *Tsai Wu Approach*. Abaqus/CAE is not incorporated in a parametric environment. Thus, the investigation requires separate FEM-analysis for every geometry investigated.

FEM-models

The finite element model from chapter 5.1.1 (Appendix A), except geometry and mesh, is used on the 18 geometries investigated. The mesh on the basic geometry was based on the location of the critical stress. When the interlocking geometry is changed, it is assumed that the location of

the critical stress might change. Thus, a modified mesh is used on the finite element models in the parametric study, see figure 39.

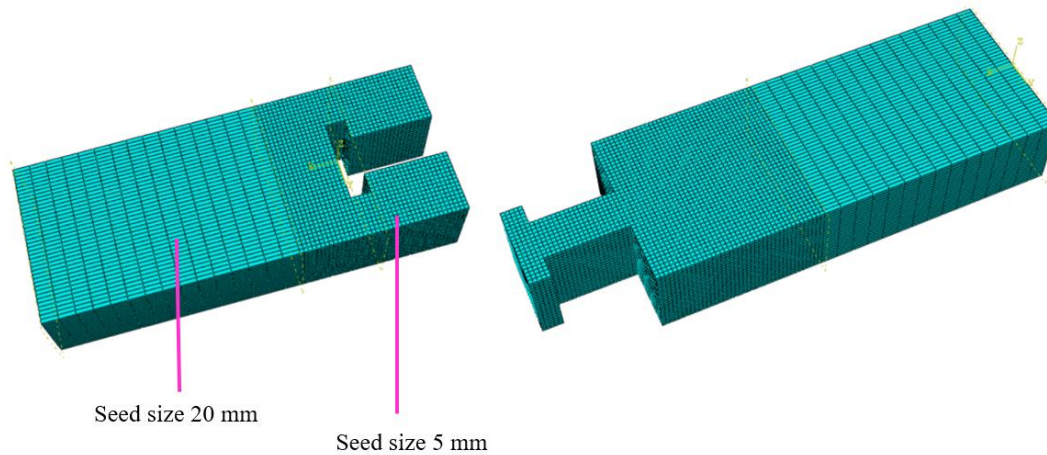


FIGURE 39) REFINED MESH APPLIES THE 18 GEOMETRIES. GLOBAL SEED SIZE 20 MM, AND LOCAL SEED SIZE 5 MM. THE 5 MM FINITE ELEMENT ARE LOCATED OVER A GREATER AREA THAN IN THE BASIC GEOMETRY

Post-processing

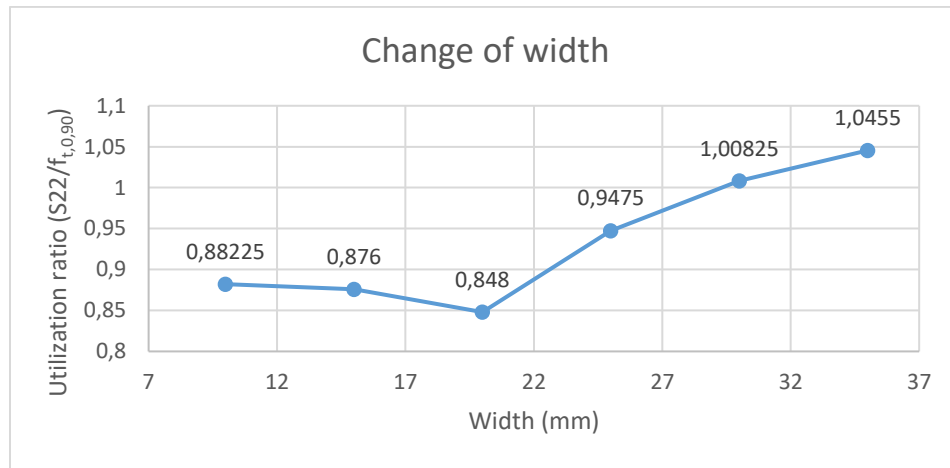
The post-processing showed that S22 was the most utilized stress tensor component in every parametric changed geometry. However, the location and magnitude of the stress varied. This change in structural behavior due to the parametrical changes will be discussed further.

The discussion is based on intuitive assumptions without any further structural analysis. However, the assumptions made are based on visual deformation and contour plots in Abaqus/CAE.

5.1.2.1 CHANGE OF WIDTH

To investigate the effect of changed width parameters, the utilization ratio of the most critical stress in the six models with different width values are compared, se table 2, chapter 5.1.

TABLE 10) UTILIZATION RATIO OF HIGHEST TENSION S22 STRESS WITH DIFFRENTH WIDTH PARAMETER



In Geometry 1 (10 mm width) and Geometry 2 (15 mm width) the highest level of S22 tensile stress is in the corner of the mortise. In Geometry 3, 4, 5 and 6, the highest level of tensile stress is in the corner of the tenon, see figure 40.

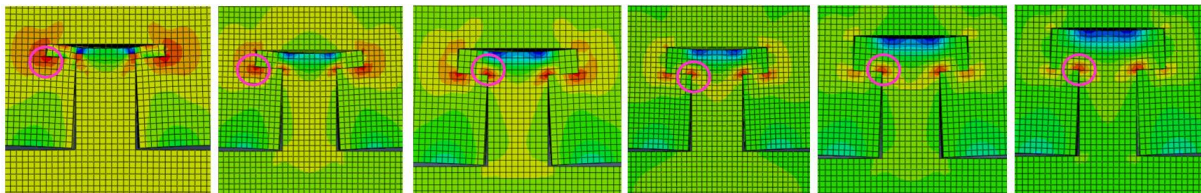


FIGURE 40) FROM LEFT, WIDTH: 10 MM, 15 MM, 20 MM, 25 MM, 30MM, 35 MM. HIGHEST S22 STRESS IS MARKED WITH A PINK CIRCLE

The utilization ratio decreases as the width changes from 10 mm to 20 mm. This could be a result of increased stiffness of the tenon feature. A stiffer tenon feature results in smaller bending deformations, see figure 41. This affects the utilization of the active area. As the width increases, the contact area between the joint members increases (the active area).

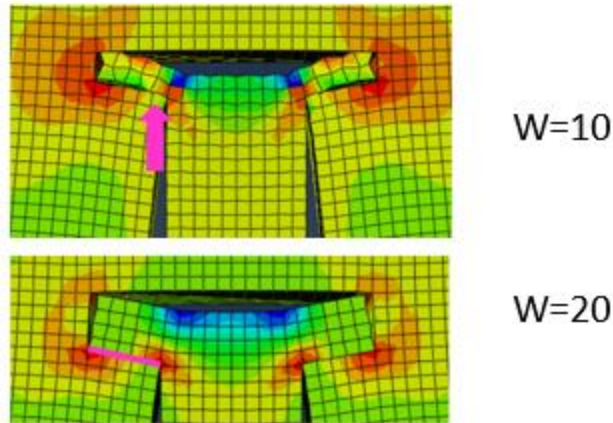


FIGURE 41) TENON FEATURE WITH 10 MM AND 20 MM WIDTH, WITH CONTACT AREA MARKED IN PINK.

Geometry 1 (width 10 mm) can be compared to an encased cantilever with a point load on the free end, see figure 42. The point load on the cantilever will create a moment in the encased end. Similar behavior of Geometry 1 creates tension stress tensor component S22 in the corner of the mortise. As the contact area is increased in Geometry 2, the load is distributed over a greater area of “the cantilever”, and the tension stress component S22 in the encased end becomes smaller. In Geometry 3, the contact area is assumed to be fully utilized.

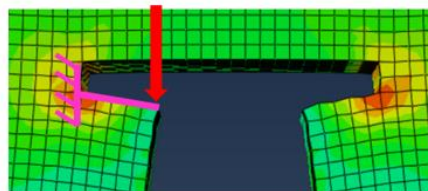


FIGURE 42) ILLUSTRATION OF COMPARISON OF GEOMETRY 1 AND A CANTILEVER WITH POINT LOAD

Another observation is that the utilization ratio increases when the width is further increased from 20 mm to 35 mm. This could be a result of the change in ratio between the height of the tenon web and the width of the tenon feature. Further investigation is required to validate this assumption.

5.1.2.2 CHANGE OF LENGTH

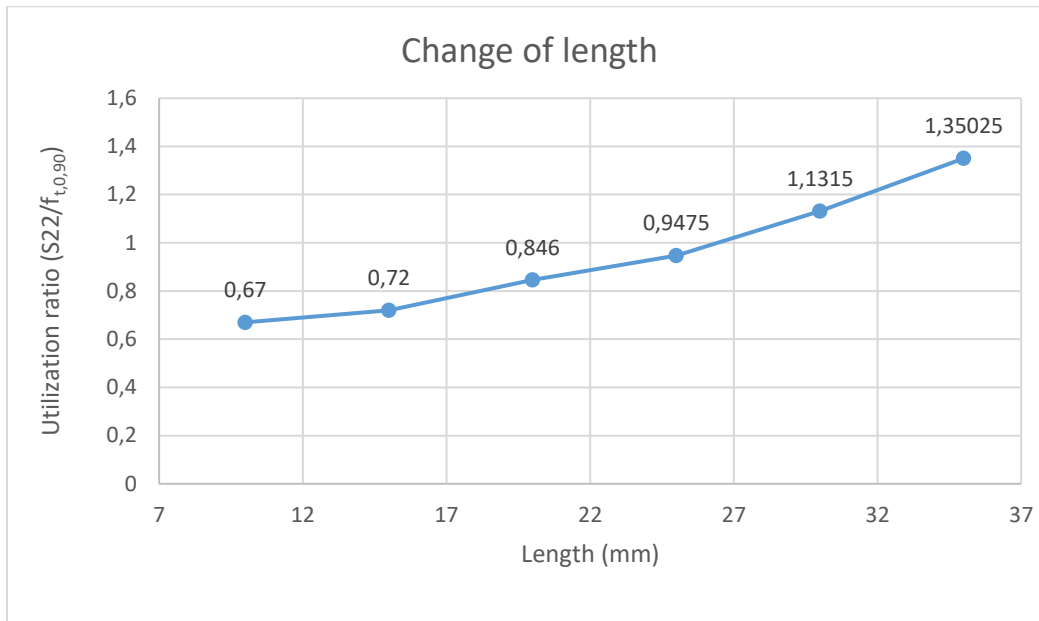


FIGURE 43) UTILIZATION RATIO OF MOST CRITICAL STRESS WHEN THE LENGTH PARAMETER IS CHANGED

The utilization ratio of the highest S22 stress increases as the length parameter is increased, see figure 43. In contrast to the change in width, the location of the highest S22 stress is not changed with the length parameter. This is assumed to be because with the constant width of 25 mm, the contact area is fully utilized. The highest S22 stress is located in the corner of the tenon, like the basic geometry in chapter 5.1.1.

This structural behavior could be explained by the contact pressure on the tenon from the active area. The contact pressure is assumed even distributed on the active area, and the corner of the tenon is considered as the fixed end of this area. The phenomena are further compared to bending of a cantilever subjected to evenly distributed load. As the active area of the tenon increases by an increased length parameter, the fixed end is subjected to a higher level of S22 stress.

However, a length smaller than 20 mm is considered unrealistic, due to geometrical imperfections and production challenges.

5.1.2.3 CHANGE OF HEIGHT

The location of the highest S22 stress is in the corner of the tenon on every geometry with changed height parameter. The utilization ratio decreases as the height increases and tends to reach a stable level after certain height, see figure 44.

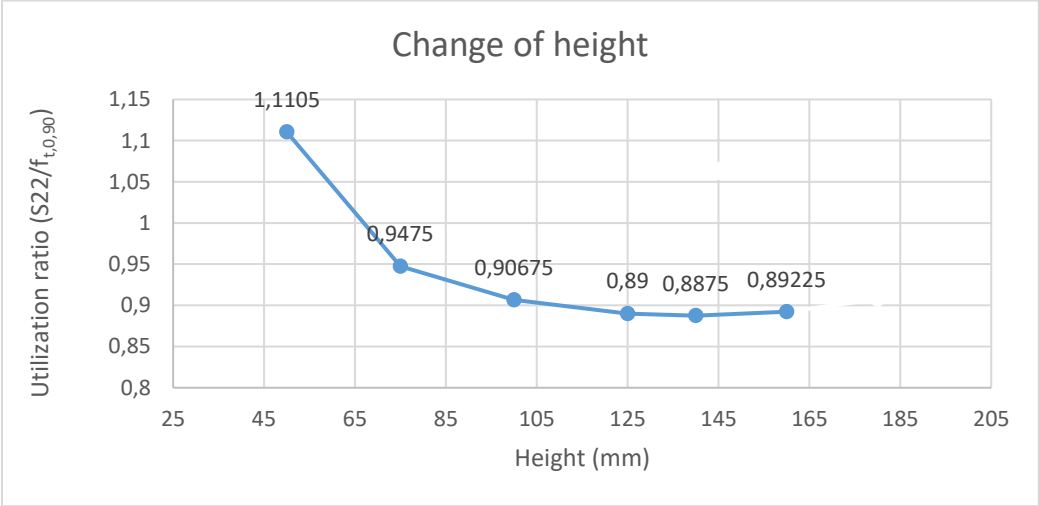


FIGURE 44) UTILIZATION RATIO WITH CHANGE OF HEIGHT PARAMETER

The phenomenon resulting in higher S22 stress level with a height of 50 mm compared with a height of 140 mm, might be caused by changes in the stress flow close to the corner of the tenon. Assumed stress flow is illustrated in figure 45. As the height is increased, the stress flow close to the corner of the tenon is assumed to give a greater stress component in the 1- direction than in the 2-direction close to the corner of the tenon (see chapter for direction description), see figure 46.

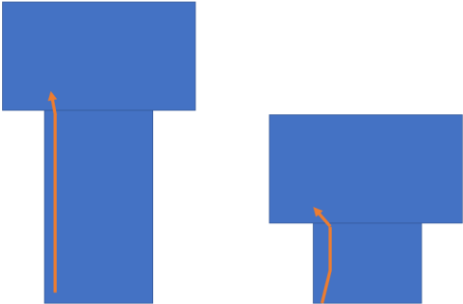


FIGURE 45) ILLUSTRATION OF STRESS FLOW CLOSE TO THE CORNER OF THE TENON WITH DIFFERENT HEIGHTS OF THE TENON WEB.

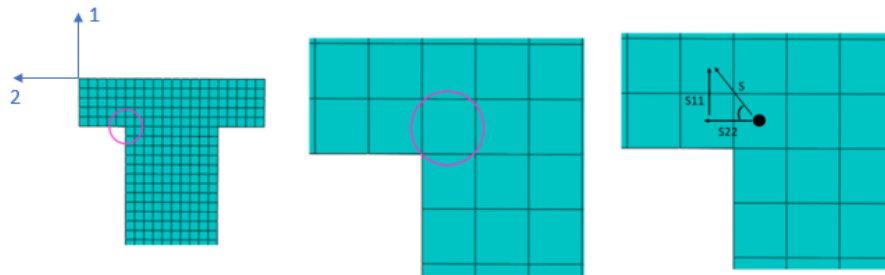


FIGURE 46) ILLUSTRATION OF COMPONENT ANGLE

Combination geometry

From the investigation done of the 18 geometries, the preferred height, width and length parameters are given in table 11. The preferred variables are based only on the highest level of S22 stress in the tenon and mortise joint.

To optimize the structural behavior of the joint, the preferred parametrical length, width and height are combined into one geometry. Thus, a geometry with a height of 125 mm, width of 20 mm and length of 20 mm was created, and a finite element analysis was performed.

The highest S22 stress result gave a utilization ratio of 0.734, see table 11, compared to the separate changes of parameters, the combination geometry has the lowest S22 stress level due to its geometry.

TABLE 11) OPTIMAL PARAMETERS

Optimal geometries:	Utilization ratio:
Geometry 9 (length =20 mm)	0,846
Geometry 16 (height =125 mm)	0,89225
Geometry 3 (width =20 mm)	0,848
Combination (20 mm, 125 mm, 20 mm)	0,734

So far in the parametric study, the combination geometry is considered to have the most favorable structural geometry. However, this is only based on the highest level of stress in one single node (S22 tensor stress component result). From chapter 5.1.1 (of the basic geometry), this is not considered to determine the capacity of the joint.

Thus, the Tsai Wu Approach (see chapter), will be performed on several of the geometries considered in this chapter. This involves geometry 1,3,9,6,7,12,13 and 16 from table 2 chapter 5, as well as the combination geometry. Two different geometries representing every parameter (width, height, length). For a description of this method see chapter 5.1.1.

The results are presented in figure 47. Every color represents a different geometry, and every point in the same color represents a different nodal point along Path 1. The nodal result for each geometry which appears to be the most critical is highlighted in the figure. As one point only represents one nodal result, the most optimal geometry cannot be considered based on the highlighted points.

To find the geometry that has the highest capacity (according to this approach), the load must be increased until all the points of all the geometries are outside the Tsai Wu boundary curve. While the imposed load is frequently increased, the geometry that last “steps outside” the Tsai Wu curve with all its points, is assumed to have the highest capacity.

The aim of the investigation done in Chapter 5 is to find a potential method of evaluating the structural behavior of integral attachment timber joints. Thus, as Abaqus/CAE is not included in a parametric environment, the process of finding the capacity of each geometry is considered inefficient.

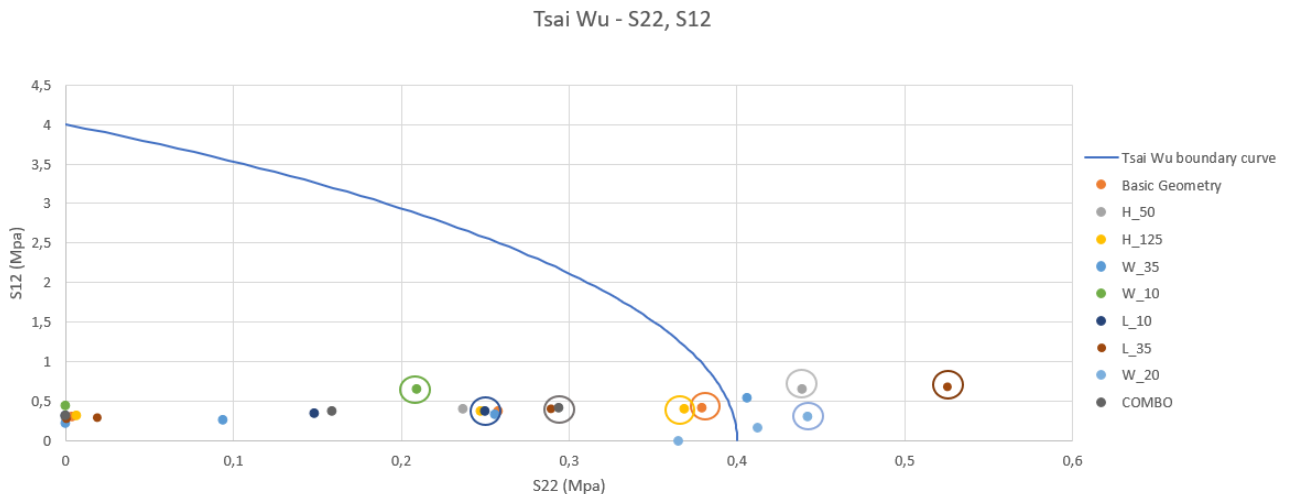


FIGURE 47) TSAI WU BOUNDARY CRITERION CURVE. THE GEOMETRIES COMPARED WITH THE TSAI WU CRITERION CURVE IS GIVEN ON THE RIGHT SIDE OF THE FIGURE.

5.2 COMPRESSION JOINT

In this subchapter, further investigation of integral attachment joint configurations will be performed. The investigation is based on knowledge from analysis in previous subchapters and experience from the workshop at Advances in Architectural Geometry (AAG) 2018 (see chapter 3).

The purpose is to understand the structural behavior of an integral attachment timber joint in compression, hereafter referred to as compression joint.

The following investigation is a parametric study of a joint configuration by three interlocking joint members subjected to pure compression force. The joint members' configuration, cross-section dimensions and imposed force are not parametrically changed, see figure 48. The joint geometry without the interlocking geometry is referred to as the basic joint configuration. The geometry in figure 48 is drawn in Rhino, without any parametric variables. The three joint members are of Norwegian spruce strength class C24, and have a cross-section with a height of 100 mm and width of 100 mm. General nomenclature of the basic compression joint configuration is given in figure 49.

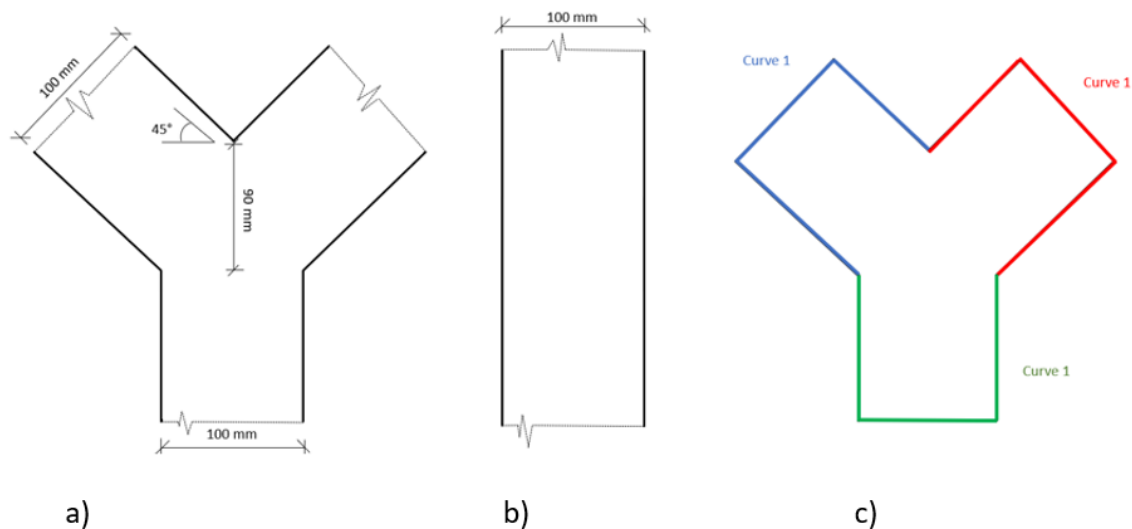


FIGURE 48 A) BASIC COMPRESSION JOINT CONFIGURATION, DIMENSIONS B) BASIC JOINT CONFIGURATION, DIMENSIONS C) N BASIC JOINT CONFIGURATION BOUNDARY CURVES IN RHINO

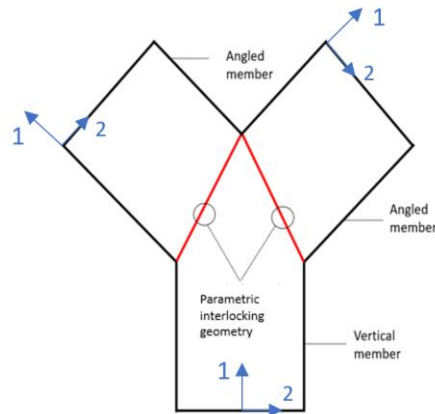


FIGURE 49) NOMENCLATURE OF THE COMPRESSION JOINT. THE ORTHOTROPIC DIRECTIONS OF THE JOINT MEMBERS ARE GIVEN BY THE BLUE ARROWS. .

Parameters considered

The parametric geometry of the compression joint considered is the interlocking surfaces between the intersecting joint members, see figure 49. The interlocking geometry is modeled in Grasshopper. As previously mentioned, Abaqus/CAE is not included in a parametric environment. Hence, nine different interlocking geometries on the basic joint configuration geometry are exported to Abaqus/CAE from Rhino. The geometries are given in figure 50, with associated names. The nine geometries are divided into three categories, based on parameters considered.

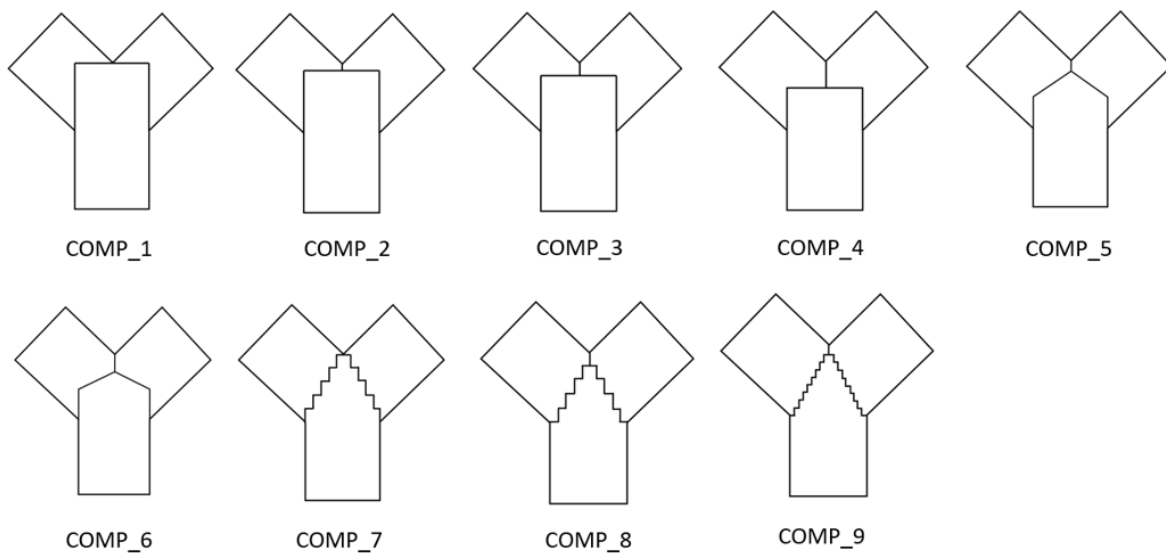


FIGURE 50) 9 INTERLOCKING GEOMETRIES OF THE BASIC JOINT CONFIGURATION.

Category 1)

In the first category, the vertical member has a fixed rectangular geometry. The parametric interlocking geometry is the interfering surface between the “angled members”, see figure 49. Thereby, the parameter considered is the height (H) of this interfering surface, see figure 51.

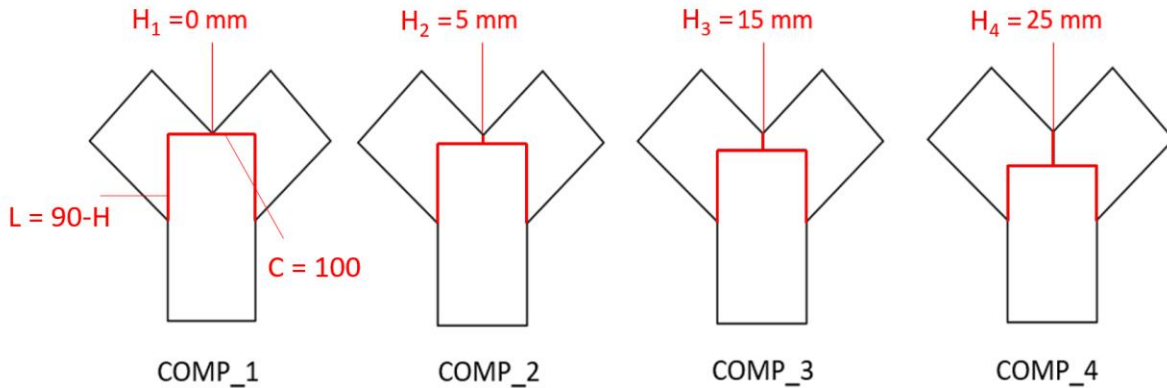


FIGURE 51) PARAMETRIC MODEL CATEGORY 1. THE PARAMETER CONSIDERED IS GIVEN AS H, AND THE ASSOCIATED CHANGE OF “L” IS ILLUSTRATED.

Category 2)

In the second category, all joint members have a parametric interlocking geometry. The vertical member has a triangular interlocking geometry, adjusted with the interfering area between the two remaining members (angled members, see figure 52). The parameter considered is the height (H) of this interfering surface, see figure 52.

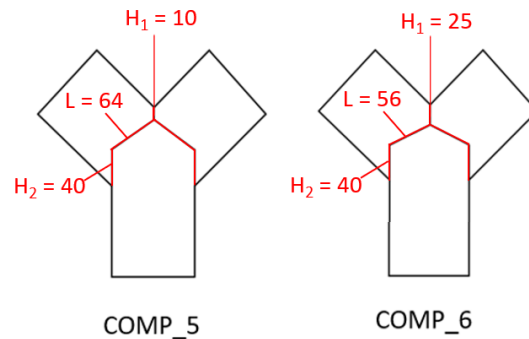


FIGURE 52) INTERLOCKING GEOMETRY CATEGORY 2.

Category 3)

The third category has an interlocking geometry with varying numbers of “steps”, see figure 53. The number of steps is the parameter considered and decides the length and height of each step.

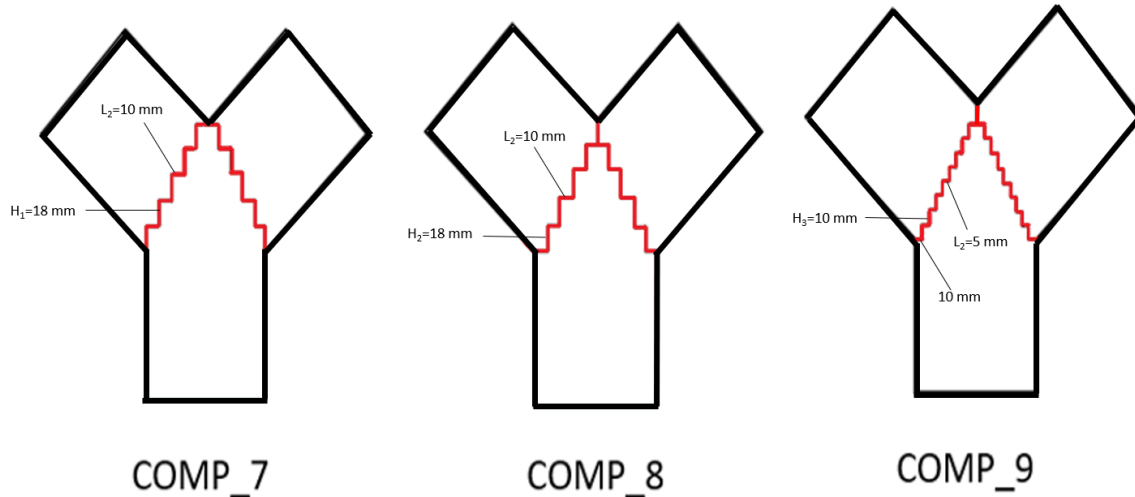


FIGURE 53) INTERLOCKING GEOMETRY CATEGORY 3.

5.2.1.1 FINITE ELEMENT METHOD MODEL

The mathematical model describing the physical problem of the compression joints in this subchapter is based on the finite element method model (Abaqus/CAE) in subchapter 5.1.1, see Appendix X. This finite element method model is adapted to the compression joint geometry.

Briefly summarized are the joints modeled with C3D8R solid finite elements, frictionless tangential contact behavior, hard normal pressure contact behavior and material properties describing the orthotropic behavior of the timber members. To simulate pure compression force acting on the joint, the force is applied as normal pressure 1 megapascal (positive sign) on the boundary surfaces of the angled members (see figure 49). The boundary conditions of the joints are illustrated in figure 54. The loaded surfaces on the angled members are restricted against movement in the tangential and radial direction of the surface plane, but free to move in the normal direction of the plane. The boundary surface on the vertical members is restricted against any movements (fixed).

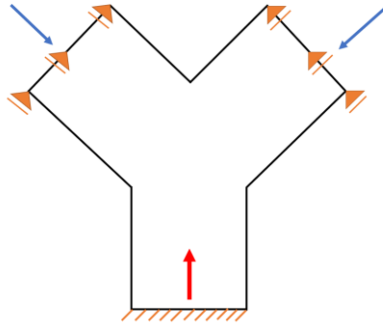


FIGURE 54) COMPRESSION JOINT WITH ILLUSTRATED BOUNDARY CONDITIONS AND IMPOSED LOAD (BLUE)

Active area

The interfering surface between the joint members are assumed to transfer the imposed load as contact pressure only in the Abaqus/CAE model. The simplification of a frictionless contact behavior is assumed not to be sufficient for actual physical behavior. However, the simplification is done to save computer time. Tangential frictional behavior should be taken into account in further calculation of the capacity but will not be done in this thesis.

5.2.1.2 FINITE ELEMENT METHOD MODEL

The finite element method models of the ten geometries created were further submitted for automatic finite element method analysis in Abaqus/CAE.

5.2.1.3 POST-PROCESSING

Utilization ratio

From the results of the Finite Element Method analysis in Abaqus/CAE of nine geometries, the most utilized stress tensor components are calculated. The definition of the stress tensor component is given in chapter 5.1.1, and the direction complies with the direction definition in figure 49. Similar to the mortise and tenon joint in subchapter xx, the tensile stress tensor component S22 is the most utilized stress component in every geometry investigated. The average values of each stress tensor component from the nine geometries are calculated and compared in figure 55.

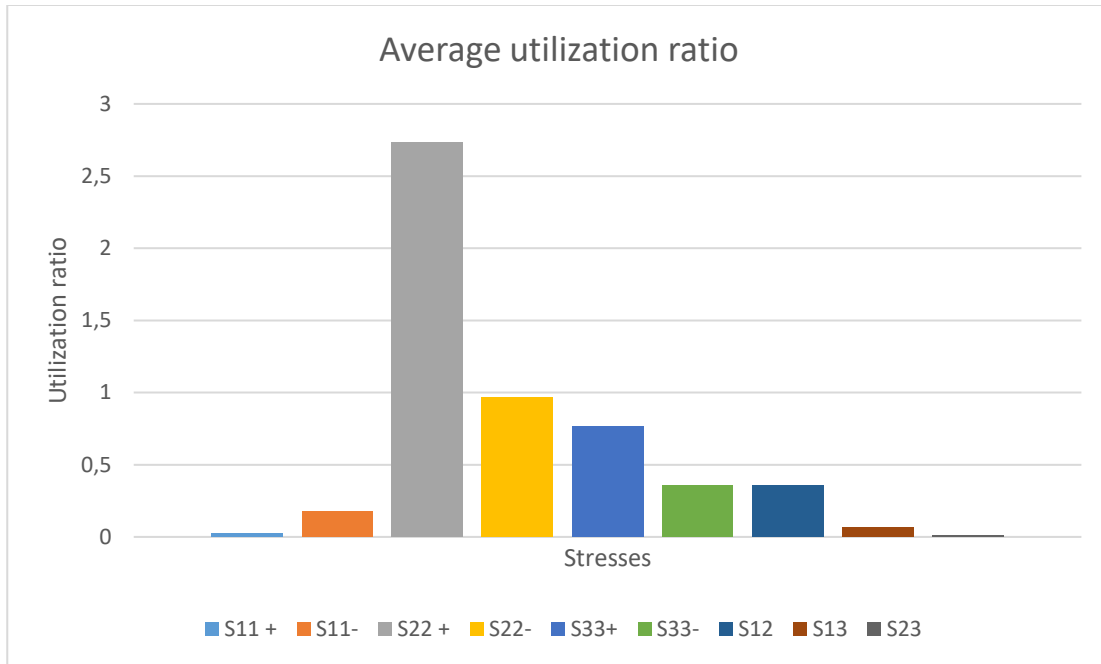


FIGURE 55) AVEGADE VALUE (FROM EACH GEOMETRY) OF UTILIZATION OF EACH STRESS TENSOR COMPONENT

Location

The location of the highest S22 tensile stress on every geometry is given in figure 56. From comparison with the investigation of the tenon and mortise joint in chapter 5.1.1, the location of the most utilized stress tensor component is again localized in the sharp corner of the structural components in contact.

Discussion – S22 and location

The assumed reason for the high utilization of S22 tensile stress is the low tensile strength perpendicular to the fiber direction. The strength limit is easily reached. When the joint members in the joint configuration are compressed in their longitudinal direction, they “want” to expand in the orthogonal directions of the compression force, causing stress perpendicular to the fibers.

In addition, in every geometry the stress flow (from the angled members boundary surfaces subjected to pressure) “meets” a sharp corner at the intersection with the vertical joint member (see figure 57). As the stress meets the sharp corner, the direction changes. This results in a higher S22 tensile stress component in the angled member close to the corner, see figure 57.

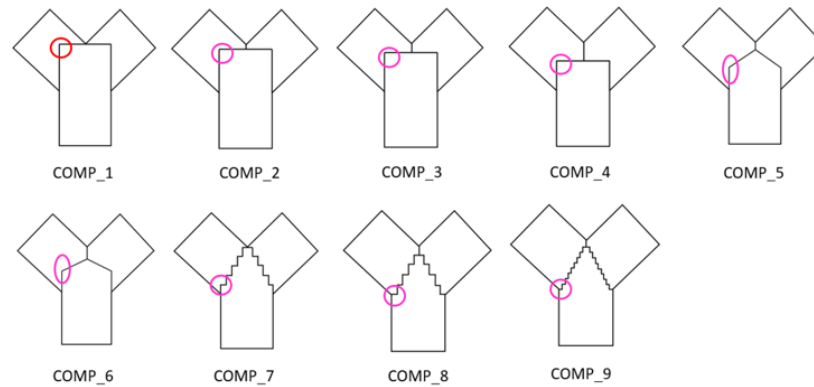


FIGURE 56) THE LOCATION OF THE HIGHEST S22 TENSILE STRESS IS MARKED IN RED AND PINK. THE PINK CIRCLES INDICATE THAT THE LOCATION IS ON THE ANGLED MEMBER. THE RED COLOR INDICATES THAT THE LOCATION IS ON THE VERTICAL MEMBER.

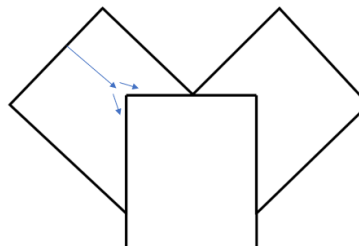


FIGURE 57) THE BLUE ARROWS ILLUSTRATE THE STRESS FLOW, ORIGINATING FROM THE SUBJECTED PRESSURE, "MEETING" THE SHARP CORNER OF THE VERTICAL MEMBER.

Comparing the geometries

The structural behavior of the nine interlocking joint geometries are further compared based on the utilization of stress perpendicular to the fibers in second direction, see figure 58. COMP_1 has the highest utilization ratio, while COMP_8 is the least utilized.

To explain this change in structural behavior due to geometrical differences, a general observation is made. As the sharp corners, where the highest level of S22 stress is located, are “unloaded” by other features on the interlocking geometry, the S22 stress tensor component decreases. These features of the interlocking geometry are either other sharp corners (steps in parametric category 3) or an increased interfering surface between the angled members.

However, from observation and discussion in subchapter 5.1., the high level of S22 stress in the sharp corners is most likely caused by singularity in the finite element method model in Abaqus/CAE. Thus, a convergence test is conducted of COMP_8.

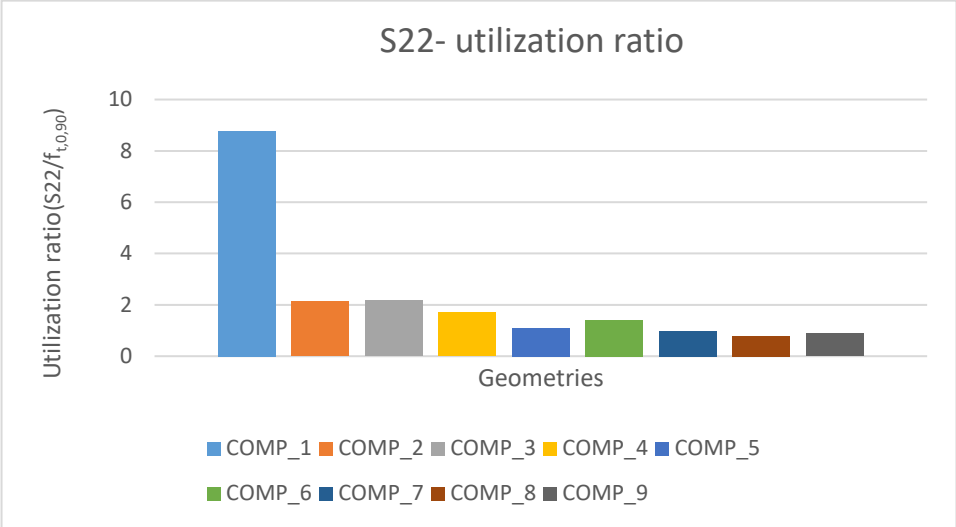


FIGURE 58) COMPARED UTILIZATION RATIO OF EACH GEOMETRY

Convergence test

The convergence test is made with a global mesh refinement, see figure 59. From this convergence test, the critical S22 stress is assumed to be a result of singularity in the Finite Element Method model in Abaqus/CAE.

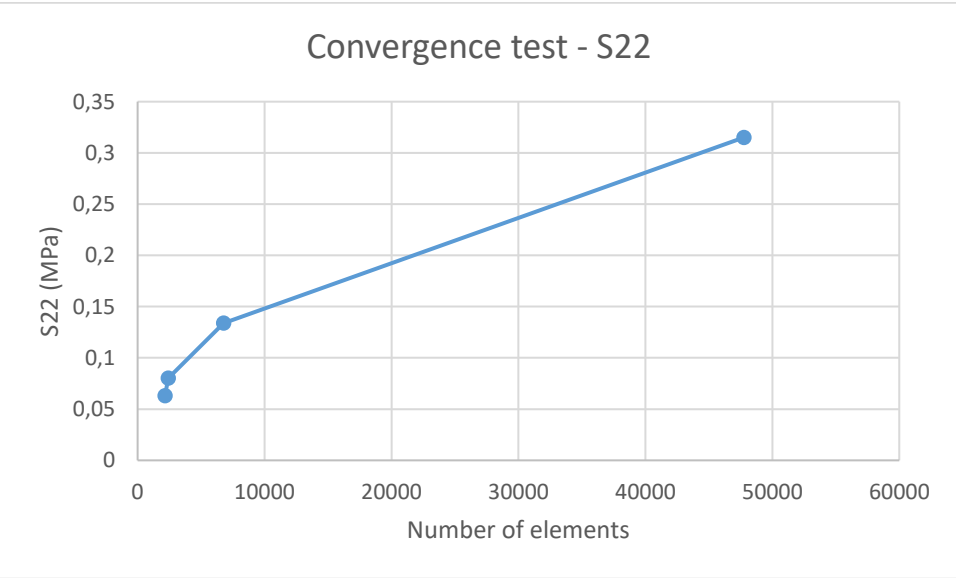


FIGURE 59) FINITE ELEMENT SIZE VARYING FROM 5, 10, 15 AND 20 MM.

Critical section

After investigation of the structural behavior based on stresses in a point of the interlocking geometries, the actual failure of the joint was considered.

To evaluate the structural performance of the joint, its capacity investigated. This is done using the Tsai Wu Approach developed in subchapter 5.1. Before the capacity can be evaluated, the failure mechanism of the joint must be predicted.

After investigating the structural behavior based on the most utilized point in the joint, the actual failure mechanism of the joint is further considered. The critical S22 stress is assumed to be a singularity in the Finite Element Method model. However, it is further assumed that the high values of stress components indicate a stress concentration that needs to be considered in a further investigation.

For the stress tensor components S11, S22 and S33, both negative and positive maximum (absolute) values are obtained, to investigate both compressive and tensile stresses.

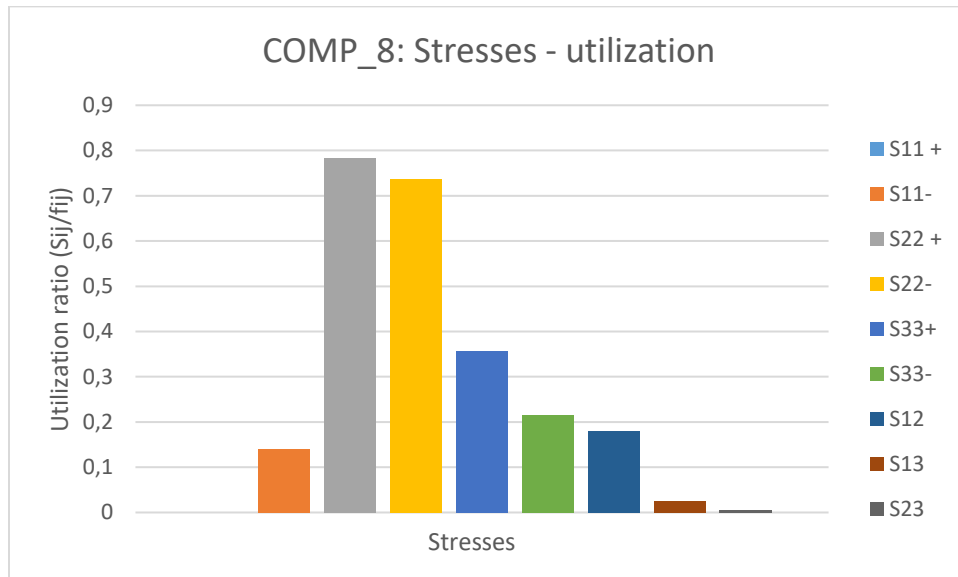


FIGURE 60) UTILIZATION RATIO OF THE HIGHEST STRESS TENSOR COMPONENT VALUES I COMP_8

The locations of all stress tensor components are further investigated (S11, S22, S33, S12, S13, S23), and the contour plots of each component are examined. Based on the observation of the contour plots, graphical stress flow maps are create, see figure 61. These stress flow maps are assumed to contribute in the evaluation of stress concentrations, as well as finding the critical section of the joint.

In figure 62, the locations of the most critical stress tensor components are located. This implies the highest level of all stress components, both tensile stress and compressive stress. The stress tensor components S13 and S23 are neglected due to relatively low values. This indicates a high level of compression stress (negative sign) at the top of the joint, where the angled members interfere. The critical tensile stresses are located in the corner of the “first step” on the interlocking geometry, see figure 63. High levels of S12 were observed in both areas.

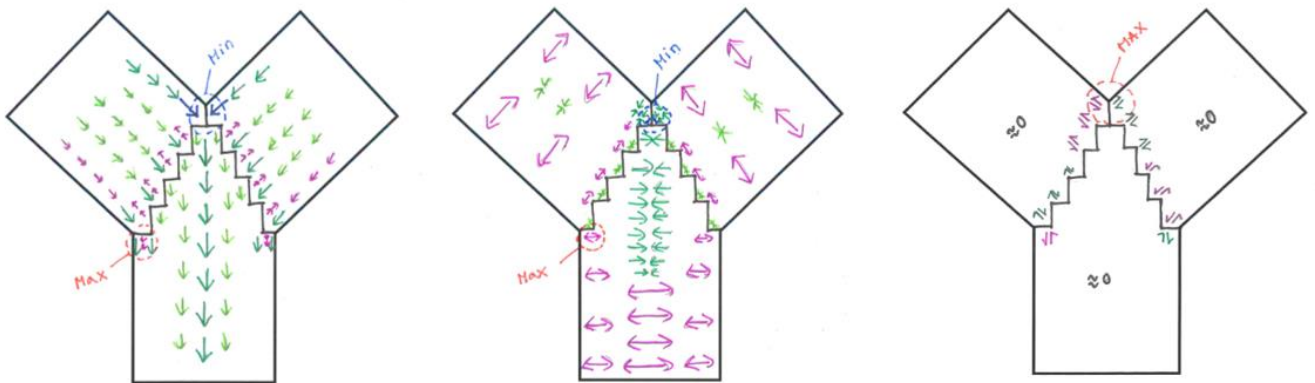


FIGURE 61) STRESS FLOW MAP

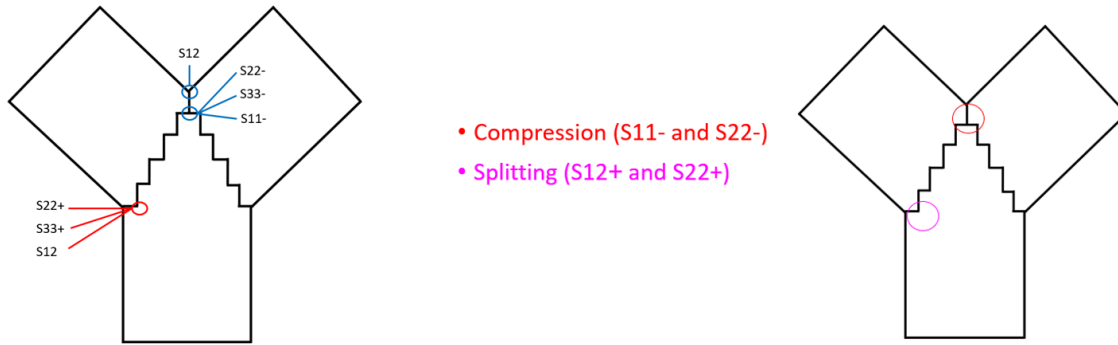


FIGURE 62) TO THE LEFT, THE LOCATION OF THE MOST CRITICAL VALUES OF THE STRESS TENSOR COMPONENTS. TO THE RIGHT, THE CRITICAL AREAS ARE HIGHLIGHTED.

Based on these observations, two critical areas that could determine the capacity of the joint are assumed. One of these areas is due to the high level of compression stresses. The other critical area can be compared with the critical section in chapter 5.1. With a high level of S22 stress combined with S12 shear stress, a crack can propagate and cause the “splitting” of fibers. The critical areas are further investigated by the method used in chapter 2.1, by creating two paths, each representing one critical area, see figure 63.

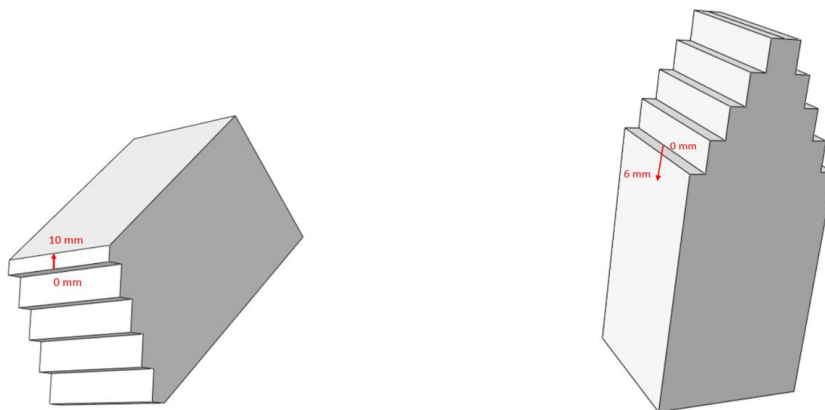


FIGURE 63) TO THE LEFT: PATH 1, 10 MM LONG AND INVOLVES 5 ELEMENTS AND 6 NODES. TO THE RIGHT: PATH 2, 5 MM LONG AND INVOLVING THREE ELEMENTS AND 4 NODES.

Refined Mesh

The mesh in the critical areas is refined with local seed sized finite elements of 2 mm, and the finite element analysis updated. This is done to avoid distorted finite elements close to the interlocking geometry in COMP_8.

The Tsai Wu Approach

The calculation of the plane stress situations in both critical sections involves three stress tensor components of high values. However, in this investigation only two parameters will be considered in the Tsai Wu approach. In further development of the Tsai Wu criterion, all critical components should be evaluated.

Based on the stress flow map combined with the stress utilization ratios, S_{22} and S_{11} along path 1 (compression zone) is given in figure 64, with the adapted Tsai Wu criterion curve, see figure 64. From this figure, we can observe that a point in the material along path is close to fully utilized. However, it must be taken into consideration that this is represented by the highest S_{22} stress tensor component in one point and can be a singularity. For further capacity investigation, each point representing stress along the path could “step outside” the Tsai Wu curve.

The S_{12} and S_{22} stress along path 2 can be found in figure 65. This combination of stress represents the same failure phenomena as in chapter 5.2.

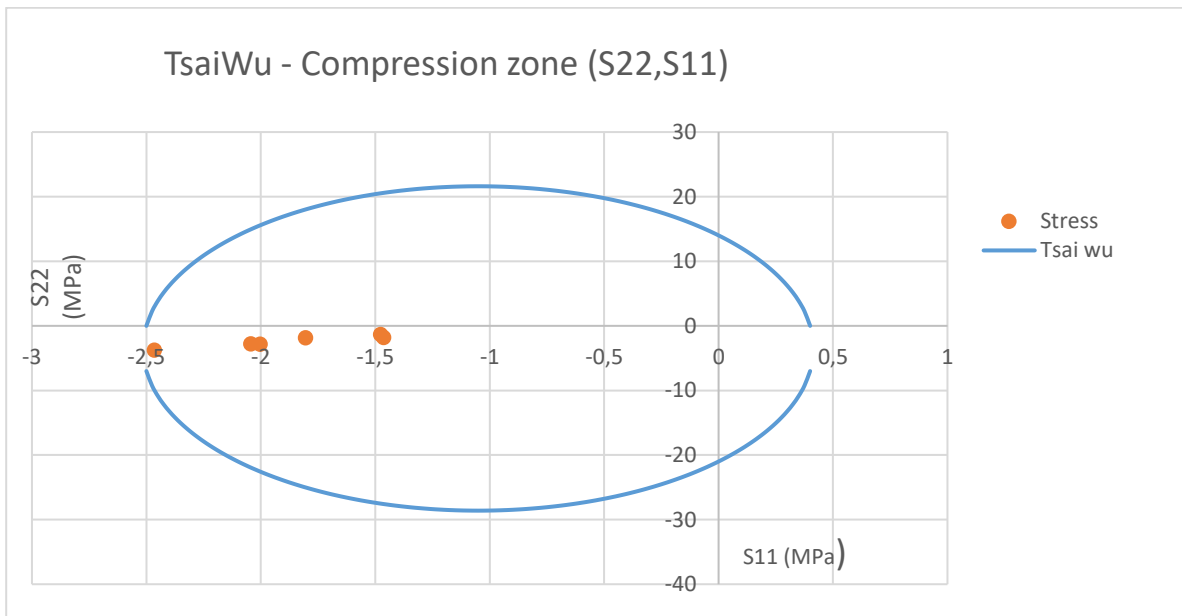


FIGURE 64) TSAI WU APPROCH OF COMPRESSION PATH 1. ORGANGE POINTS REPRESENTING S22 AND S11 IN ALONG THE PATH

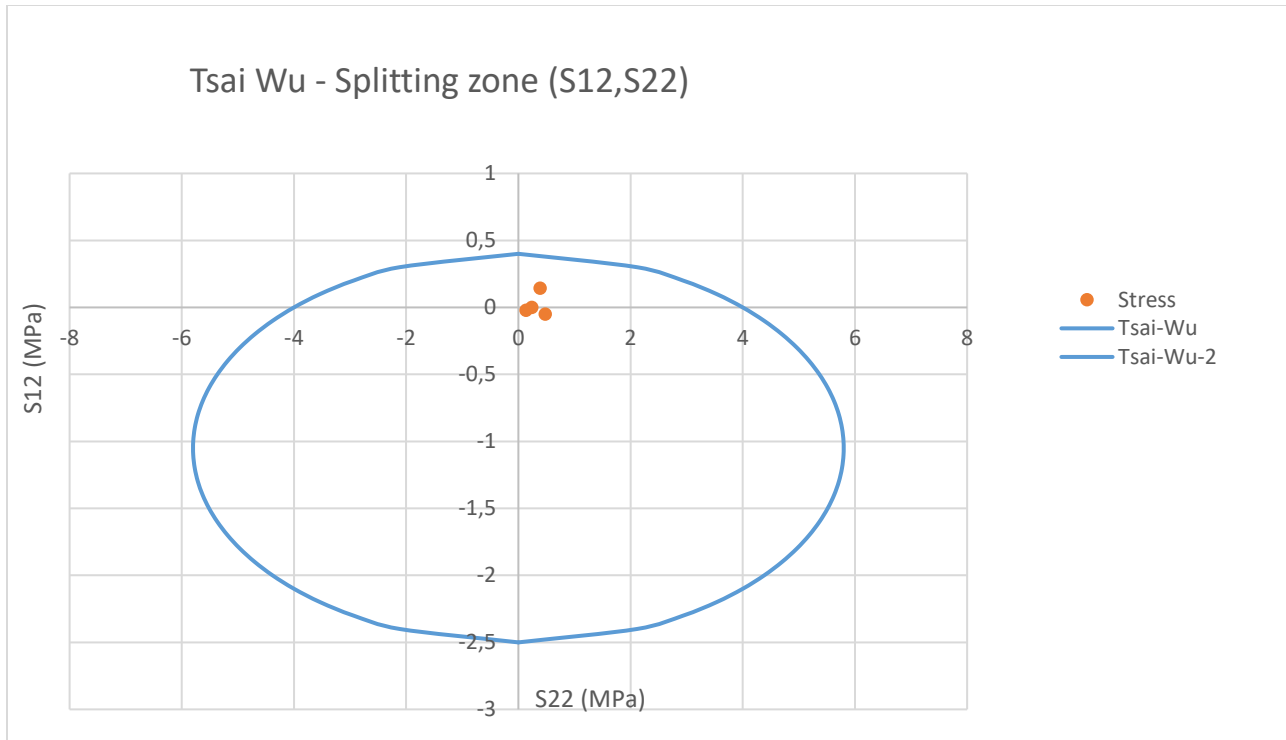


FIGURE 65) TSAI WU APPROCH OF COMPRESSION PATH 1. ORGANGE POINTS REPRESENTING S22 AND S12 IN ALONG THE PATH

Further capacity control of this joint will not be done in this investigation. However, by observing the stress flow, the Tsai Wu approach and intuitive consideration of the structural situation, the investigations done in chapter 5 can be used in further development of a potential form-finding method of integral attachment timber joints.

6 FORM-FINDING OF A JOINT IN A GLOBAL WORKFLOW

Through the preceding chapters, I have managed to collect and sort information about integral attachment timber joints. Moving on into this chapter, I would like to combine this knowledge gained, in seeking to design a complex structure with integral attachment timber joints. In order to do this, a parametric code of a structure with implementation of a parametric integral attachment joint design will be established.

6.1 GENERAL WORKFLOW

A potential form-finding of the integral attachment timber joints will be considered implemented in a digital workflow of parametric structural design, referred to as the “General Workflow” given in Appendix A. This workflow is considered for grid shell structures of timber members only, constructed by robot assembly. The workflow is based on previous research done by the Conceptual Structural Design at the Department of Structural Engineering, at NTNU[6]. The design and form-finding of the shell shape is assumed to follow the theoretical workflow developed by Åshild Huseby and Marie Eliasson, presented in their master thesis «The Digital Workflow of Parametric Structural Design - Developing Grid Shells in a Nordic Climate» .

In addition, the General Workflow is influenced by the method of designing, producing and assembling interlocking shell segments, used at the AAG 2018 workshop. Details and information about this workshop are elaborated in chapter 3. This involves a method of designing interlocking joints on a standard joint configuration. The design is further transposed to every nonstandard joint configuration on the final shell shape, which allows the construction method of robot assembly. Hence, simulation of robot fabrication and robot assembly is considered important elements in the implementation of the General Workflow.

6.2 POTENTIAL FORM-FINDING METHOD

Before the design of integral attachment timber joints are implemented in a global parametric model, the potential form-finding method obtained on a base by the structural analysis and observations made in preceding chapter, is further elaborated in this subchapter.

Optimal shape

To develop a form-finding method, an “optimal shape” must be defined based on the purpose of the structural feature considered. In this context, the optimal shape of an integral attachment timber joint is assumed fulfilment of following requirements:

- Embedded assembly logic
- Possible to fabricate with available manufacturing tools
- Enable unit complexity
- Optimal load-bearing capacity (structural optimization)

Further elaboration of the potential form-finding method will consider the requirements of structural optimization.

The most critical section

To find the shape of the integral attachment timber joint with optimal load-bearing capacity, the considered failure mechanism must be defined. The interlocking functionality of integral attachment joints is ensured by the integral attached features. For that reason, the bearing-capacity of the integral attachment feature is assumed to decide the capacity of the joint. From structural analysis in chapter 5, the joint is further assumed to fail as the utilization of the “most critical section” in the integral attachment feature is exceeded. Hence, the most critical section must be found in every shape investigated.

Tsai- Wu criterion

To evaluate the capacity of structural shapes, an adequate material failure criterion is required. By the assumption of failure due to exceeded capacity of *the most critical section*, a criterion which evaluates the complexity of a plane stress situation in an anisotropic material is required. Based on the investigations/discussions in chapter 5, the Tsai Wu material failure criterion is suggested.

Utilization calculations of the integral attachment timber joints in chapter 5, based on characteristic strength properties (chapter 5) and the Tsai Wu failure criterion, resulted in the following conclusion:

- The capacity of the joint cannot be decided by high stress levels in a single point (singular points and stress concentrations).
- The most critical section of the integral attachment joint must be detected.
- The most critical section depends on the joint configuration and subjected load (compression joint vs. tension joint, in chapter 5).

It is further assumed that as the interlocking geometry of the integral attachment feature is parametrically changed, so is the most critical section. In addition, the most critical section depends on the joint configuration and its imposed loads. This observation is based on the results from the tension- and the compression joints in chapter 5.

In previous subchapters, the detection of the most critical section was done manually (intuitive investigation of Abaqus/CAE-results). To achieve a rapid form-finding method, this process should be automatized. However, this will not be further investigated in this form-finding proposal.

Potential form-finding method

The proposed potential form-finding method is illustrated by a graphical map given in Appendix A. The method will further be explained in steps from 0- 4, based on this graphical map.

Step 0.

A *basic joint configuration* with an initial interlocking geometry is created visually in Rhino by Grasshopper. This is the starting point for generating the interlocking geometry. The basic joint configuration is given by the shell grid projected into a two-dimensional plane (see General workflow). There can be one or more basic joint configurations, depending on the two-dimensional shell grid geometry. The basic joint configurations are defined by the intersecting points in the two-dimensional shell grid, with associated intersecting members. A specific basic joint configuration has the same number of intersecting members and is imposed on the same load. The imposed load refers to the forces in the joint members calculated from the global structure. As input for generating the interlocking geometry, the imposed load on the basic joint configuration is set to unit magnitude.

Step 1.

Further, an adequate finite element model of the basic joint configuration is generated with a subsequent finite element analysis. The tensor stress components at the most critical section of the joint members are obtained from the FEM-results, see chapter

Step 2.

In the next step, the stresses on the most critical section obtained are compared with the Tsai Wu criterion- curve (chapter 5).

In an iterative manner step 1 and step 2 are repeated as the magnitude of the imposed load is increased (unite magnitude in step 0.). The iteration process stops as the stress-curve (stress along the critical section) “steps outside” the criterion-curve, see (chapter 5). The most critical section is fully utilized.

Step 3.

The load-bearing capacity of the joint can be calculated from load causing full utilization of the integral attachment feature.

The steps described above (step 1- step 3) are repeated, as a parametric adjustment of the interlocking geometry is done between step 1 and step 3. Changing numbers of interlocking steps in the “staircase”-geometry of the compression joint in previous chapter (5.2), is an example of such parametric adjustment.

Step 4.

When all investigated shapes, controlled by parameters in the parametric model, have been evaluated the joint geometry with the highest capacity is detected. Hence, the optimal integral attachment timber joint design is found. The global workflow of the structure can continue.

6.3 IMPLEMENTATION OF JOINT DESIGN IN A GLOBAL PARAMETRIC MODEL

GLOBAL GRID SHELL

A global model of a grid shell is modelled in Grasshopper, making Rhino only a visual environment to make the model as parametric as possible. However, the shape of the grid shell is not the focus of this parametric model. As the aim of this parametric code is to implement a parametric joint design into the global model, the structure is a simple two-dimensional grid shell of hexagonal cells. The grid shell is further assumed to be in pure compression.

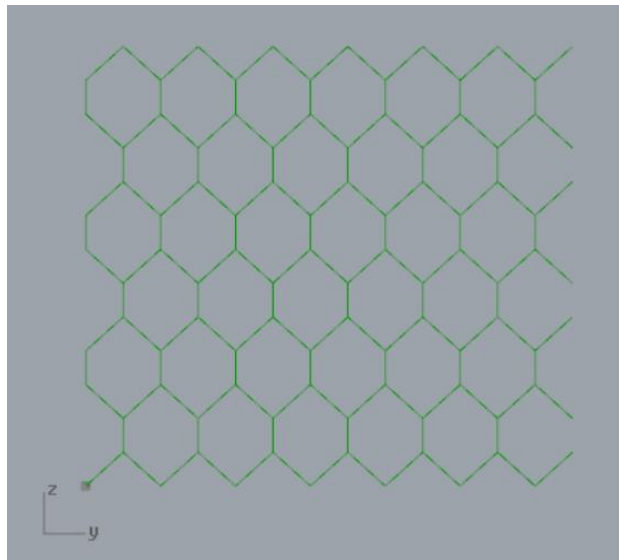


FIGURE 66) GLOBAL GRID SHELL

Parameters considered in the global shape

The parameters considered in the geometry of the grid shell is the size (hence number of) cells in the grid. The number of intersecting points can be changed in the horizontal and vertical directions, changing both the size and the number of cells.

INTERLOCKING JOINT GEOMETRY

The parametric modeling of the grid shell is so far a geometry of simple lines. The structural members with its interlocking geometry will be applied in the following.

From the geometry of the global grid shell, there is only one type of basic joint configuration. This joint configuration consists of three intersecting members (see figure 56), subjected to pure

compression. A parametric interlocking geometry will further be created on the basic joint configuration.

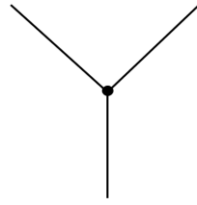


FIGURE 67) BASIC JOINT CONFIGURATION

Following the General workflow (Appendix A), the cross-section data of each joint member is assumed given by an optimization process of the global grid shell. A parametric interlocking line which represents the interference surfaces between the joint members is created, see figure 57. Each joint member has an integral attachment joint geometry given by this interlocking line.

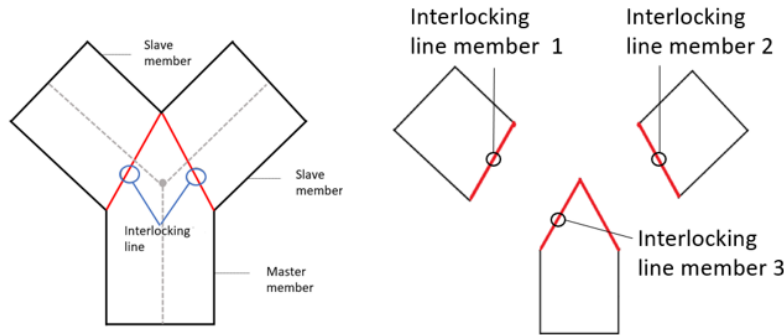


FIGURE 68) JOINT CONFIGURATION WITH PARAMETRIC MODELLED INTERLOCKING LINE.

Parameters considered on the interlocking geometry

The parameters considered are based on the investigations done in chapter 5.2. The interlocking line is parametrically designed as a “steps in a stair” (see figure 58). By adjusting a slider, the number of steps can be adjusted. See step 4 in figure 58.

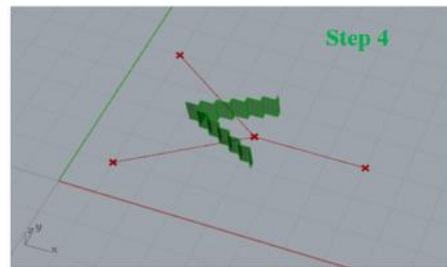
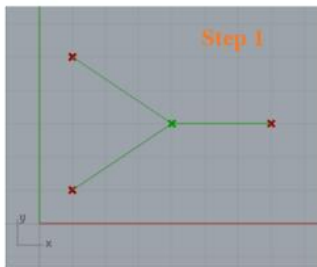
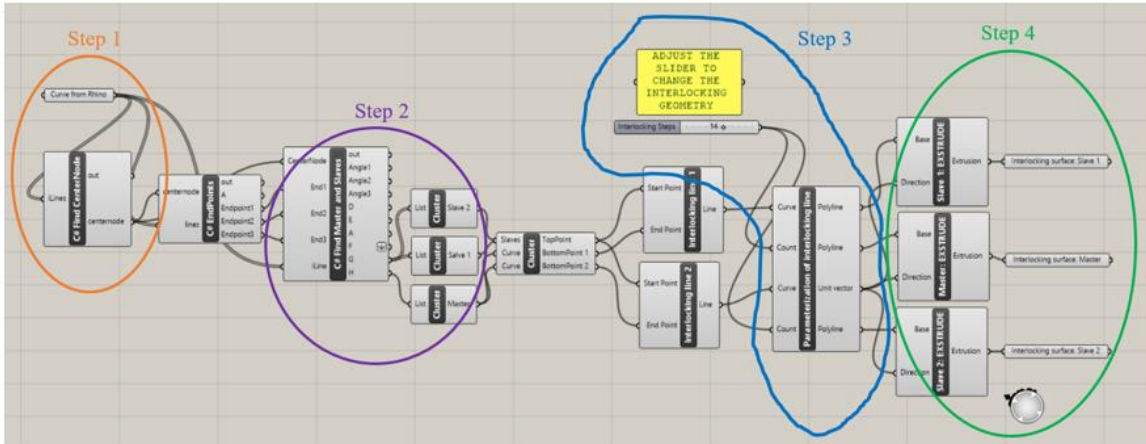


FIGURE 69) CODE IN GRASSHOPPER WITH VISUALIZATION OF EACH STEPS. STEP 1) IDENTIFYING THE INTERSECTION POINT AND THE ASSOCIATED INTERSECTION MEMBERS STEP 2) DEFINING “MASTER” AND “SLAVE” 3) CREATE A 2D INTERLOCKING PARAMETRIC “STAIR” 4) EXTRUDING THE GEOMETRY INTO A INTERLOCKING SURFACE

Nonstandard joint configurations

The interlocking geometry is modeled to adapt to any nonstandard joint configurations. This means that the interlocking geometry can be applied to any joint configuration geometry with the same number of joint members in the grid shell. The joint member with the smallest angle between their axes is defined in Grasshopper as “slaves”. The remaining member is defined as “master” (see figure 57). Using these definitions, the interlocking geometry will adapt to the new nonstandard configuration.

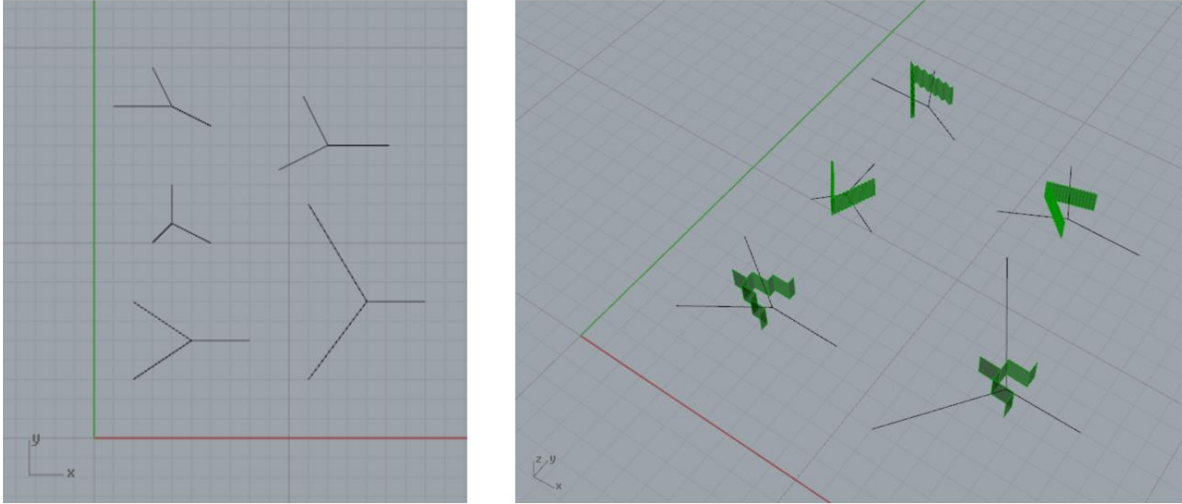


FIGURE 70) INTERLOCKING GEOMETRY ON NONSTANDARD JOINT CONFIGURATIONS.

Interlocking geometry applied grid shell

The interlocking geometry created is assigned to each intersection point in the global model. As a result of the identifications as “slaves” and “masters”, the interlocking geometry will assume the correct configuration according to its intersecting members. The interlocking geometry represents the interfering surface between the joint members in each joint. The structural members can now be created by extruding between the interlocking surfaces on each end (connection end of the member), see figure 60. The result is a global grid shell with a parametric modeled interlocking joint geometry.

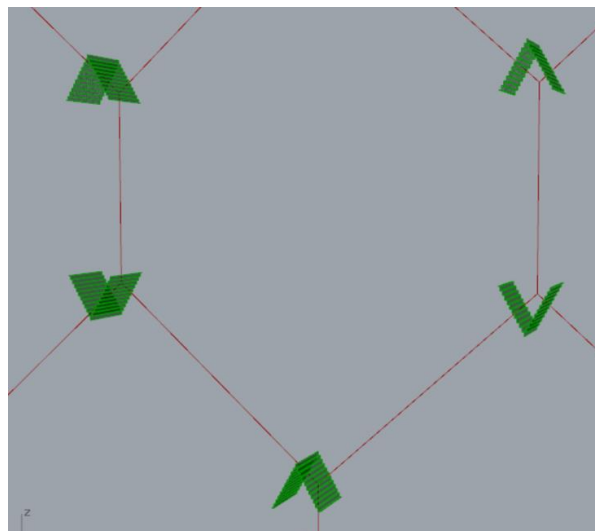


FIGURE 71) THE GLOBAL GRID WITH INTERLOCKING GEOMETRY

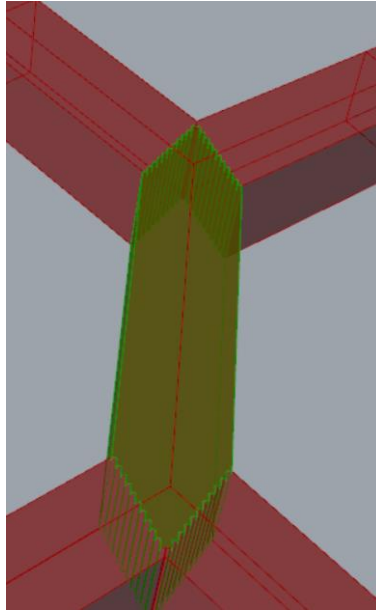


FIGURE 72) JOINT MEMBER WITH INTERLOCKING GEOMETRY ON EACH END.

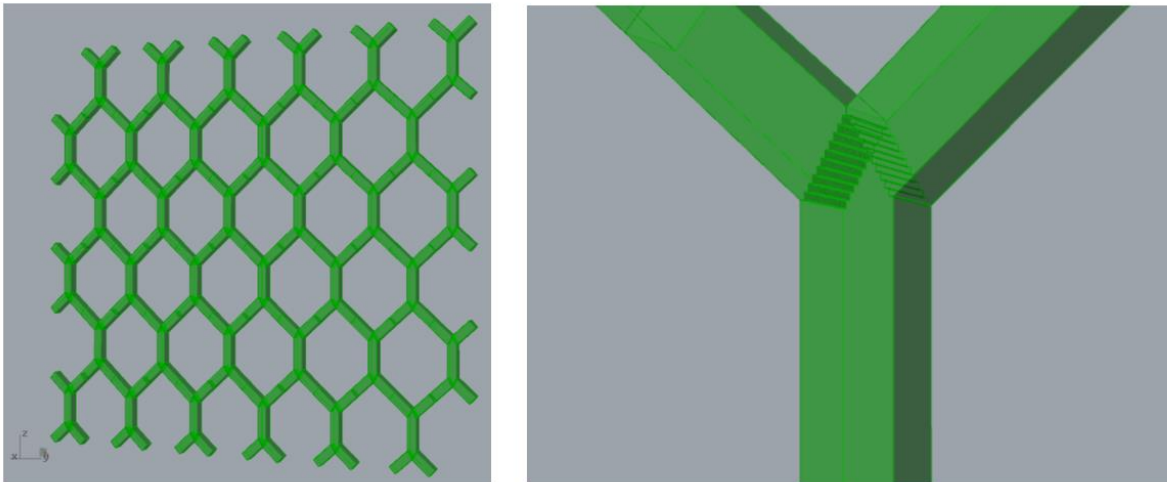


FIGURE 73) GLOBAL GRID WITH THE PARAMETRIC MODELED JOINT GEOMETRY

- Future work include the form-finding in the parametric model

7 CONCLUDING REMARKS

Through the work of this master thesis my knowledge on computer design, finite element method, timber and design of structural joints has grown. The process has been highly educational. From this project I have been given the opportunity to learn sophisticated digital designing tools from high skilled people, that have taken their time to educate me. I have also experienced the advantages of a digital workflow of parametric structural design, and the future opportunities. I am also left a better understanding on how structural joints works, and the importance in their details.

Further Work

In this master thesis a potential form finding method for integral attachment timber joint have been investigated, but the work is far from done. By further work, an automatized method for finding the critical section in an integral attachment timber joint should be elaborated. However, before any final evaluation of the method created (the Tsai Wu criterion) can be done, the study should be compared with empirical investigations.

A parametric tool for structural analysis with solid finite elements, should be incorporated in the parametric environment of Rhino and grasshopper. This would enable rapid structural analysis of a wide range of shapes.

8 REFERENCES

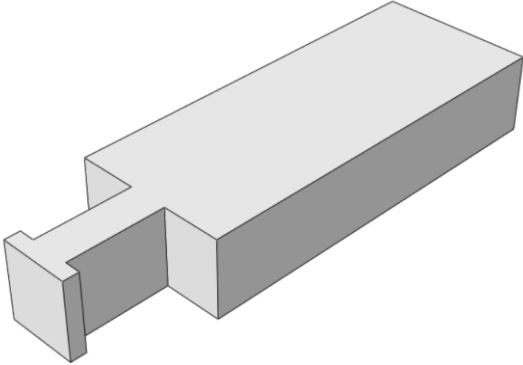
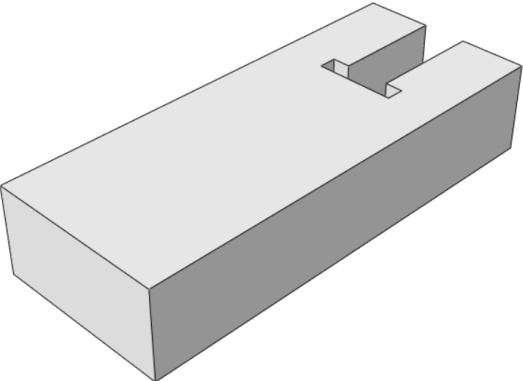
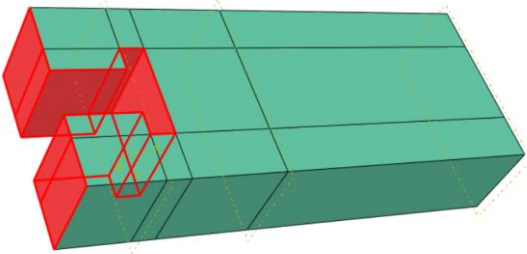
- [1] Veenendaal D. Adrianssens, Block P, Williams C., and Veenendaal D. *Shell structures for architecture: Form finding and optimization*. Routledge.
- [2] Kolbein Bell. 2014. *FINITE ELEMENT ANALYSIS of linear structural mechanics problems*. fagbokforlaget.
- [3] BillWagner. C# Programming Guide. Retrieved January 31, 2019 from <https://docs.microsoft.com/en-us/dotnet/csharp/programming-guide/>
- [4] Kristian Berbom Dahl. Mechanical properties of clear wood from Norway spruce. 140.
- [5] Christian Fossen. Digital production and assembly - Research - Conceptual Structural Design - Department of Structural Engineering. Retrieved January 19, 2019 from <https://www.ntnu.edu/kt/research/csdg/research/digital>
- [6] Christian Fossen. Research - Conceptual Structural Design - Department of Structural Engineering. Retrieved January 31, 2019 from <https://www.ntnu.edu/kt/research/csdg/research>
- [7] Scott Davidson created this Ning Network. Grasshopper. Retrieved January 31, 2019 from <https://www.grasshopper3d.com/>
- [8] Marcia Patton-Mallory and Steven M Cramer. 1987. Fracture mechanics: a tool for predicting wood component strength. *For. Prod. J.* 37, 7 (1987), 9.
- [9] Jack Porteous and Abdy Kermani. *Structural Timber Design to Eurocode 5*. John Wiley and Sons Ltd.
- [10] AAG 16 Admin User. AAG 2018. Retrieved January 31, 2019 from <http://www.architecturalgeometry.org/aag18/>
- [11] AAG 16 Admin User. Workshop 15: Interlocking-based Robotic Fabrication of Segmented Shells: Formwork-free and mortar-free assembly. AAG 2018. Retrieved January 31, 2019 from <http://www.architecturalgeometry.org/aag18/workshop-15-interlocking-based-robotic-fabrication/>
- [12] Robert W. Messler. 2004. *Joining of materials and structures : from pragmatic process to enabling technology*. Amsterdam ; Boston : Elsevier, ©2004.
- [13] Robert W. Messler. 2011. *Integral Mechanical Attachment: A Resurgence of the Oldest Method of Joining*. Butterworth-Heinemann; 1 edition.
- [14] Robert W. Messler. 2011. *Integral Mechanical Attachment: A Resurgence of the Oldest Method of Joining*. Butterworth-Heinemann; 1 edition.
- [15] Eric W. Weisstein. Ruled Surface. Retrieved January 31, 2019 from <http://mathworld.wolfram.com/RuledSurface.html>
- [16] 2013. 9 spa by a21studio. *Dezeen*. Retrieved January 31, 2019 from <https://www.dezeen.com/2013/06/19/9-spa-by-a21studio/>
- [17] 2014. Landesgartenschau Exhibition Hall / ICD/ITKE/IIGS University of Stuttgart. *ArchDaily*. Retrieved January 31, 2019 from <http://www.archdaily.com/520897/landesgartenschau-exhibition-hall-icd-itke-iigs-university-of-stuttgart/>
- [18] 2017. frihetsgrad – fysikk. *Store norske leksikon*. Retrieved January 28, 2019 from http://snl.no/frihetsgrad_-_fysikk
- [19] Stonehenge. *English Heritage*. Retrieved January 31, 2019 from <https://www.english-heritage.org.uk/visit/places/stonehenge/>
- [20] Pantheon | building, Rome, Italy. *Encyclopedia Britannica*. Retrieved January 31, 2019 from <https://www.britannica.com/topic/Pantheon-building-Rome-Italy>
- [21] Form Finding Lab – Princeton University. Retrieved January 19, 2019 from <http://formfindinglab.princeton.edu/>
- [22] The Meticulous Art of Traditional Japanese Woodworking. Retrieved January 30, 2019 from <https://www.stonebridge.com/sbp-blog/the-meticulous-art-of-traditional-japanese-woodworking>
- [23] Pinterest. *Pinterest*. Retrieved January 31, 2019 from <https://no.pinterest.com/pin/703687510504607109/>
- [24] Eurocode 3: Design of steel structures - Part 1-8: Design of joints (1993-1-8) 1.4.4 ,.
- [25] Eurocode 3: Design of steel structures - Part 1-8: Design of joints (1993-1-8) ,1.4.3.
- [26] McNeel Europe - Contact us. Retrieved January 31, 2019 from <http://www.mcneel.com/contact>
- [27] Abaqus CAE - SIMULA™ by Dassault Systèmes®. Retrieved January 31, 2019 from <https://www.3ds.com/products-services/simulia/products/abaqus/abaquscae/>

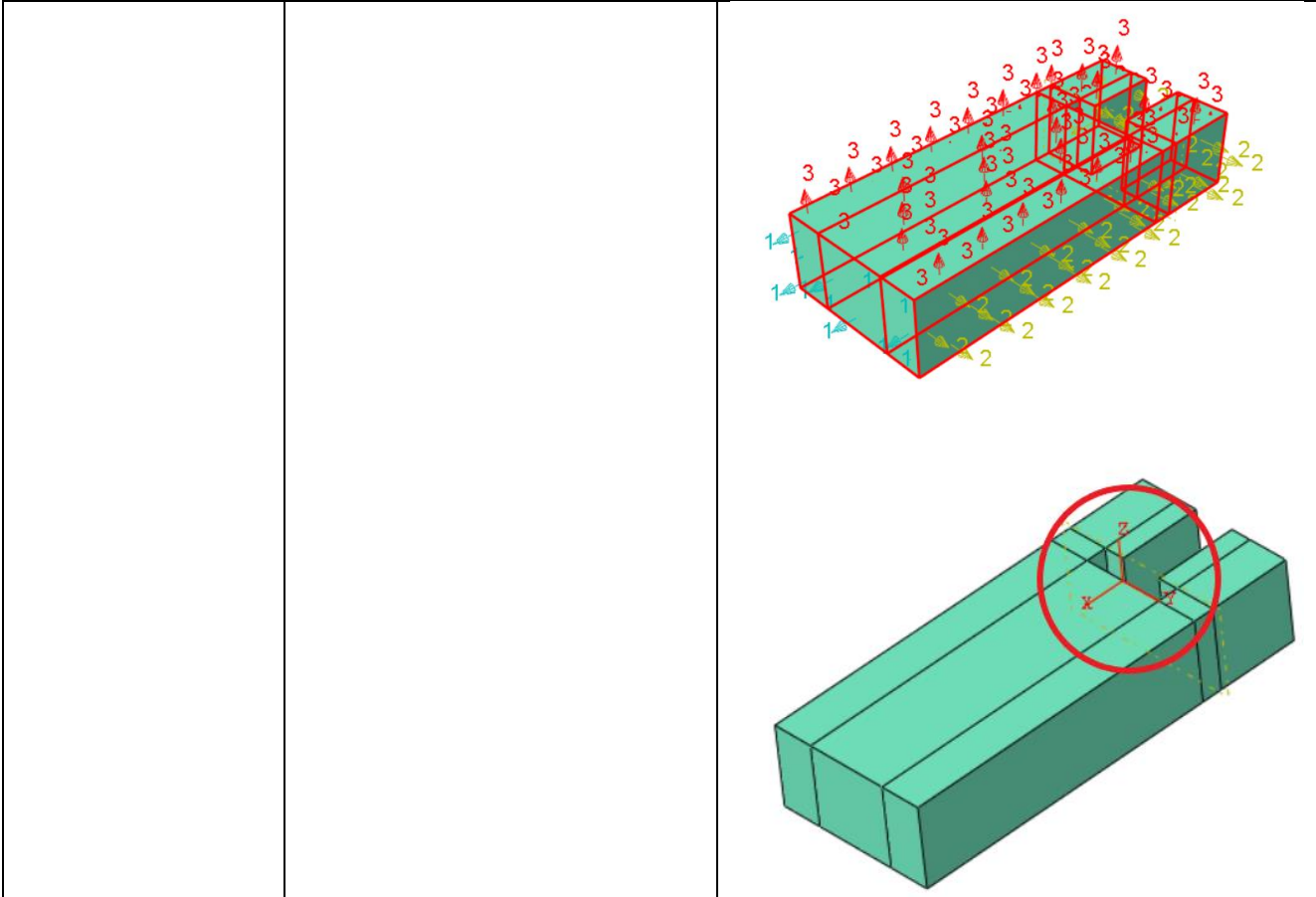
- [28] Industrial_Robots_2016_Chapter_1_2.pdf. Retrieved January 31, 2019 from https://ifr.org/img/office/Industrial_Robots_2016_Chapter_1_2.pdf
- [29] industrial intelligence 4.0_beyond automation. KUKA AG. Retrieved January 31, 2019 from <https://www.kuka.com/en-se>
- [30] MORPH | meaning in the Cambridge English Dictionary. Retrieved January 31, 2019 from <https://dictionary.cambridge.org/dictionary/english/morph>
- [31] EN1995_5_Leijten.pdf. Retrieved January 29, 2019 from https://eurocodes.jrc.ec.europa.eu/doc/WS2008/EN1995_5_Leijten.pdf
- [32] Cross section of a tree. *Tree Growth and Structure*. Retrieved January 31, 2019 from <http://treegrowthstructure.weebly.com/cross-section-of-a-tree.html>
- [33] (kilde) EN 1995-1-1 Design of timber structures-Part 1-1: General- Common rules and rules for buildings. EC5, section 5- structural analysis requirements for timber structures).
- [34] EN 338 - Table 1 - Strength classes - Characteristic Values.
- [35] Rhino 6 for Windows. Retrieved January 31, 2019 from <https://www.rhino3d.com/>
- [36] Abaqus Analysis User's Guide, vol3. 707.
- [37] Matter, elements, and atoms. *Khan Academy*. Retrieved January 31, 2019 from <https://www.khanacademy.org/science/biology/chemistry--of-life/elements-and-atoms/a/matter-elements-atoms-article>
- [38] 2017 SOLIDWORKS Help - Tsai-Wu Failure Criterion. Retrieved January 31, 2019 from http://help.solidworks.com/2017/english/SolidWorks/cworks/r_tsaiwu_failure_criterion.htm

9 APPENDIX

Pre-processing: Basic analysis (Abaqus/CAE) Chapter 5

Definitions on information given in this table can be found on the Abaqus/CAE home page [34]

Process	Explanation	Visualization								
<p><u>Parts</u> The geometry made in Grasshopper Imported as “Parts” into Abaqus where they are assigned structural properties</p> <p>a) Features b) Sets c) Surface d) Section Assignment e) Orientation f) Mesh</p>	<p>a) <u>Feature:</u></p> <ul style="list-style-type: none"> - Geometry import from GH as a SAT-fil - Partitioning parts into meshable cells to select “structured meshing technique”. <p>b) <u>Surface:</u></p> <ul style="list-style-type: none"> - Defining surfaces on the tendon and the mortise part that are interacting with each other. <p>c) <u>Section assignment:</u></p> <ul style="list-style-type: none"> - Assigning the part created section (See property’s) <p>d) <u>Orientation</u></p> <ul style="list-style-type: none"> - Assign the part a coordinate system with 1-,2- and 3 -axis to assign local material <table border="1" data-bbox="505 1031 842 1194"> <thead> <tr> <th>Axis XYZ-CSYS</th> <th>Axis 123- CSYS</th> </tr> </thead> <tbody> <tr> <td>x</td> <td>1</td> </tr> <tr> <td>y</td> <td>2</td> </tr> <tr> <td>z</td> <td>3</td> </tr> </tbody> </table> <p style="text-align: center;">orientation:</p> <p>e) <u>Mesh</u></p> <ul style="list-style-type: none"> - Assign chosen mesh to parts (See mesh) 	Axis XYZ-CSYS	Axis 123- CSYS	x	1	y	2	z	3	<p>Two solid ACIS geometries:</p> <p>Part 1) Tendon</p>  <p>Part 2) Mortise</p>  <p>Interacting surfaces on part 2</p> <ul style="list-style-type: none"> - Green color means that the part is assigned section properties - Red color is the defined surface  <p>Orientations according to created coordinate system on parts</p>
Axis XYZ-CSYS	Axis 123- CSYS									
x	1									
y	2									
z	3									



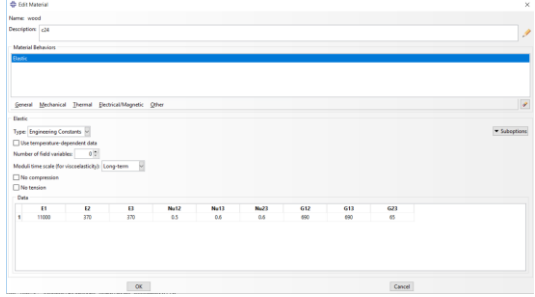
Property
 Defining structural properties
 a) Material
 b) Section

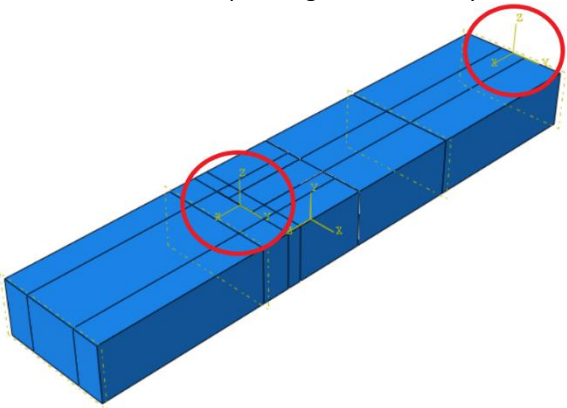
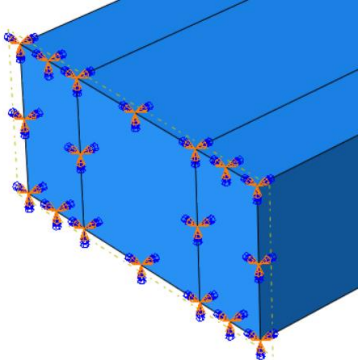
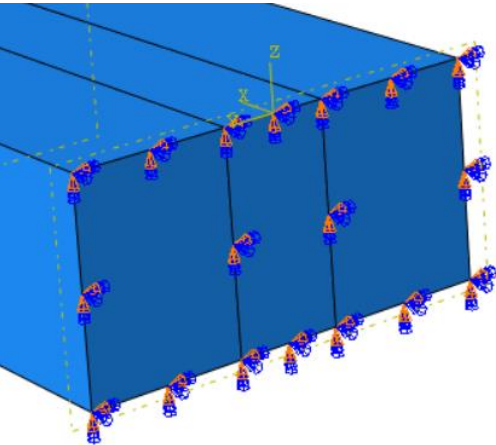
- a) Material – Wood
- Elastic material behavior
 - Structural timber (softwood), strength class C24, Norwegian spruce
 - Orthotropic behavior
 - Engineering constants:

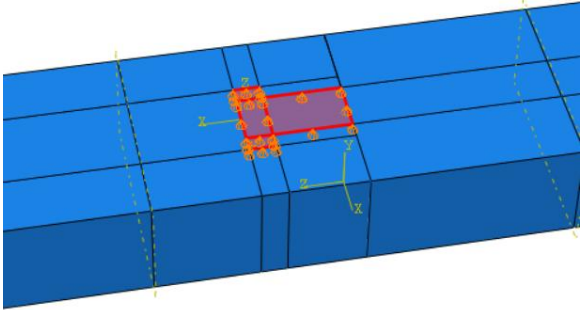
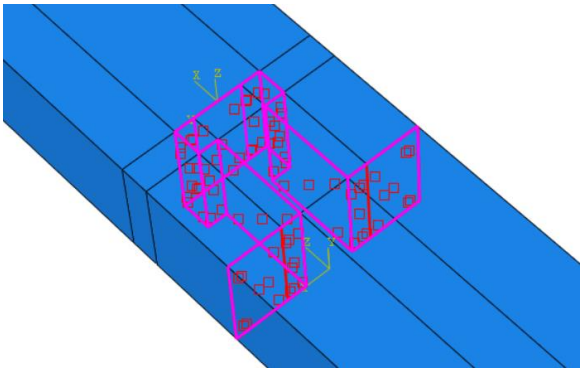
E ₁	10991
E ₂	716
E ₃	435
NU ₁₂	0.42
NU ₁₃	0.48
NU ₂₃	0.5
G ₁₂	682
G ₁₃	693
G ₂₃	49

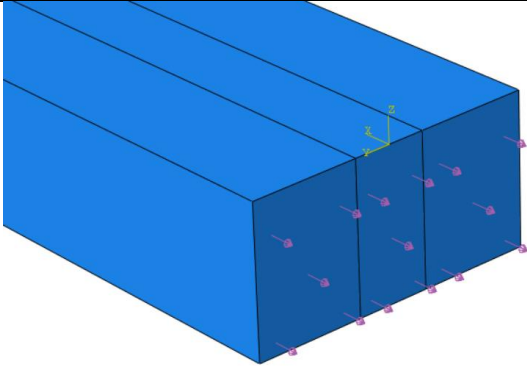
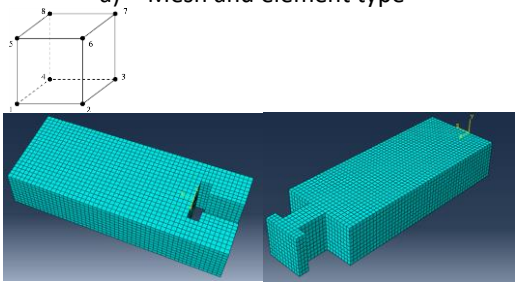
- b) Section
- Creating a section defined as a homogeneous solid assigned with the defined material -Wood

Abaqus Material definition
 c) Material properties in Abaqus

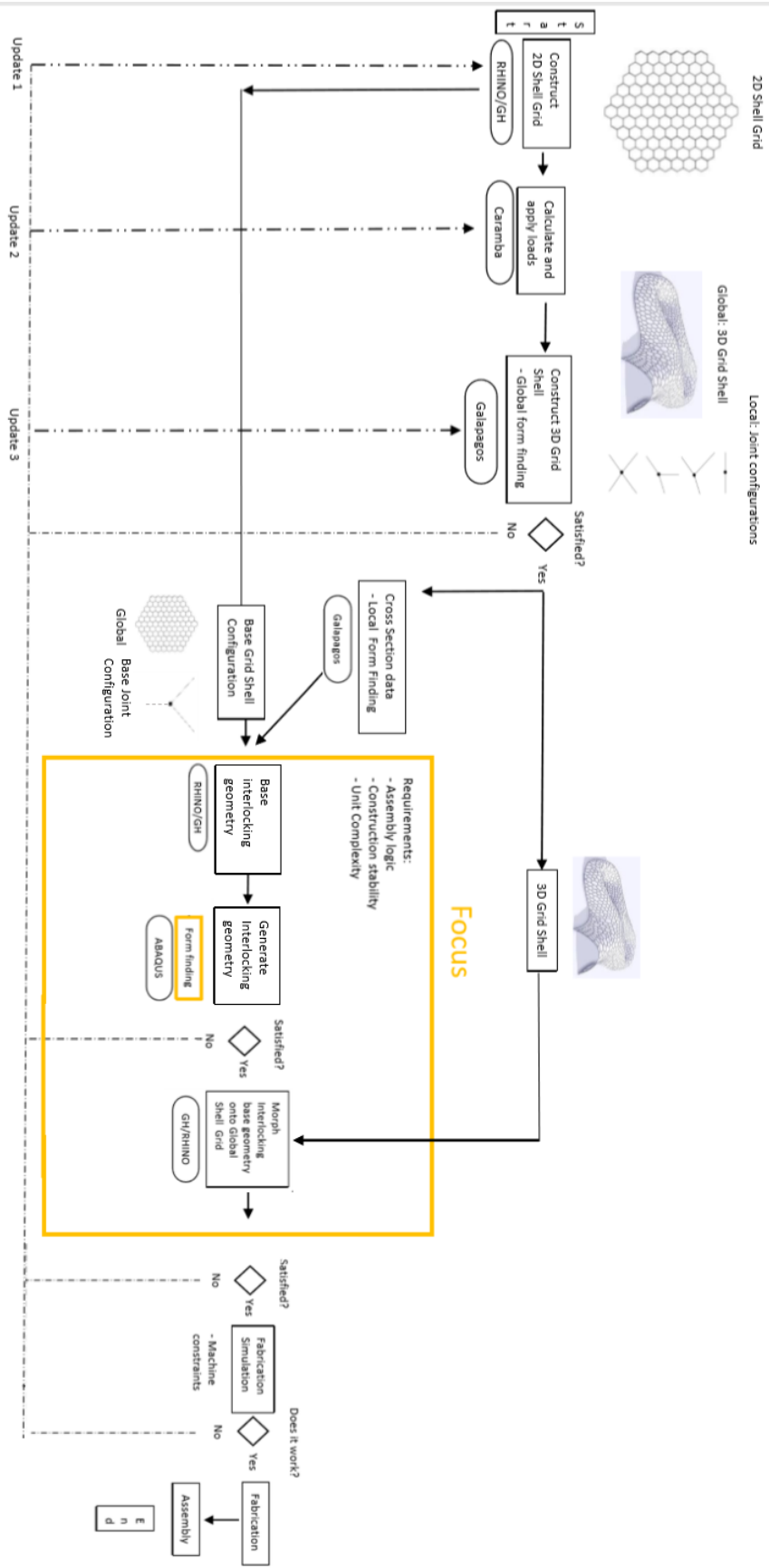


<p>Assembly Parts are assembled into one instance as a structural system</p> <p>a) Instance</p>	<p>a) Parts 1 and 2 are assembled to one connection/joint in interlocking position Collecting part 1 and 2 in the right position by choosing coincident points on interacting surface The coordinate systems assigning the local material orientations on each part needs to correspond in the assembled instance</p>	<p>Instances with corresponding coordinates system</p> 																																				
<p>Steps Abaqus follows two steps</p> <p>a) The Initial step</p> <p>b) Analysis step</p>	<p>a) The initial step</p> <ul style="list-style-type: none"> - Procedure: static, general - Creating boundary conditions: <ol style="list-style-type: none"> 1. Encased mortise- <table border="1" data-bbox="475 982 870 1283"> <tr><td>U1</td><td>x-displacement</td><td>0</td></tr> <tr><td>U2</td><td>y-displacement</td><td>0</td></tr> <tr><td>U3</td><td>z-displacement</td><td>0</td></tr> <tr><td>UR1</td><td>Rotation about the x-axis</td><td>0</td></tr> <tr><td>UR2</td><td>Rotation about the y-axis</td><td>0</td></tr> <tr><td>UR3</td><td>Rotation about the z-axis</td><td>0</td></tr> </table> <p style="text-align: center;">end:</p> <ol style="list-style-type: none"> 2. Tendon- end that can move in longitudinal direction <table border="1" data-bbox="475 1520 870 1820"> <tr><td>U1</td><td>x-displacement</td><td>-</td></tr> <tr><td>U2</td><td>y-displacement</td><td>0</td></tr> <tr><td>U3</td><td>z-displacement</td><td>0</td></tr> <tr><td>UR1</td><td>Rotation about the x-axis</td><td>0</td></tr> <tr><td>UR2</td><td>Rotation about the y-axis</td><td>0</td></tr> <tr><td>UR3</td><td>Rotation about the z-axis</td><td>0</td></tr> </table> 3. Restriction against 	U1	x-displacement	0	U2	y-displacement	0	U3	z-displacement	0	UR1	Rotation about the x-axis	0	UR2	Rotation about the y-axis	0	UR3	Rotation about the z-axis	0	U1	x-displacement	-	U2	y-displacement	0	U3	z-displacement	0	UR1	Rotation about the x-axis	0	UR2	Rotation about the y-axis	0	UR3	Rotation about the z-axis	0	<p>Encased end</p>  <p>Move in longitudinal direction</p>  <p>Restriction against movement in z/3 direction</p>
U1	x-displacement	0																																				
U2	y-displacement	0																																				
U3	z-displacement	0																																				
UR1	Rotation about the x-axis	0																																				
UR2	Rotation about the y-axis	0																																				
UR3	Rotation about the z-axis	0																																				
U1	x-displacement	-																																				
U2	y-displacement	0																																				
U3	z-displacement	0																																				
UR1	Rotation about the x-axis	0																																				
UR2	Rotation about the y-axis	0																																				
UR3	Rotation about the z-axis	0																																				

	<p>movement in z(3)-direction on top of joint surface close to interlocking between mortise and tendon</p> <table border="1" data-bbox="475 369 870 575"> <tr><td>U1</td><td></td><td>-</td></tr> <tr><td>U2</td><td></td><td>0</td></tr> <tr><td>U3</td><td></td><td>-</td></tr> <tr><td>UR1</td><td></td><td>-</td></tr> <tr><td>UR2</td><td></td><td>-</td></tr> <tr><td>UR3</td><td></td><td>-</td></tr> </table> <p>(see figure)</p> <p>b) Analysis step: Step-1</p> <ul style="list-style-type: none"> - Static general step after initial step default settings - Adding boundary conditions (propagated from initial step), interactions (propagated from initial step) and load to analysis 	U1		-	U2		0	U3		-	UR1		-	UR2		-	UR3		-	
U1		-																		
U2		0																		
U3		-																		
UR1		-																		
UR2		-																		
UR3		-																		
<p>Interactions</p> <p>a) Interaction</p> <p>b) Interaction properties</p>	<p>a) When surfaces are in contact, in interaction pair, one surfaces need to be assigned as master surfaces and one as slave</p> <table border="1" data-bbox="542 1241 805 1310"> <tr><td>Master:</td><td>Mortise</td></tr> <tr><td>Slave:</td><td>Slave</td></tr> </table> <p>b) The interaction properties between interacting pairs are set to frictionless tangential behavior and “hard” contact as “pressure-overclosure” normal behavior.</p>	Master:	Mortise	Slave:	Slave	<p>Interaction surfaces</p> 														
Master:	Mortise																			
Slave:	Slave																			
<p>Loads</p> <p>a) Created in analysis step: step-1</p>	<p>a) Load 1</p> <ul style="list-style-type: none"> - Uniform pressure on boundary end surface of tendon. The magnitude is with negative sign to simulate tension force behavior. <table border="1" data-bbox="513 1860 833 1896"> <tr><td>Load:</td><td>Magnitude:</td></tr> </table>	Load:	Magnitude:	<p>Pressure on tendon-end boundary surface, arrows in purple</p>																
Load:	Magnitude:																			

	<table border="1"> <tr> <td>(Mpa)</td> <td></td> </tr> <tr> <td>Pressure</td> <td>-0.5</td> </tr> </table>	(Mpa)		Pressure	-0.5	
(Mpa)						
Pressure	-0.5					
Mesh a) Element type b) Global Seed size	a) Element type: - Hexagon with default values: C3D8R (8-node linear brick, reduced integration, hourglass control) b) Global seed size : 5 mm - Covering the whole instance	a) Mesh and element type 				
Job	- Submit - Computer time: ca. 20 minutes	Submitted: Thu Oct 25 10:23:48 2018 Started: Analysis Input File Processor Completed: Analysis Input File Processor Started: Abaqus/Standard Completed: Abaqus/Standard Completed: Thu Oct 25 10:43:40 2018				

General Workflow



Form finding

